JYVÄSKYLÄ STUDIES IN BIOLOGICAL AND ENVIRONMENTAL SCIENCE
325

Mari Martikainen

Development of Novel Probes for Enterovirus B Group to Study Uncoating and Infection

JYVÄSKYLÄN YLIOPISTO

JYVÄSKYLÄ STUDIES IN BIOLOGICAL AND ENVIRONMENTAL SCIENCE 325

Mari Martikainen

Development of Novel Probes for Enterovirus B Group to Study Uncoating and Infection

Esitetään Jyväskylän yliopiston matemaattis-luonnontieteellisen tiedekunnan suostumuksella
julkisesti tarkastettavaksi yliopiston Ambiotica-rakennuksen salissa YAA303,
joulukuun 16. päivänä 2016 kello 12.

Academic dissertation to be publicly discussed, by permission of
the Faculty of Mathematics and Science of the University of Jyväskylä,
in building Ambiotica, hall YAA303, on December 16, 2016 at 12 o'clock noon.

UNIVERSITY OF JYVÄSKYLÄ

JYVÄSKYLÄ 2016

Development of Novel Probes for Enterovirus B Group to Study Uncoating and Infection

JYVÄSKYLÄ STUDIES IN BIOLOGICAL AND ENVIRONMENTAL SCIENCE 325

Mari Martikainen

Development of Novel Probes for Enterovirus B Group to Study Uncoating and Infection

UNIVERSITY OF JYVÄSKYLÄ

JYVÄSKYLÄ 2016

Editors
Varpu Marjomäki
Department of Biological and Environmental Science, University of Jyväskylä
Pekka Olsbo, Ville Korkiakangas
Publishing Unit, University Library of Jyväskylä

Jyväskylä Studies in Biological and Environmental Science
Editorial Board

Jari Haimi, Anssi Lensu, Timo Marjomäki, Varpu Marjomäki
Department of Biological and Environmental Science, University of Jyväskylä

URN:ISBN:978-951-39-6868-7
ISBN 978-951-39-6868-7 (PDF)

ISBN 978-951-39-6867-0 (nid.)
ISSN 1456-9701

Jyväskylä University Printing House, Jyväskylä 2016

"To infinity and beyond." –Buzz Lightyear

-Walt Disney Pictures
Toy Story

ABSTRACT

Martikainen, Mari
Development of novel probes for enterovirus B group to study uncoating and infection
Jyväskylä: University of Jyväskylä, 2012, 60 p.
(Jyväskylä Studies in Biological and Environmental Science
ISSN 1456-9701; 325)
ISBN 978-951-39-6867-0 (nid.)
ISBN 978-951-39-6868-7 (PDF)
Yhteenveto: Uudenlaisten markkereiden kehittäminen enterovirus B ryhmän virusten kapsidin aukeamisen ja infektion tutkimiseen
Diss.

Enterovirus B group (EV-B) viruses are important human pathogens which cause a variety of diseases from mild respiratory illnesses to more severe acute infections such as myocarditis and meningitis. EV-Bs have also been associated with chronic infections and autoimmune diseases such as type I diabetes. Because of their significance, better and more accurate methods are necessary to track and visualize viruses *in vitro* and *in vivo*. This thesis focus on the development of novel probes to label viruses site-specifically and track infection *in vitro*. First, we established a covalent conjugation between gold nanocluster markers and EV-B viruses. We were able to visualize through electron microscopy site-specific labelling of cysteines on the viral capsid surface. Second, we developed probes targeted to the hydrophobic pocket of the enterovirus capsid. The probes were synthesized based on a hydrophobic pocket binding drug pleconaril. Successful binding of the probe was confirmed with nuclear magnetic resonance measurements. The probe was conjugated to a fluorescent KU Orange 2 dye or Au102 gold nanocluster, and further studied by confocal and electron microscopy. The third section of this thesis studied the infectious entry pathway of three different coxsackievirus B1 (CVB1) strains. All of the studied strains appeared to use the previously suggested EV-B group entry pathway: macropinocytic entry dependent on Na^+/H^+ and Rac1 and independent of acidification. However, strain specific kinetic differences in the infection of non-polarized cells were revealed. Importantly, one of the CVB1 strains infected cells independently from endosomal sorting complexes required for transport (ESCRT) driven multivesicular bodies (MVBs), and initiated the virus uncoating with slower kinetics. The results indicate that the ESCRT driven biogenesis of MVBs is required for efficient uncoating and infection. Thus, the viruses show remarkable similarities to other well studied EV-B viruses.

Keywords: Coxsackievirus B1; enterovirus B species; gold nanocluster; hydrophobic pocket; multivesicular body; virus tracking

Mari Martikainen, University of Jyväskylä, Department of Biological and Environmental Science, P.O. Box 35, FI-40014 University of Jyväskylä, Finland

Author's address Mari Martikainen
Department of Biological and Environmental Science
P.O. Box 35
FI-40014 University of Jyväskylä
Finland
mari.r.e.martikainen@jyu.fi

Supervisor Docent Varpu Marjomäki, Ph.D
Department of Biological and Environmental Science
P.O. Box 35
FI-40014 University of Jyväskylä
Finland

Reviewers Professor Renate Fuchs
Department of Pathophysiology and Allergy Research
Medical University Vienna
Waehringer Guertel 18-20
A-1090 Vienna, Austria

Docent Tero Ahola, Ph.D
Department of Food and Environmental Sciences
Division of Microbiology and Biotechnology
PO Box 56 (Viikinkaari 9)
00014 University of Helsinki
FINLAND

Opponent Professor Dieter Blaas
Max F. Perutz Laboratories
Medical University of Vienna
Institute of Medical Biochemistry, Vienna Biocenter (VBC),
Dr. Bohr Gasse 9/3,
A-1030 Vienna, Austria,

CONTENTS

LIST OF ORIGINAL PUBLICATIONS

The thesis is based on the following original articles, which will be referred to in the text by their Roman numerals I-III.

I Marjomäki V., Lahtinen T., Martikainen M., Koivisto J., Malola S., Salorinne K., Pettersson M. and Häkkinen H. 2014. Site-specific targeting of enterovirus capsid by functionalized monidisperse gold nanoclusters. *Proceedings of the National Academy of Sciences*. 111(4):1277-81

II Martikainen M., Salorinne K., Lahtinen T., Malola S., Permi P., Häkkinen H. and Marjomäki V. 2015. Hydrophobic pocket targeting probes for enteroviruses. *Nanoscale*. 7(41):17457-67

III Martikainen M., Sioofy-Khojine A., Hyöty H. and Marjomäki V. CVB1 shows strain specific differences infecting cells leading to different outcomes. Manuscript

RESPONSIBILITIES

Article I: The original idea and design of the research was by Varpu Marjomäki and Hannu Häkkinen. The research was performed by Varpu Marjomäki, Tanja Lahtinen, Mari Martikainen, Jaakko Koivisto, Sami Malola, and Kirsi Salorinne. Specifically, I performed the cellular experiments, virus-gold nanocluster conjugations, most of the column purifications, and most of the TEM imaging. Functionalized gold nanoclusters were synthesized by Kirsi Salorinne and Tanja Lahtinen, and analyzed by Jaakko Koivisto. All authors participated in the writing process.

Article II: The original idea and design of the research was by Varpu Marjomäki, Tanja Lahtinen, Kirsi Salorinne, and Hannu Häkkinen. Probes were synthesized and characterized by Kirsi Salorinne and Tanja Lahtinen. The NMR studies were completed under the supervision of Perttu Permi. The analysis and modeling of the gold nanoclusters on the virus structure was done by Sami Malola. I participated in planning and performing the virus-probe conjugation, cellular experiments, thermal stability experiment, and confocal and transmission electron microscopy (TEM) imaging. I wrote the biological aspects of the article together with Varpu Marjomäki. The chemical and physical aspects were written by Tanja Lahtinen, Kirsi Salorinne, Sami Malola, and Hannu Häkkinen.

Article III: The original idea and experimental planning was done by Varpu Marjomäki, Amirbabak Sioofy-Khojine, Heikki Hyöty, and Mari Martikainen. I performed all of the experiments and analysis of data except for the single step growth curve assay. I wrote the article together with Varpu Marjomäki.

ABBREVIATIONS

ATP	adenosine triphosphate
Au	gold
CAR	coxsackie and adenovirus receptor
Cys	cysteine
CVA9	coxsackievirus A9
CVB1	coxsackievirus B1
CVB3	coxsackievirus B3
DAF	decay acceleration factor
DN	dominant negative
EEA1	early endosome antigen 1
EIPA	5-(N-ethyl-N-isopropyl)-amiloride
ESCRT	endosomal sorting complexes required for transport
EV	enterovirus
E1	echovirus 1
GTP	guanosine triphosphate
Hrs	hepatocyte growth factor receptor substrate
ILV	intraluminal vesicle
IgG	immunoglobulin G
Lamp	lysosomal-associated membrane protein
MVB	multivesicular body
NMR	nuclear magnetic resonance
NR	neutral red
Pak1	p21-activated kinase-1
PCR	polymerase chain reaction
PI3K	phosphoinositide-3-kinase
PKC	protein kinase C
PLC	phospholipase C
QD	quantum dot
RGS	Arg-Gly-Asp
RO	replication organelle
scFv	single chain variable fragment
STD	saturation transfer difference
TEM	transmission electron microscopy
Tf	transferrin
TJ	tight junction
T1D	type 1 diabetes
VP	viral protein
WT	wild type

1 INTRODUCTION

Enteroviruses (EVs) are important human pathogens. They cause symptoms ranging from mild respiratory diseases to more severe, e.g. polio-like, symptoms. Moreover, by the end of 1960s, EV infections were associated with the development of type 1 diabetes (T1D). Enterovirus infection begins at the cell surface where the virus binds to its cellular receptor. To infect cells, the virus must transport its genome into the cell cytoplasm where replication and production of new viral proteins take place. Often, the virus needs to be internalized into endosomal carriers of the cell. The infectious entry cycle of the virus is mediated by different cellular factors regulating the events leading to uncoating, genome replication, and production of new viral particles. Currently, there is no exact information about the mechanism of virus uncoating nor the release of the genome from the endosomes. The development of novel antiviral strategies requires more detailed information about the infectious entry route of the virus. Despite their significance, there are only three commercial vaccines available for picornavirus associated diseases. Research, also outside the conventional fields of biology and medicine, is constantly building novel applications in the hope that a better understanding of viral pathogenesis can lead to significant progress in disease prevention or cure.

This PhD thesis concentrates on EV research in two ways: 1) Developing novel techniques to track and visualize EV-B species viruses *in vitro* and 2) studying the differences between three coxsackievirus B1 (CVB1) strains, including the entry mechanisms and infection cycle into non-polarized cells. Specifically, we developed novel strategies to label EV-B virus capsids with site-specific probes and to track EV-B infection *in vitro*. We also observed that CVB1 shows remarkable similarities to other EV-B species viruses studied by us. However, based on the results of the current study, we showed that CVB1 has some strain specific differences in the infection of the cells such as infection kinetics and importance of the MVBs.

2 REVIEW OF THE LITERATURE

2.1 Enteroviruses

EVs are human and animal pathogens belonging to the family of *Picornaviridae*. They infect via the fecal-oral route or through the respiratory track, causing various diseases, but mainly mild respiratory infections (Tuthill *et al.* 2010).

The EV genus consists of 12 species classified mainly by their phylogenetical relations. These species are EVs from A to J and rhinoviruses from A to C. The species EV-B contains 63 serotypes, including echovirus 1 (E1), coxsackievirus A9 (CVA9), coxsackievirus B1 through 6 (CVB1–6), over 30 serotypes of echoviruses, and 20 other know serotypes (Tuthill *et al.* 2010).

EV-B infection (Fig. 1) starts at the plasma membrane where the virus binds to its receptor. The viruses are then internalized into cytosolic vesicles which mature into multivesicular structures. The release of the RNA genome into the cytoplasm enables translation by the host cell machinery. This is followed by polyprotein cleavage and replication, and then production of new virus progeny which are released, often by cell lysis.

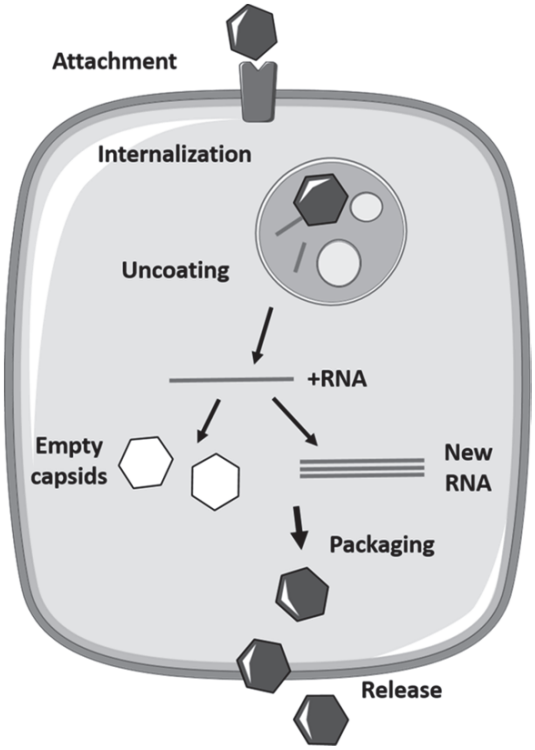

FIGURE 1 Simplified schematic representation of enterovirus B group (EV-B) infection cycle in human cells. Infection starts by the virus binding to its cellular receptor. Next, the virus is internalized into endosomes followed by the release of its genome into the cytoplasm, genome replication, and protein production. The newly formed empty viral capsids are packed with the produced RNA. Finally, new virions are released from the cell by cell lysis. Figure is by drawn using components of the Servier Medical Art Powerpoint image bank (smart.servier.fr/servier-medical-art).

2.1.1 Receptors

A virus receptor is a cellular protein interacting with the virus and promoting infection at the cell surface. Receptors have different cellular and physiological functions that facilitate infection. The first and the most straightforward task is the binding of the virus to the receptor, followed by the concentration of the virus on the cell surface. Typically, this initiates other events important to the infection cycle. Other important functions include: initiating conformational changes and RNA release, targeting the virus to intracellular compartments, and inducing intracellular signals (Bergelson 2010).

E1 and CVA9 use members of the integrin superfamily as their cellular receptors or co-receptors (Bergelson *et al.* 1992; Roivainen *et al.* 1994; Williams *et al.* 2004; Heikkilä *et al.* 2009). Integrins are transmembrane cell adhesion proteins important in cell-cell contacts and cell-extracellular matrix interactions. Their heterodimer structure consists of α- and β- subunits which can be in

active or inactive positions. Also, the intracellular section of the integrin is either in an open or closed conformation (Hynes 2002).

E1 binds to an inactive form of α2β1 integrin on the plasma membrane (Bergelson *et al.* 1992). Furthermore, E1 seems to favor the closed conformation of the integrin. Naturally α2β1 integrin binds to collagen and laminin, component of the extracellular matrix (Elices and Hemler 1989). The binding site of collagen is different from the virus binding site. Moreover, it has been shown that the binding affinity of E1 to the α2-subunit is 10-fold higher than the affinity of the collagen binding protein (Xing 2004). When E1 binds to the α2β1 integrin on the plasma membrane, the integrins cluster, leading to the internalization of the E1-integrin complex (Marjomäki *et al.* 2002; Upla *et al.* 2004).

CVA9 binds to αVβ3 and αVβ6 integrins that typically act as vitronectin and fibronectin receptors, respectively (Roivainen *et al.* 1994; Williams *et al.* 2004; Takada *et al.* 2007; Heikkilä *et al.* 2009). CVA9 is known to attach to integrins via the Arg-Gly-Asp (GRD)-motif (Roivainen *et al.* 1994; Williams *et al.* 2004). In contrast to E1, CVA9 does not co-localize with the integrin receptors during the internalization process (Heikkilä *et al.* 2009). Additionally, αVβ6 integrin is known to have some kind of an effect on CVB1 infection in human colon cancer cells (Agrez *et al.* 1997).

In addition to integrins, E1 and CVA9 have been shown to interact to some extent with β2 microglobulin (Ward *et al.* 1998; Triantafilou *et al.* 1999; Marjomäki *et al.* 2002). β2 microglobulin is a non-glycosylated protein that compose functional major histocompatibility complex class I molecules at the cell surface. Other molecules involved in CVA9 infections are GRP78 (also known as HSPA5 or BiP) and heparin sulfate (Triantafilou *et al.* 1999; Merilahti *et al.* 2016).

All CVBs bind to the coxsackie and adenovirus receptor (CAR) (Cohen *et al.* 2001). Like integrins, CAR is a transmembrane protein and expressed abundantly in many different tissues and cells where it functions in cell-cell adhesions. CAR is in charge of virus internalization, and initiates the conformational changes to the virus capsid that are ultimately needed for the release of the viral RNA (Milstone *et al.* 2005). CAR is mostly expressed at the tight junctions (TJ) of polarized cells and tissues (Cohen *et al.* 2001). In adenocarcinoma human epithelial cells (A549 cells), CAR has been shown to be localized predominantly at cell-cell contacts. However, in more permissive human cervical cancer cells (HeLa MZ cells), CAR is expressed throughout the cell surface (Bordería *et al.* 2015). In polarized cells, CAR is not internalized with the virus, whereas in non-polarized cells, CAR has been visualized with the virus in cytoplasmic vesicles (Patel *et al.* 2009).

Due to the challenging location of CAR in polarized cells, the virus needs a secondary receptor for primary attachment. In such cases, CVB1, CVB3 and CVB5 have been known to use the decay-accelerating factor (DAF) as their secondary receptor (Shafren *et al.* 1995). At least in polarized cells, DAF has an important role in transferring the virus from the apical surface to the TJs to meet CAR. DAF conjugation also initiates signaling events that aid the entry

(Coyne and Bergelson 2006). Like CAR, DAF also has different expression levels depending on the cell line. Permissive Hela cells are known to express DAF in much higher levels than non-permissive A549 cells (Bordería *et al.* 2015). In addition to CAR and DAF, αVβ6 expression is also shown to have a role in CVB1 infection of human colon cells (Agrez *et al.* 1997).

2.1.2 Infectious entry route

The entry route (Fig. 2) of E1 and CVA9 seems to be distinct from the normal, acidifying endosomal pathway of the cell. The internalization of E1, CVA9, and CVB3 starts from lipid raft domains at the plasma membrane (Triantafilou and Triantafilou 2003; Coyne and Bergelson 2006; Patel *et al.* 2009). Virus binding causes clustering of the receptors, triggering signaling events leading to internalization to cytoplasmic vesicles (Upla *et al.* 2004; Coyne and Bergelson 2006; Heikkilä *et al.* 2009). The internalization is mostly independent of clathrin (Bergelson *et al.* 1997; Pietiäinen *et al.* 2004; Coyne and Bergelson 2006; Upla *et al.* 2008; Heikkilä *et al.* 2009; Patel *et al.* 2009; Delorme-Axford *et al.* 2013; Krieger *et al.* 2013). Moreover, cholesterol appears to play a role in E1 and CVB3 infection (Marjomäki *et al.* 2002; Pietiäinen *et al.* 2004; Coyne and Bergelson 2006; Patel *et al.* 2009; Siljamäki *et al.* 2013). The internalization of E1, CVA9, and CVB3 is dependent on the activation of membrane-associated enzymes phospholipase Cs (PLCs) that are in charge of generating inositol triphosphates and diacylglycerol. These are necessary for the downstream activation of protein kinase Cs (PKCs). PKCs are serine-threonine kinases which phosphorylate different protein targets involved in diverse cellular signaling pathways (Upla *et al.* 2004, 2008; Karjalainen *et al.* 2008; Bozym *et al.* 2010; Krieger *et al.* 2013; Huttunen *et al.* 2014).

Next, a small Rho type GTPase Rac1 is activated (Coyne and Bergelson 2006; Karjalainen *et al.* 2008; Huttunen *et al.* 2014). Rac1 is known to regulate the dynamics of actin (Ridley 2006). The activated Rac1 causes actin remodeling and downstream phosphorylation of Pak1. Pak1 is associated with macropinocytosis and fluid-phase endocytosis (Dharmawardhane *et al.* 2000). Interestingly, CVA9 internalization is independent of Pak1 activation (Huttunen *et al.* 2014). In cell line dependent manner, viruses containing clathrin-independent carriers are pinched from the plasma membrane by dynamin or CtPB/BARS (Pietiäinen *et al.* 2004; Karjalainen *et al.* 2008; Heikkilä *et al.* 2009; Patel *et al.* 2009; Delorme-Axford *et al.* 2013). The inhibition of several macropinocytic factors strongly suggests that macropinocytotic entry is used with E1 and CVA9 (Karjalainen *et al.* 2008; Huttunen *et al.* 2014). Table 1 lists the cellular factors involved in E1, CVA9, and CVB3 entry.

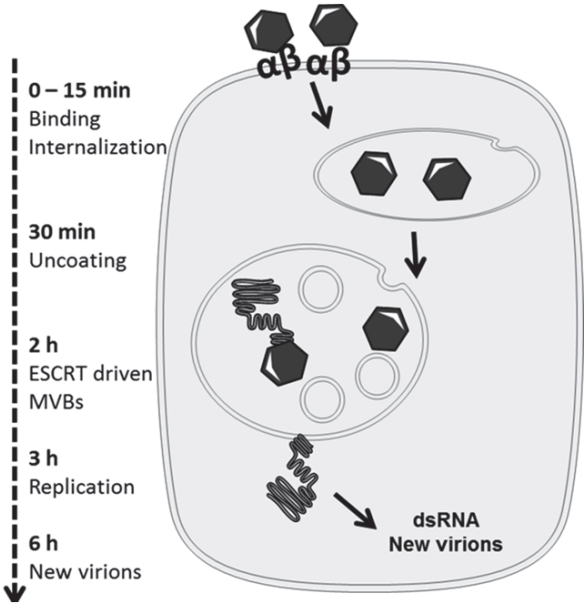

FIGURE 2 Schematic representation of echovirus 1 (E1) and coxsackievirus A9 (CVA9) entry into non-polarized cells. E1 and CVA9 bind to integrins at the cell surface. At 15 min post infection (p.i.), viruses are internalized into cytoplasmic vesicles. These vesicles develop to tubulovesicular structures, and mature into endosomal sorting complexes required for transport (ESCRT) driven multivesicular bodies (MVBs). The uncoating of the virus begins around 30 min p.i. and increases steadily until 2 h p.i. while viruses are still in the MVBs. The replication starts around 3 h p.i. followed by synthesis of capsid proteins and infectious virions. Figure is adapted from Marjomäki et al., (2016) using components of Servier Medical Art Powerpoint image bank (smart.servier.fr/servier-medical-art).

After 15 to 30 minutes post infection (p.i.), E1 and CVA9 are found in cytoplasmic tubulovesicular endosomes lacking early endosomal markers or transferrin (Marjomäki *et al.* 2002; Upla *et al.* 2004; Heikkilä *et al.* 2009; Karjalainen *et al.* 2011; Krieger *et al.* 2013; Huttunen *et al.* 2014). These structures mature into multivesicular bodies (MVBs) that are distinct from the late endosomes. The biogenesis of these MVBs is driven by endosomal sorting complexes required for transport (ESCRT). In contrast to acidic endosomes, MVBs containing these enteroviruses have a neutral environment based on imaging of endosomal pH (Karjalainen *et al.* 2011; Huttunen *et al.* 2014). E1, CVA9, and CVB3 infection is not dependent on acidity (Patel *et al.* 2009; Rintanen *et al.* 2012; Huttunen *et al.* 2014). Uncoating of E1 and CVA9 takes place in MVBs from 30 min p.i. onwards (Pietiäinen *et al.* 2004; Siljamäki *et al.* 2013; Huttunen *et al.* 2014). Finally, the genome is released into the cytoplasm, followed by replication and production of new viral progeny. Information concerning CVB3 uncoating and whether it accumulates into MVBs is still lacking.

TABLE 1 Relevant cellular factors studied by different treatments in E1 and CVA9 infection cycle. The dependence on the target molecule is stated with a plus sign (+) and independence with a minus sign (-). A minor effect is stated with plus and minus sign (+/-). Phospholipase C (PLC), protein kinase C (PKC), phosphoinositide-3-kinase (PI3K), endosomal sorting complex required for transport (ESCRT).

Target	Effect on E1	Effect on CVA9	Effect on CVB3	References
Dynamin	+/-	+	+/-	Upla et al., 2008; Krieger et al., 2013; Huttunen et al., 2014; Patel et al., 2009; Delorme-Axford et al., 2013
CtBP/BARS	+			Karjalainen et al., 2011; Krieger et al., 2013
PLC	+	+	+/-	Karjalainen et al., 2008; Huttunen et al., 2014: Upla et al., 2004
PKC	+		+	Upla et al., 2004; Pietiäinen et al., 2004; Coyne et al., 2007; Delorme-Axford et al., 2013 Krieger et al., 2013;
Rac1	+	+	+	Coyne et al., 2006 Karjalainen et al., 2008; Huttunen et al., 2014
Pak1	+	-	+	Karjalainen et al., 2008; Krieger et al., 2013; Huttunen et al., 2014
PI3K	+/-	-	-	Karjalainen et al., 2008; Heikkilä et al., 2010; Delorme-Axford et al., 2013; Huttunen et al., 2014
Na^+/H^+ exchanger	+	+	+	Coyne et al., 2007; Karjalainen et al., 2008; Krieger et al., 2013; Delorme-Axford et al., 2013; Huttunen et al., 2014

Target	Effect on E1	Effect on CVA9	Effect on CVB3	References
Acidification	-	-	-	Heikkilä et al., 2010; Krieger et al., 2013; Huttunen et al., 2014
ESCRTs	+	+		Karjalainen et al., 2011; Huttunen et al., 2014
Microtubules	-	-	+	Pietiäinen et al., 2004; Coyne et al., 2007; Heikkilä et al., 2010; Delorme-Axford et al., 2013; Huttunen et al., 2014

2.1.3 Enterovirus structure

EVs have a single-stranded RNA genome with positive polarity (Fig. 3A) and the genome is roughly 7,500 nucleotides long. A small virus-encoded protein (VPg) is linked covalently to the 5′ end, whereas the 3′ end is polyadenylated. VPg functions as a primer for the RNA polymerase $3D^{pol}$ (Paul *et al.* 1998). The viral RNA acts as messenger RNA upon uncoating. The internal ribosomal entry site at the 5′ end allows the initiation of direct translation of the polyprotein (Wimmer and Paul 2010). The polyprotein is first processed into precursor proteins P1, P2, and P3. P1 is then proteolytically cleaved into structural proteins VP1-4, whereas P2 and P3 are processed into seven non-structural proteins associated with replication. The EV genome is tightly packed within the protein capsid at a concentration of roughly 70 mg/ml (Wimmer and Paul 2010).

The non-enveloped icosahedron shaped EV capsid is formed by 60 structural units called protomers (Fig. 3B). Each protomer consists of VP1, VP2, VP3, and VP4. Proteins VP1–3 are expressed on the outer surface of the capsid whereas VP4 forms the inside of the capsid with the N-terminus of VP1. VP4 is observed in association with RNA in poliovirus (Lentz *et al.* 1997).

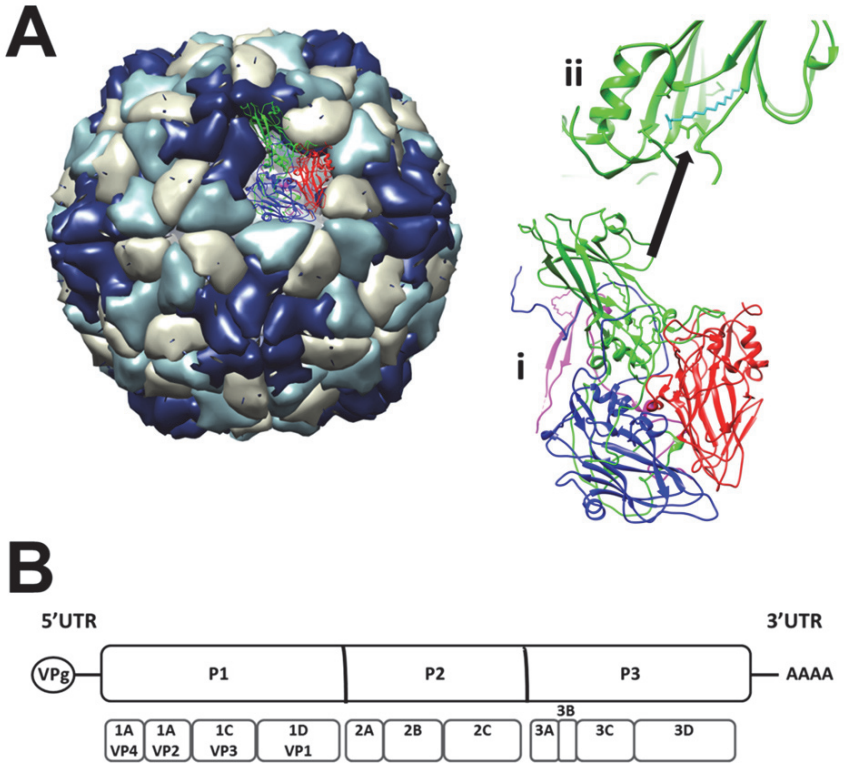

FIGURE 3 Schematic representation of enterovirus B (EV-B) capsid structure and genome. A) Crystal structure of echovirus 1 (E1). EV-B capsid represent has icosahedron symmetry and consists of 60 copies of structural units, protomers. (i) A protomer is formed by viral proteins (VP) 1 to 4. Here, VP1 (green), VP2 (red) and VP3 (blue) form the outside surface of the capsid, whereas VP4 (magenta) is inside the capsid. (ii) Within VP1 there is a hydrophobic pocket that is occupied by a pocket factor (cyan). Images drawn with Chimera based on E1 crystal structure, PDB code 1EV1. B) The genome of EV-B consists of P1 region coding the structural proteins, and P2 and P3 regions coding the non-structural protein needed for replication.

VP1 proteins surround the five-fold axis and VP2 and VP3 locate around the two- and three-fold axes. The β-barrel of VP1 contains a hydrophobic pocket which is, in most cases, occupied by a pocket factor (Filman *et al.* 1989). The entrance of the pocket is located at the canyon-like depression that is surrounds the five-fold axis. The pocket factor is a small, non-protein molecule. In bovine enterovirus the most frequent pocket factor is palmitic acid (Smyth *et al.* 2003). Pocket factors are believed to have a role in capsid stability and are most likely released upon uncoating (Filman *et al.* 1989; Smyth *et al.* 2003).

Dynamic, reversible exposition of internal proteins from the virus capsid, called "breathing", has been observed with many picornaviruses including poliovirus (Li *et al.* 1994), rhinoviruses (HRV14 and HRV16) (Lewis *et al.* 1998; Katpally *et al.* 2009), and swine vesicular disease virus (Jiménez-Clavero *et al.*

2000), and CVA9 (Pulli *et al.* 1998). Moreover, VP4 and the N-terminus of VP1 of HRV14, due to breathing, can be extruded temporarily from the capsid (Lewis *et al.* 1998). Similarly, the aminoterminus of VP1 of poliovirus 1 has been shown to be outside of the capsid close to the 2-fold axis where uncoating possibly occurs (Li *et al.* 1994). This emphasizes that capsid breathing is part of the capsid dynamics and possibly leads to the uncoating process (Smyth 2002; Reisdorph *et al.* 2003; Roy and Post 2012).

2.1.4 Clinical relevance

EVs include numerous important human pathogens, generating a wide range of symptoms from mild respiratory disease to severe acute and chronic infections, such as poliomyelitis, aseptic meningitis, myocarditis, and pancreatitis. Today, two of the most studied enteroviruses are EV-71 and EV-D68, causing foot-and-mouth-disease and respiratory illness, as well as polio-like-symptoms (Tokarz *et al.* 2012; Tan *et al.* 2014). Globally, EVs initiate epidemics and outbreaks, more frequently infecting neonates and young children.

In various studies, EV infection has been associated as a causative environmental factor for T1D (Gamble *et al.* 1969; Jenson *et al.* 1980; Coppieters *et al.* 2012). Through various methods, the presence of EV RNA and VP1 has been associated with the onset of T1D in patient samples (Ylipaasto *et al.* 2004; Krogvold *et al.* 2015). Particularly, CVB1 has been shown to cause insulitis, islet cell damage, and induction of islet beta-cell autoimmunity. Moreover, it has the capacity to infect human pancreatic islets *in vitro* (Jenson *et al.* 1980; Frisk and Diderholm 2000; Roivainen *et al.* 2000, 2002; Laitinen *et al.* 2014). Recent birth cohort studies in different European populations indicate risk association between CVB1 and T1D (Oikarinen *et al.* 2008; Laitinen *et al.* 2014). CVB1 infection has been studied in greater detail and the two clinical isolates of CVB1, CVB1-CDC7, and CVB1-CDC11, have been shown to cause differing immune responses in human peripheral blood mononuclear cells, as well as in isolated pancreatic islets. Moreover, the CVB1-CDC11 strain is known to have a more aggressive infection in the islets (Anagandula *et al.* 2014; Hämäläinen *et al.* 2014).

2.2 Visualization and tracking of viruses

The visualization and tracking of viruses is essential to understand the mechanisms of the infectious entry. Knowledge of the characteristics of receptor binding and internalization, genome release, and the production of new viral progeny is necessary for diagnostic purposes and the development of novel antiviral strategies. Furthermore, high resolution visualization of the virus structure is essential to study the intricacies of viral uncoating in endosomes.

EVs are small-sized viruses, making them more difficult to visualize both *in vitro* and *in vivo*. In recent applications, studies in tissues and cells often

involve fluorescent or colloidal gold markers for various microscopy techniques. Usually, these markers are bound to viruses indirectly via antibodies. Furthermore, viral RNA can be detected from tissues, blood, and serum through different methods. Specific 3D viral structures can be determined with cryo-electron microscopy reconstructions and by crystallization.

2.2.1 Antibody labeling and immunofluorescence techniques

Antibodies are host proteins produced by the immune system to recognize and neutralize pathogens such as bacteria and viruses. These proteins, also known as immunoglobulins (Ig), are large, Y-shaped molecules approximately 150 kDa in size. They differ in structure, forming five different classes in mammalians: IgM, IgD, IgG, IgA, and IgE.

Antibodies are composed of four polypeptides: two identical copies of light and heavy chains bound together with disulphide and non-covalent bonds (Fig. 4). Additionally, the structure is divided into constant and variable regions with antigen binding sites located at the tips of the Y-shaped structure. Antibody molecules can either be poly- or monoclonal, depending on whether they were produced by all lymphocytes or by one lymphocyte clone, respectively (Litman *et al.* 1993; Lipman *et al.* 2005).

Antibody molecules can be cleaved into smaller fragments and retain their full binding capacity. The arm of the Y-shaped molecule is called a Fab fragment and is roughly 50,000 Da in size. The even smaller IgG fragment is the single-chain variable fragment (scFv), also called a nanobody (Fig. 4) Nanobodies are man-made fragments composed of an N-terminal, variable domain of the heavy chain and an N terminal, variable domain of the light chain linked together with a peptide linker (Fig. 4). A nanobody is only 25,000 Da in size. The small size is beneficial when efficient penetration into cells and tissues is needed (Ahmad *et al.* 2012). However, the small size also has disadvantages, e.g. lack of stability and a tendency to form aggregations (Nieba *et al.* 1997; Wörn and Plückthun 1999). The production and selection of nanobodies can be done by phage display library, wherein the target protein, e.g. a virus, is exposed to a large library of peptides. This allows for efficient and low-cost screening, called bio-panning (McCafferty *et al.* 1990). Selected nanobodies can be used as antibodies in various applications.

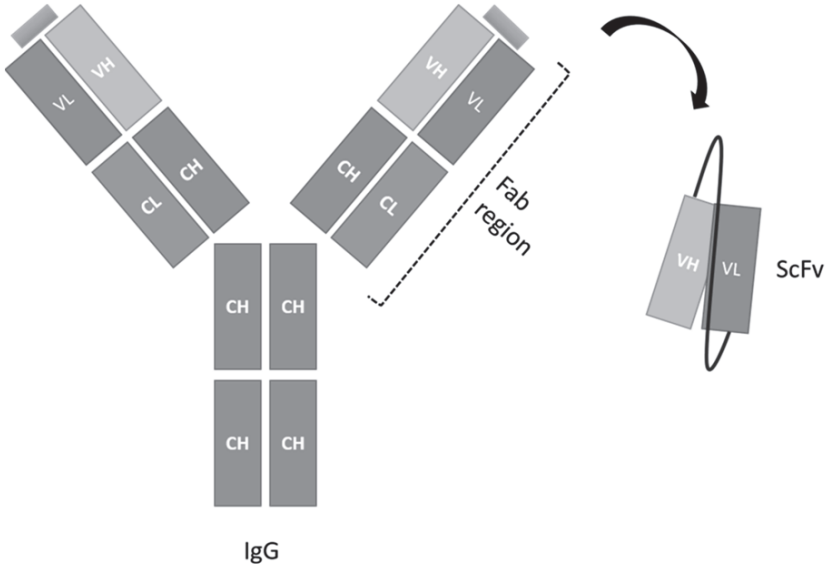

FIGURE 4 Simplified representation of immunoglobulin G (IgG) structure. The IgG molecule is composed of constant (C) and variable (V) regions and light (L) and heavy (H) chains. At the end of V regions are antigen binding sites. The "arms" of the Y shaped molecules can be cleaved as smaller Fab and single chain variable (ScFv) fragments.

Antibodies have the ability to bind to an antigen with high affinity and specificity, and subsequently they have been used in a variety of medical and scientific applications. These applications include analysis, purification, and enrichment methods as well as mediation and modulation methods. Some of the most popular methods for virus analysis are immunoblotting and immunoprecipitation, Enzyme-linked immunosorbent assays, X-ray crystallography, flow cytometry analysis, immunohistochemistry, and immunofluorescence (Lipman *et al.* 2005). The basic element of all antibody techniques is the antibody's capacity to recognize its epitopes in the specimen which is then detected via different markers.

In immunofluorescence labeling, target proteins or antigens are recognized in a section of tissue or cells with specific antibodies which are conjugated to a fluorescent dye. The light emitted by the fluorescent dye is visualized with an optical microscope. Immunofluorescence labeling can be done directly or indirectly. When using the direct method, the primary antibody is labeled with a fluorescent dye, whereas in the indirect method, the primary antibody is labeled with a secondary antibody bound to a fluorescent dye (Fig. 5). Generally, fixed immunofluorescence samples are prepared on glass slides which makes it possible to maintain the normal 3D structure of the cells (Fritschy and Härtig 2001).

One of the weaknesses of immunofluorescence labeling is the unspecific binding of antibodies which may cause background noise and unreliable results. This is problematic, especially when small sized proteins or a small

number of target proteins are being visualized, e.g. a viral capsid or RNA. In addition, challenges also arise because of the lack of long-term stability of fluorescent probes and the weak interactions of antibody binding. However, suitable usage and correct analysis make antibodies one of the most powerful reagents in science.

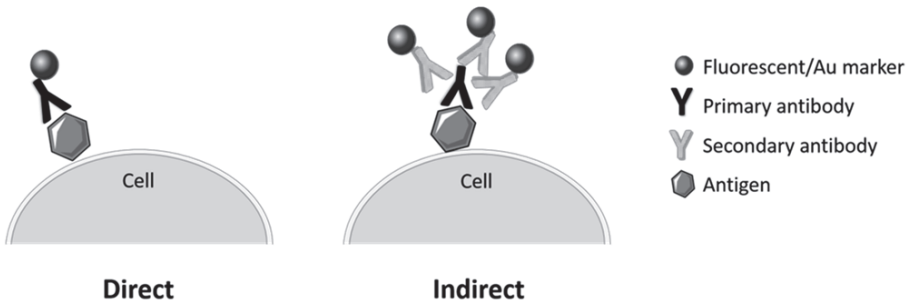

FIGURE 5 Example of direct and indirect immunolabeling. In both techniques, the antigen is recognized by a primary antibody. When the direct method is used, the primary antibody is conjugated to a fluorescent or colloidal marker depending on the imaging technique. By contrast, the indirect method requires a secondary antibody, conjugated to the marker, which recognizes the primary antibody.

2.2.2 Live imaging

As described, in common immunofluorescence labeling, target proteins are observed in fixed cells. To gain more information about cellular and viral dynamics, live cell imaging can be used. In live imaging, dynamics are visualized over time using time-lapse microscopy. In combination with the fluorescent labeling of different proteins and molecules, this technique enables visualization of interactions, associations, and other processes in real time. Live cell imaging is a useful tool to study biological mechanisms. This makes it significant in visualizing the functions and dynamics of many cellular and virological processes.

An essential aspect of imaging is that it is performed close to the natural state of the living cells to avoid abnormal cellular behavior. A challenge is the choice of an appropriate fluorescent probe as it may cause problems, such as phototoxicity and photobleaching (Tan *et al.* 2010). Moreover, commercially available probes may not be suitable for the target protein.

Conventional immunofluorescence labeling can also be applied for live cell imaging. In this case, an antibody is attached to its antigen at the plasma membrane prior to internalization into the cell. For example, integrin clustering and recycling has been studied with fluorescent bound Fab-fragments that were conjugated to integrins on the plasma membrane (Rintanen *et al.* 2012). However, this type of indirect labeling is vulnerable to degradative processes inside endosomes and thus may not reliably visualize the localization of the target.

Brandenburg *et al.* (2007) visualized the entry and genome release of the poliovirus in live cells. They produced an infectious poliovirus with both their capsid and genome specifically labeled by fluorescent probes. Over 20 RNA binding dyes were screened to fit the criteria for successful labeling as the dye needed to be membrane permeable and non-cytotoxic. Moreover, sufficient binding to RNA was needed to visualize the single RNA release. Additionally, it was necessary for the dye not to compromise the infectivity nor interfere with RNA incorporation into the virus capsid. Only one suitable dye was found matching the criteria—Syto82. Thus, RNA was labeled non-covalently with Syto82 and the capsid was labeled covalently with Cy5. With double labeling, it was shown that poliovirus uncoating takes place in the early infection. Similar types of capsid labeling, wherein the fluorescent dye reacts with the amines of the capsid, have been used, originally with simian virus 40, but also in our earlier studies with E1 (Pelkmans *et al.* 2001; Pietiäinen *et al.* 2004). More recently, outside of the EV group, the rabies vaccine strain virus entry into Vero cells was visualized with the help of Cy5 labeling of the capsid (Xu *et al.* 2015).

Live-cell imaging has been used also to visualize the formation of CVB3 replication organelles (ROs) (van der Schaar *et al.* 2016). In this study, a small split-system green-fluorescent-protein was introduced into CVB3 genome, more specifically into the well-known RO-resident protein 3A. The formations of ROs was visualized with the double labeling of the Golgi apparatus and ROs using immunofluorescence and correlative light electron microscopy. This technique is a novel tool to study the dynamics of ROs directly in living cells. In older studies, the formation of poliovirus ROs have been visualized in live cells that express a fluorescently labeled cellular protein (Belov *et al.* 2007).

2.2.3 Immunogold labeling

Likely the most popular electron microscopy (EM) detection technique is immunogold labeling. This technique is similar to conventional immunofluorescence labeling in its simplicity except antibodies detecting cell structures and other biomolecules are attached to colloidal gold (Au) probes. Colloidal Au is a colloidal suspension that contains similarly sized colloidal Au particles (< 10% variation), that, however, varies in the number of Au atoms they have. Colloidal Au size can vary from 5 to 250 nm (Ackerson *et al.* 2010). In immunogold labeling, secondary antibodies or Protein-A are non-covalently attached to colloidal Au particles (Roth 1982). This is how Au particles are targeted to the primary antibodies in the sample. However, since the attachment is not covalent, the protein gradually disengages from the colloidal Au particle.

Similar to immunofluorescence labeling, immunogold labeling is also carried out either directly or indirectly (Fig. 5). Au is an electron dense material which can be clearly visualized through transmission electron microscopy (TEM) and scanning electron microscopy. The advantages of this technique are that it allows the quantification of Au markers inside tissue and cells; and it enables the staining of the microscopic sample to enhance the visualization of

cellular structures (Paul *et al.* 2012). With immunogold labeling, the structure-function relationships, as well as protein distributions, can be studied in high resolution. Immunogold labeling has been an essential part of resolving the infectious entry route of E1 and CVA9 (Marjomäki *et al.* 2002; Upla *et al.* 2004; Karjalainen *et al.* 2011; Huttunen *et al.* 2014).

Two of the most common immunogold techniques are pre- and post-embedding methods. Before or after the labeling, the sample requires a suitable sample preparation which generally involves the following steps: fixation, dehydration, embedding, and sectioning. Proper sample preparation is necessary to generate high quality samples.

When using the pre-embedding technique, a sample is labeled before embedding and sectioning. Whereas in the post-embedding procedure, samples are first fixed, embedded and sectioned, and then finally labeled. Depending on the labeling method, samples are either prepared for resin-embedding or for cryo-sectioning. The former retains the cellular structures. When the pre-embedding technique is applied, antigens are already labeled at the plasma membrane in a manner similar to that as described for live cell immunofluorescence labeling. This method ideally provides low background noise and allows for the tracking of target proteins in real time. It works especially well when there are a sufficient number of target proteins and a sensitive enough antibody, e.g. the internalization of integrin is easy to visualize with this method since it is highly expressed throughout the cell surface (Karjalainen *et al.* 2011; Rintanen *et al.* 2012; Soonsawad *et al.* 2014). However, it is difficult to label proteins and biomolecules inside the cell.

By contrast, ultra-thin cryo-sections sample preparations preserve the antigen binding properties and immunogold labeling is completed after the sectioning. With this technique, a greater variety of proteins can be targeted. However, different cellular structures in cryo-sections are not as well-preserved as in resin-embedded sections.

2.2.4 Detection of RNA

Different methods, such as polymerase chain reaction (PCR) and *in situ*-hybridisation, can be used to detect the viral genomic material in cells and tissues. EVs release their positive sense RNA into the cytoplasm of the cell. Then, RNA can be targeted with specific primers or probes.

Reverse transcription-PCR (RT-PCR) is a widely used method in virology. The high sensitivity and rapidity of the technique also allows for PCR usage for diagnostics purposes. The technique can detect EV sensitively via specific primers that are targeted to the RNA of the virus (Rotbart 1991). The selectivity of virus detection depends on the quality of the primers and the purity of the sample. A virus can be also detected directly from tissues (Shibata *et al.* 1988). However, a virus cannot be localized into specific cells.

In situ-hybridization (ISH) can be used for more sensitive detection in cells and animal models. ISH is a hybridization method where genomic material is detected with complementary RNA. With ISH in particular, the localization of

the target genome can be studied in greater detail. The RNA binding probes are visualized by microscopic means depending on the marker (radio-, fluorescence- or antigen labeled). The fluorophore binding poliovirus and E1 RNA has been visualized via fluorescence ISH (FISH) (Bolten *et al.* 1998; Pietiäinen *et al.* 2004).

As with PCR, the sensitivity of the detection is highly dependent on the quality of the probe. Laiho *et al.* (2015) developed a highly selective, novel probe specifically detecting EV RNA from formalin-fixed paraffin embedded tissue samples. The probe can also be used to distinguish between virus serotypes.

2.2.5 Click chemistry

Click chemistry is an orthogonal reaction in which a single desired product is efficiently synthesized from a group of reactions. Typically, the requirements for click reactions are effective for selective biomolecule labeling. Reactions need to proceed rapidly and in high yields under specific conditions to yield the desired product. These reactions are bio-orthogonal in nature since they proceed in high yields under biological surroundings and the precursor does not disturb the common biochemical processes (Best 2009). However, thus far, viral tracking based on click chemistry has not been successful in live cells due to the cytotoxicity of the method.

Click chemistry can be used either for detection of viral capsids or the genome (Wang *et al.* 2003, 2013). In an early study, Wang *et al.* (2003) used azide-alkyne cycloaddition to derive the cowpeac mosaic virus. Azide or alkyne groups were introduced to either lysine or cysteines on the viral surface. Whereas, in a more recent study, viral surfaces were modified via click reactions for viral vector targeting purposes (Chu *et al.* 2016).

Viral DNA trafficking in single cells has been visualized and quantified at single viral DNA resolution in mammalian cells. Adenovirus, herpes virus, and vaccinia virus DNA was metabolically labeled by ethynyl-modified nucleosides. Then, newly synthesized viral DNA was labeled with copper(I)-catalyzed azide-alkyne cycloaddition click reactions and tracked with super resolution microscopy (Wang *et al.* 2013). With similar procedures, click chemistry makes it possible to follow and quantify the effect of a viral infection on host cell RNA synthesis (Kalveram *et al.* 2013).

2.3 Virus detection in nanotechnology

The goal of detecting biological macromolecules linked to viral infection directly from diagnostic samples has impelled researchers to develop novel tools with nanotechnology. The current medical diagnostics of clinical virulence primarily relies on the detection of viral genomic material by PCR techniques. As described, antibody detection is not typically useful in the early stages of

infection. While PCR can detect viral genomes with great specificity, it does not reveal information about its localization in infected cells or their types. A sensitive method to selectively detect individual virus particles in clinical samples would have a significant impact on health care. Such a sensitive method could enable the diagnosis of disease in its early stages.

Single influenza A virus viral particles have been selectively detected using antibody functionalized nanowire field-effect transistors (Patolsky *et al.* 2004). Silicon nanowires were synthesized with 20 nm gold nanoclusters, silane, and diborane. The basic idea of this process is that a viral particle binds to the antibody on the nanowire device, generating a change from the baseline conductance value. Within the array, different nanowires can be modified with antibodies to provide a platform for the simultaneous detection of multiple viruses (Patolsky *et al.* 2004).

Single virus particles can be also detected with spectroscopic means via whispering gallery modes (Vollmer *et al.* 2008; Zhu *et al.* 2011). Whispering galley modes are waves that can travel across a concave surface. The detection of these waves is based on an optical measurement that does not require labeling of the sample. Vollmer et al. (2008) observed a label-free virus particle producing changes in the resonance frequency of a whispering-gallery mode excited in a micro-spherical cavity. In addition to the detection of the virus, the viral size and mass were recognized. Moreover, Zhu *et al.* (2011) applied whispering gallery modes to a label free spectrometry scheme that allowed for influenza A virus detection in an ultra-high-Q resonator. In addition to whispering gallery modes, other kinds of spectroscopic measurements can be used for viral detection, e.g. Ruokola *et al.* (2014) observed detailed signatures of E1 and its uncoating intermediate produced by heating, as well as the disrupted particle with Raman spectroscopy.

A novel single virus tracking technique includes quantum dots (QD) as labels. Recently, the infectious entry routes of different animal viruses have been characterized with the help of QD labeling (Joo *et al.* 2011; Liu *et al.* 2012b). QDs are inorganic nanocrystals with unique properties. These make them ideal for optical purposes, in many ways exceeding the characteristics of normal fluorescent proteins. They have excellent photostability, high brightness, a moderate size, and are multicolored (Bruchez *et al.* 1998; Liu *et al.* 2016). Moreover, they have excellent resistance and high quantum yields.

To be suitable for a cellular environment, QDs need to go through biofunctionalization (Bruchez Jr. *et al.* 1998; Chan and Nie 1998). Depending on the target viral component, QDs can be attached to a virus via different methods, typically divided into four categories: direct labeling via chemical reaction, biotin-streptavidin reaction, antibody-antigen interactions, and peptide residues. QD bound viruses can be visualized *in vivo* or *in vitro* via different imaging methods, such as total internal reflection imaging, confocal imaging, super-resolution imaging, and 3D imaging (Liu *et al.* 2016). There is a discrepancy in the field concerning QD toxicity *in vivo* and *in vitro.* However, each QD is a unique design with a combination of physiochemical properties which do not always make them toxic (Tsoi *et al.* 2013).

2.3.1 Gold nanoclusters and bioconjugation

Conventional indirect colloidal Au labelling has poor signal-to-noise ratio and is based on weak, electrostatic interactions. This has led researchers to determine solutions for direct labeling methods using the site-specific labeling of biomolecules by size-specific Au nanoclusters (Häkkinen 2008). An Au nanocluster is a cluster of Au atoms containing multiple Au-Au bonds, typically protected or stabilized by a ligand layer. In contrast to colloidal Au particles, Au clusters are constructed of a precise number of Au atoms (Ackerson *et al.* 2010). Au clusters are also relatively easily modified (Wang and Ma 2009). Au nanoclusters have unique properties that enable their use in nanotechnology, e.g. medicine, biochemistry, photonics, and sensors. Some of these properties are catalytic activity and size dependent optical, electronic, and photothermal properties. Furthermore, there are well-established methods of synthesizing gold nanoparticles into specific and consistent sizes and shapes (Ackerson *et al.* 2010). These properties have led researchers to develop novel labelling strategies for viruses.

Generally, three different bioconjugation chemistries are used: 1) Linker mediated bioconjugtion, 2) Direct gold-biomolecule bonding, and 3) His-tag binding by chemical reactions. Linker mediated binding forms a link between an Au cluster and cysteine, amine, or Ni(II)-His_6 cross-links. Moreover, linker mediated binding and direct Au-biomolecule conjugation are based on covalent binding of molecules, whereas an Au cluster functionalized with a derivative of nitrilotriacetic acid (NTA) is targeted to form a strong bond for His-tags (Ackerson *et al.* 2010). There are also commercially available Au cluster labels for these purposes. Direct Au binding eliminates the organic link between a protein and the Au core (Ackerson *et al.* 2010). However, this method is more complicated than the linker mediated method. Moreover, the structure of Au affects the chemistries of biomolecule bonding, e.g. the coating of the Au core affect the cluster's electrostatic properties (Jackson *et al.* 2004; Ghosh *et al.* 2011; Kim *et al.* 2012; Liu *et al.* 2012a).

2.3.2 $Au102(pMBA)_{44}$ cluster

The $Au102(pMBA)_{44}$ cluster (Fig. 6) is an all-thiolate-protected, stable, water-soluble Au nanocluster with a core size of 1.5 nm. The atomic structure of the cluster has been determined. The cluster consists of 102 Au atoms which are protected by 44 para-mercaptobenzoic acid $SC_7O_2H_5$ (pMBA). More specifically, the cluster core is composed of 79 Au atoms in charge-neutral metallic states and 23 Au oligometric RS–(AuSR)x units are in an oxidized state (Jadzinsky *et al.* 2007; Walter *et al.* 2008; Salorinne *et al.* 2014).

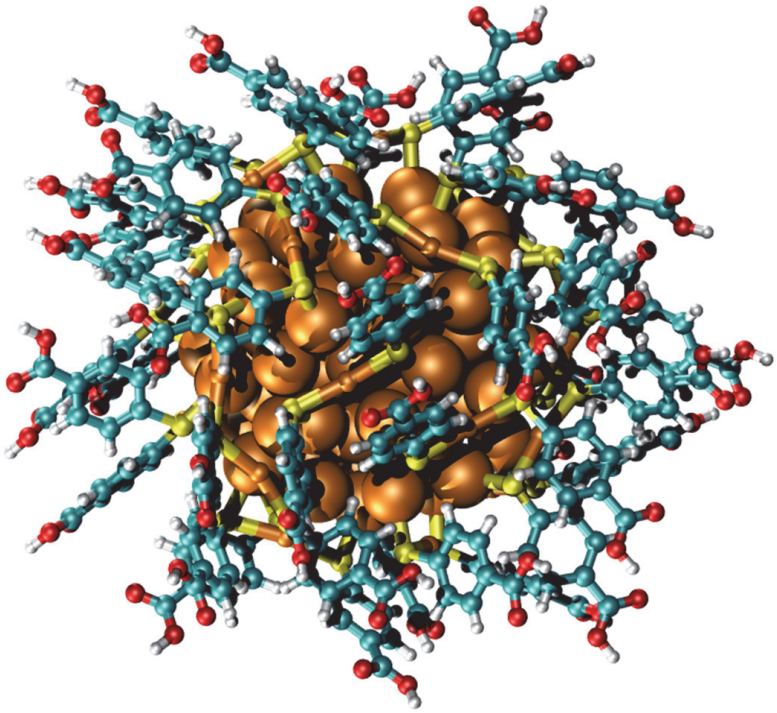

FIGURE 6 Schematic presentation of the structure of $Au102(pMBA)_{44}$ cluster drawn from the crystal structure. Au atoms (gold), carbon (turquoise), oxygen (red), sulfur (yellow), and hydrogen (white). Image courtesy of Sami Malola.

2.3.3 Au-virus conjugations

Colloidal Au particles have been encapsulated in brome mosaic virus (Dragnea *et al.* 2003). The encapsulation enables the observation of individual virus signals via Rayleigh resonance spectroscopy. The negatively charged RNA of the virus was partially replaced by citrate covered Au particles, 2.5–4.5 nm in diameter. Virus particles were disassembled and then reassembled in the presence of Au clusters. The success of Au encapsulation was visualized by TEM. Virus-Au-complexes were analyzed in greater detail with spectroscopy and dark-field optical microscopy. In conclusion, researchers were able to present the use of Au clusters as markers for spectroscopic use (Dragnea *et al.* 2003).

In another study, Blum *et al.* (2004) bound 2 and 5 nm Au nanoparticles to mutated virus capsids via a covalent bond. The precise number of Au atoms in the used cluster was not known. Cysteine residues were engineered on selected points of the cowpeac mosaic virus capsid. The thiols of cysteines conjugated to the nanoclusters. The binding was visualized by TEM and the neighbor-neighbor distances of the Au clusters were analyzed. The results demonstrated the specific binding of Au nanoclusters on the virus surface. These kinds of Au-

virus complexes can be useful in many applications, such as molecular electronics and biosensors.

Additionally, Au nanoparticles have been bound covalently to Adenoviruses (Everts *et al.* 2006). Everts et al. (2006) visualized a successful conjugation of sulfo-NHS-ester Au nanoparticles to lysine residues, abundantly present on adenovirus capsids. The virus-Au-conjugates were separated by cesium chloride gradients and then further analyzed with TEM. The aim of the study was to develop a successful Au nanoparticle conjugated adenovirus vector targeted to tumor sites. Au photothermic properties would then enable their use as a potential cancer therapy. In addition, in another study, Au nanoparticles decorated with naturally occurring N-glycans have been used for highly sensitive detection of the influenza virus and viral hemagglutinin by dynamic light scattering and UV/Vis spectroscopy (Poonthiyil *et al.* 2015).

The unique properties of Au are an advantage when designing novel virus tracking and visualization strategies. Direct bio-conjugation of Au not only improves the Au labeling for TEM imaging but also enables the use of other detection methods such as spectroscopy. Thus, the use of Au labeling in virus detection will most probably increase in the future technologies.

3 AIMS OF THE STUDY

I Development of tools for detecting and targeting EV-B viruses and visualizing their uncoating *in vitro* (I, II).

II Entry and infection kinetics of CVB1 and its two clinical isolates into non-polarized cells (III).

4 OVERVIEW OF THE METHODS

The methods used in this study are listed in Table 2. Detailed descriptions of the materials and methods can be found in the original publications, indicated by Roman numerals.

TABLE 2 Summary of methods used in the original publications included in the current thesis.

Method	Publication
Cell culture	I, II, III
Virus production and purification	I, II, III
Virus infection	I, II, III
Drug treatments	III
Transfections	III
Chemical synthesis	I, II
Characterization methods for markers	I, II
Thermal stability assay	III
Immunofluorescence and confocal microscopy	II, III
Electron microscopy	I, II
NMR	III
Quantification of microscopic data	I, II, III
Statistical testing	I, II, III

5 RESULTS AND DISCUSSION

5.1 Cysteine targeted Au nanoclusters

Monodisperse Au102(pMBA)44 clusters were synthesized as described by Kornberg and co-workers (Levi-Kalisman *et al.* 2011). The 1.5 nm metal core was protected by a para-mercaptobenzoic acid ligand layer resulting in 2.8 nm sized water soluble particles. The quality of the clusters was characterized with TEM, NMR, UV-visible (UV-vis) spectroscopy and gel electrophoresis (I, Fig. S1-S4).

The next step in the synthesis strategy was to functionalize the Au102 clusters with a six-carbon alcohol with terminal maleimide functionality. The closest distances from the thiol end of cysteine residues to the viral surface of E1 and CVB3 was determined. The nearest cysteines for E1 were cys256, cys209, and cys73, and distances varied from 0.31–1.15 nm. For CVB3, they were cys234, cys134, and cys73, with distances from 0.88–1.24 nm. For this reason, N-6(hydroxyhexyl)maleimide, approximately 1.1 nm in length, was chosen as a linker.

The pMBA ligand provided a bond via a modified Steglich esterification reaction to the terminal alcohol producing maleimide functionalized Au102(pMBA)44-m(N-(6-hexyl 4-mercapto- benzoate)maleimide)m clusters, hereafter called Au102-MI. Functionalization was confirmed by gel electrophoresis, UV-vis, and IR spectroscopy (I, SI Appendix Fig. S3, S4 & S6). Au102-MI clusters were then targeted to the free thiols of cysteine residues of the viral surface via a Michael addition reaction. The conjugation was performed for various time periods at 37°C. Non-functionalized Au102(pMBA)44 clusters were used as a control throughout the study.

The success of site-specific binding was analyzed by TEM. Non-functionalized clusters did not show any association with the virus capsid, suggesting they could not actively bind to virus, even during long incubation periods (I, Fig. 2C & S7). By contrast, Au102-MIs showed substantial loading on E1 and CVB3 surfaces (I, Fig. 2A, B, D & S8). To get rid of free, unbound gold

clusters, after Au102-MI-virus conjugation, samples were further purified via size-exclusion chromatography to remove excess Au102-MI clusters. Virus containing structures were visualized by TEM, containing mostly virus-cluster conjugates (I, Fig. S10 & S11), whereas a similar purification process with non-functionalized clusters showed only pure, Au free virus particles (I, Fig. S12). This further confirmed that non-functionalized clusters did not bind to E1 or CVB3 during these incubation times.

As described, the positions of the three closest cysteines measured from the thiol ends were localized in the crystal structures of E1 and CVB3. These were compared to the spatial ordering of the clusters visualized with TEM. Cluster-cluster distances correlated with the thiol-thiol distances of cysteine residues. Moreover, the binding patterns of Au102-MI clusters compared to thiol positions also correlated well. Pentagonal and trigonal rotational symmetries were identified (I, Fig. 3). These results further confirmed the successful binding of Au102-MI to E1 and CVB3 capsids.

The binding of Au102-MI clusters was also observed with other cysteines of E1 and CVB3 capsids (I, Fig 2 & 3). One explanation could be that targeting is also facilitated by the natural breathing of the capsid. As described, during the capsid breathing, internal proteins are temporarily expulsed from the capsid (Lewis *et al.* 1998; Pulli *et al.* 1998; Jiménez-Clavero *et al.* 2000; Katpally *et al.* 2009). For example, poliovirus antibodies have been shown to have access to polypeptides inside the virus capsid (Lewis *et al.* 1998; Lin *et al.* 2012). These kinds of dynamic events may also play a role in Au102-MI conjugation and open transient channels for thiol accessibility.

In addition, we observed an "on-off"-loading of gold clusters on the virus surface. Specifically, most virus capsids seemed to have either generous loading of Au102-MI clusters or no clusters at all. This could be explained by the different populations of E1 capsids. Myllynen *et al.* (2016) recently found a novel open and infectious form of E1 that is naturally produced during infection. This particle has a more open structure than the native 160S E1 particle, allowing entry of small molecules such as SYBR green II or Cs+ ions inside the capsid. However, it appears to be distinct from the altered 135S particle and empty 80S particle as it still contains its VP4 and is able to bind to α2β1 integrin. This novel, intermediate particle, together with natural dynamics, could be more accessible for the abundant loading of Au102-MI clusters observed on the virus surface. Moreover, it addresses why two different populations of Au102-MI conjugated viruses were seen. It is likely that more direct and specific labeling would have required accessible thiol groups closer to the surface. Blum *et al.* (2004) described the successful covalent Au labeling of cowpea mosaic virus mutants in which cysteines were introduced at different positions of the capsid.

Finally, we showed that the infectivity of virus-Au102-MI conjugates was not compromised (I, Fig.4). For its future use as a live virus probe in cells or tissues, it is important that Au102-MI retains its infectivity and receptor binding properties.

In conclusion, we demonstrated the robust, site-specific labeling of EV-Bs. Conventional virus markers are bound to viruses via weaker interactions and are primarily dependent on the specificity of antibodies. Au102-MI markers could help in understanding biochemical and structural factors leading to the uncoating of the virus in endosomes and allow for the better visualization of viruses in cells and tissues in live assays.

5.1.1 Potential future applications of Au102-MI

Au102-MI probes require some alterations to be applied in future applications. First of all, to improve the control of targeting specific cysteine groups at the EV surface, the linker arms of Au102-MI clusters could be modified. Shorter lengths of linker arms on the Au102 surface could focus the cysteine-Au conjugations closer to the virus surface. This could also limit the number of Au clusters bound to virus capsids. Moreover, the number of linker arms on Au102 clusters could be controlled. Molecular dynamic simulations, where the physiological movements of Au102-MI clusters atoms and molecules have been studied, have shown that the more linkers Au102 has, the greater chance it has for successful binding (Pohjalainen et al. 2015, unpublished). Furthermore, the atomically known structure of an Au102 cluster could allow for the further modification of these markers for novel developments, e.g. the dual conjugation of Au and fluorescent probe on the virus surface. Recently, a covalently linked multimer of Au102 and Au144 was successfully formed (Lahtinen *et al.* 2016). This opens new possibilities to conjugate Au clusters with fluorescent probes as well.

Virus-Au102 conjugates could be detected via spectroscopy. Spectroscopic detection of viruses via Au cluster conjugation has been described already earlier with brome mosaic virus (Dragnea *et al.* 2003). Dragnea et al. showed that colloidal Au particles were partially replacing the RNA of the virus, thus the Au was located inside the virus capsid. This approach could be applied to Au102-MI conjugation, although in this case Au would be located outside the capsid.

The unique electronic, optical, and photothermal properties of Au nanoclusters would also allow virus detection and possible capsid manipulation to initiate uncoating. This could be developed further to study uncoating where different properties, e.g. different chemical environments inside the vesicular structures of cells, could be tested in the presence of virus-Au-conjugates and the movement of Au-clusters could be followed. Furthermore, the virus structure could be modified using the ability of the clusters to absorb near-infrared radiation and generate “local heat” upon de-excitation. The heat treatment could also stimulate the uncoating of the virus, thus enabling more detailed study of this process. There is only a limited amount of specific information available about EV uncoating. Au clusters could be also helpful in structural studies with cryo-EM where Au clusters would enhance the signal making it easier to detect.

The photothermal properties of Au clusters have been also suggested for potential cancer therapy applications. Everts *et al.* (2006) demonstrated the successful, covalent, conjugation of Au nanoparticles to Adenovirus vectors in the hopes of creating a new tool for tumor disruption. Similarly, EV-Au102 conjugates could be used as similar kind of disruption tools in the gut.

Probably the most usable application of Au102-MI clusters would be their use as biomolecule markers in microscopic methods. As described more detail in the literature review, there is a constant need for better tracking methods for viruses. The covalent binding of Au102-MI to the virus capsid could be strong enough to withstand the harsh cellular conditions as well as difficult conditions in the gut. This would allow the more specific tracing of intracellular pathways of the virus *in vivo* and *in vitro*. Any new information concerning virus infection routes is beneficial to development of antivirals.

5.2 Probes targeted to hydrophobic pockets

5.2.1 The development and synthesis of the probe

Recently developed drug molecules such as pleconaril, ribavirin, and their other derivatives are targeted to the hydrophobic pocket of the enterovirus virus capsid (Pevear *et al.* 1999; Thibaut *et al.* 2012; Macleod *et al.* 2013; De Colibus *et al.* 2014). However, if these molecules do not disturb the functionality or infectivity of the virus, they can also act as potential hydrophobic pocket targeted markers. Therefore, a WIN (compound produced by Sterling and Winthrop, Inc.) derivative, pleconaril, was chosen as the backbone of the probe design (II). The probe was further synthesized and conjugated to either an Au102 or KU orange 2 fluorescent marker (II, Scheme 2). The synthesized probes were: derivative (1), probe (2), gold probe (3), and fluorescent probe (4).

Previously, it has been shown that WIN compounds bind the hydrophobic pocket of the VP1 protein by replacing the naturally occurring pocket factor (Giranda *et al.* 1995; Reisdorph *et al.* 2003; Zhang *et al.* 2004; Thibaut *et al.* 2012). Originally, pleconaril had been planned for use with rhinoviruses, but it has also been shown to work with other EVs, such as CVB1, CVB5, and CVA9 (Pevear *et al.* 1999). Since then, several modifications of pleconaril structure have been made with the hope of generating new antiviral molecules (Schmidtke *et al.* 2009).

We modified the pleconaril structure to make it more suitable for the E1 hydrophobic pocket. The fluorine from the phenyl-oxadiazole ring system was removed and the carboxylic group was incorporated into the isoxazole ring. The amine group at the isoxazole ring provided an anchoring function for the probe at the opening end of the hydrophobic pocket. Moreover, the modified derivative was needed to provide a link to the bound gold cluster or fluorescent probes in addition to an anchoring group that would hold the probe at the opening of the hydrophobic pocket. Synthesis and molecular structures are seen

at II, Scheme 2 and at Fig. 7. The infectivity assays (II, Fig. 1) and thermal stability assay later discussed suggested that the binding moiety of our derivatives was changed only slightly as the infectivity properties seemed to be more or less similar to original pleconaril.

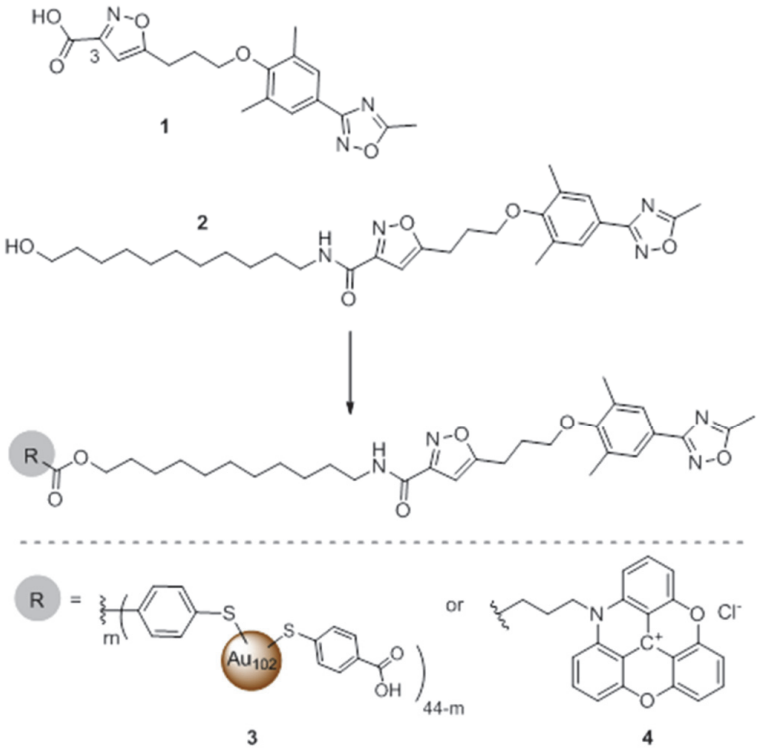

FIGURE 7 Molecular structures of probe (2), gold cluster probe (3) and fluorescent probe (4). The scheme is modified from Martikainen et al. (2014).

5.2.2 Successful binding to the hydrophobic pocket

We studied the binding of the probe into the hydrophobic pocket of E1 using saturation transfer difference (STD) NMR. The technique has been successfully used to study binding activities of compounds towards proteins (Mayer and Meyer 1999). With this method, when the virus is saturated, the magnetization is transferred from the virus particle to the bound ligand. Due to the weak interactions between the ligand and the virus, the transferred magnetization is detected when the ligand is released from the virus back into the solution (Bhunia *et al.* 2012). STD NMR is a fairly rapid technique and requires a

relatively small amount of the virus. At least a 100-fold molar excess of the ligand over the receptor should be used (Bhunia *et al.* 2012).

To perform the measurement in solution, derivative (1) was used instead of probe (2) due to a solubility issue. In a study by Benie *et al.* (2003), a 6000-fold molar excess was used to study ligand binding to the hydrophobic pockets of HRV. We chose to use a 5000-fold excess of derivative 1 over the hydrophobic binding sites and recorded the spectra with 1–3.5 s saturation times. The STD difference spectra and transfer NOESY experiment showed distinct signals to the derivative (1), indicating binding to E1 (II, Fig. 3A & S4).

As described, due to solubility issues, it was not possible to execute NMR measurements for all of the derivatives. We cannot exclude the possibility that there may have been some differences in the binding affinities. However, similar behavior in cellular experiments suggests that these differences remain trivial. Overall, we showed that derivative (1) bound successfully to the hydrophobic pocket. Furthermore, since the STD-NMR measures the magnetization of released ligands, our NMR results also suggested that the ligand binding and pocket factor release are dynamic events. The dynamic nature of the pocket factor and derivative (1) binding could be explained by capsid breathing.

The CVB3 Nancy strain was used as a negative control throughout the study. It is known that the structure of the CVB3 hydrophobic pocket is distinct from other CVB3 strains more susceptible to pleconaril due to changes in the amino acid sequence: Ile1092 has been replaced to Leu or Ile1092 to Met. This results in pleconaril not binding to the hydrophobic pocket of CVB3 Nancy (Groarke and Pevear 1999; Pevear *et al.* 1999; Schmidtke *et al.* 2009). We observed similar behaviors with our pleconaril derivatives and gold cluster probe (4). They did not change the virus infectivity or thermal stability (II, Fig. 1 & 5). Furthermore, the gold cluster probe (3) conjugation to the virus was not successful and the space filling model of the CVB3 hydrophobic pocket revealed that the probe did not have clear access to the pocket (II, Fig. 5).

5.2.3 Probes cause a delay in infection

Since the fundamental structure of the probe was based on an antiviral, we wanted to evaluate effects in the infectivity of the viruses. First, the cytotoxicity of the probe (2) and derivative (1) was studied with pleconaril as a comparison. A 3-(4,5-dimethylthiazol-2-yl)-2,5-diphenyl- tetrazolium bromide (MTT) assay did not show any significant cell death (II, Fig. S5D). The effects on infectivity were studied using several different, well-characterized approaches. The TCID50 assay quantified the 50% tissue culture infective dose and revealed that the last dilution, considered the end-point dilution, still contained infective particles. This assay did not show any significant reduction in the virus infectivity with or without the compounds (II, Fig 1A & S5). The TCID50 values were typically around 10^{10} to 10^{11} TCID50/ml.

In addition to an end-point dilution assay, we wanted to understand the effects of the compounds on a shorter time scale. A 24 h cytopathic effect (CPE)

inhibition assay was used. Schmidtke *et al.* (2001) established this method to study the antiviral effect of various compounds using a crystal violet uptake of the cells, then quantifying the lysed cells with an optical plate reader. The final calculations yielded a cell viability percentage. Furthermore, the CPE titration assay was used to quantify the half maximal inhibitory concentrations (IC50 (μM)) for each compound (II, Fig S5A). This assay showed that after 24 h the derivative (1) and probe (2) inhibited E1 and CVA9 infection by 65–70%, whereas for CVB3 inhibition was only 18%. Cell viability was also measured using a commercial kit based on ATP production of the cell (Cell Titer Glo assay). The results were similar to those observed with the CPE assay. As discussed, it has been shown that pleconaril does not fit the hydrophobic pocket of the CVB3 Nancy strain (Pevear *et al.* 1999). Also, the IC50 values were remarkably higher for CVB3 than for E1 and CVA9.

The total number of infective particles was not changed in the preparations, whereas the CPE and the CTG assay results showed around 70% inhibition of the infection at 24 h p.i. with E1 and CVA9 when bound to the probe (2). These results suggest that there is a delay in infection rather than total inhibition. We studied the delay in greater detail with confocal microscope immunofluorescence to evaluate the kinetics of the inhibition (II, Fig. 1C). The infected cells were recognized by a widespread, newly synthetized virus capsid label in the cytoplasm. The number of infected cells was quantified at different time points and the analysis revealed that the infection was delayed rather than completely halted.

Typically, E1 and CVA9 are seen in the cytoplasmic endosomes at 2 to 3 h p.i. After replication and protein production have started, virus capsid proteins are usually widely observed in the cell cytoplasm (Marjomäki *et al.* 2002; Karjalainen *et al.* 2011; Huttunen *et al.* 2014). Further observations with confocal microscopy revealed that there was no apparent difference in the amount of viruses internalized into the cell with or without the probe, ensuring that receptor entry was not disturbed. In conclusion, the results indicated that viruses treated with the probe remained longer in the endosomes and produced new viral proteins slower than non-treated virus. Since the infection was not totally blocked, it indeed open possibilities to use these probes as markers during the infection cycle. Pleconaril had the most effect on E1 and CVA9, as expected. In addition, all compounds had the least effect on CVB3.

5.2.4 Probe increases the thermal stability of the virus

The slowing of virus infectivity suggested that there may be a measurable stabilizing effect on the virus. A stabilizing effect of hydrophobic pocket targeted antivirals has been shown with poliovirus (Tsang *et al.* 2000). Thus, we studied this with a particle stability thermal release assay where the capsid opening and RNA release can be observed via RNA binding dye SYBR Green II upon virion heating (Walter *et al.* 2012). This method has been used to describe the stabilizing effects of hydrophobic pocket binding drug molecules in other

recent studies with EV-71 and EV-D68 (Plevka *et al.* 2013; De Colibus *et al.* 2014; Liu *et al.* 2015).

In the particle stability thermal release assay, the uncoating of the virus is stimulated by gradually heating the sample in solution. Next, RNA binding SYBR Green fluorescence is detected over time (II, Fig. 2A). The melting temperature (T_m) is determined, which, for enteroviruses, is typically around 50°C. In our measurements without any probes, the values were 50.5°C, 50°C and 44.5°C for E1, CVA9, and CVB3, respectively (II, Fig. 2B). The thermal lability of CVB3 is in agreement with early observations by Groarke and Pevear (1999), where pleconaril resistant CVB3 strains had dramatically decreased thermal stabilities. Probe (2) showed only a minor effect on capsid stability whereas derivative (1) increased the melting temperature by 2.5°C and 4°C for E1 and CVA9, respectively. This indeed demonstrates that these compounds affect capsid stability which may cause a delay in infection.

There is a consensus in the field that pocket factors have a role in capsid stability (Ismail-Cassim *et al.* 1990; Oliveira *et al.* 1993; Smyth *et al.* 2003). For example, the foot and mouth disease virus (FMDV) has been shown to be highly thermolabile (Rincón *et al.* 2014). The lack of thermal stability is due to the lack of hydrophobic pocket altogether in FMDV capsids. This contributes to arguments considering the importance of the pocket factor in EVs. Moreover, the dynamic events of the capsid leading to the uncoating of the virus can be stabilized with capsid binding molecules (Reisdorph *et al.* 2003; Roy and Post 2012).

5.2.5 Gold cluster and fluorescent probes allow virus detection and the fluorescent probe is released after capsid opening

The probe (1) was conjugated either to 2 nm Au102 or to a fluorescent dye (Fig. 6) which were then bound to virus capsids (II, Scheme 2). The binding of the gold cluster probe (3) into E1 and CVA9 hydrophobic pockets was monitored with TEM (II, Fig. 3B & 3C, S7A & B). The negatively stained samples revealed successful binding on virus surfaces. Gold cluster probes were observed in pentamer-like-symmetries, similar to those modelled to be with the locations of the hydrophobic pocket (II, Fig. 3D). Furthermore, the TEM visualization suggested that only some of the 60 hydrophobic pockets were occupied by the gold cluster probe. There is no present specific information about the occupancy of these pockets. Because the viruses appeared to remain intact after gold probe binding, it is possible that some dynamic exchange between our probe and the pocket factor may have occurred. It is also possible that the probe has better affinity to the pocket than the lipid moiety inside. The virus-gold cluster conjugation was also strong enough to withstand a short Sephacryl-300 column purification (size exclusion to exclude excess, unbound gold clusters).

To follow viruses in cells with confocal microscopy, the fluorescent probe (4) was used. Fluorescent probe-virus conjugation was prepared like the gold probe-virus except that unbound excess dye was dialyzed away. The virus-fluorescent probe conjugates were allowed to internalize into A549 cells. Cells

were fixed and virus capsids were labeled with a specific antibody as we wanted to confirm that the virus and fluorescent probe were in the same cellular structures (II, Fig. 4 & S8). We were able to verify that the virus and fluorescent probe were indeed in the same vesicular structures. In addition, the appropriate concentration of dye did not internalize in cells as a bulk fluid-phase marker but rather stained cellular membranes with low efficiency, likely due to its hydrophobic properties. As observed with the other probes, the fluorescent probe (4) also slowed the infection and virus-fluorescent probe conjugates accumulated in the vesicular structures for longer periods of time than the native virus, causing a slight slow-down in infection (II, Fig. 4B).

Interestingly, the fluorescent probe (4) dissociated from the capsid label during the infections, most likely because of the capsid opening. The fluorescent dye was then visible in the cytoplasm of the cell due to leakage from the endosomes from 6 h p.i. onwards (II, Fig. 4C). The released dye was observed close to the endosomes at 6 to 8 h p.i., whereas after longer periods (12 to 24 h p.i.), the fluorescent signal had already leaked out (II, Fig. S10). As shown with the derivative (1), the fluorescent probe (4) most likely stabilizes the E1 capsid, causing a delay in infection. Additionally, live imaging of fluorescent probe-virus conjugates was performed. We observed high loading of the fluorescent probe in the endosomes which decreased over time, suggesting that the release of the probe and separation of the virus occurred (II, Fig. S9).

Collectively, these results indicate that we were able to develop novel probes targeting the hydrophobic pocket of E1 and CVA9 that can be successfully used to label these viruses. Differing from conventional virus capsid labels with antibodies or direct fluorescent label (Brandenburg *et al.* 2007), the dynamic nature of the probes may provide new information about the function of the hydrophobic pocket and its importance in the virus life cycle.

5.2.6 Potential applications to study uncoating and infection

As mentioned above, the hydrophobic pocket targeted probes could give valuable information about the function of the pockets. The most throughout study of the hydrophobic pockets and the pocket factors is made by Smyth et al. (2003) where they showed by mass spectroscopy that the palmitic acid was the most used fatty acid in bovine enterovirus pocket. However, there is no exact knowledge how well the hydrophobic pockets are occupied by the pocket factor, and whether all of the pocket factors or only some of them are expulsed during uncoating. In our study we showed that the gold cluster probes (3) were bound only to some of the 60 hydrophobic pockets. Whether these pockets were already empty or there was an exchange between the pocket factor and the probe (3) remains to be studied.

Combinatorial use of the hydrophobic pocket fluorescent probe (4) with capsid or genome binding dye will help to monitor the release of the pocket factor upon uncoating *in vitro* and in endosomes *in vivo*. In addition, the gold

clusters may be used as platforms that combine also other probes e.g. those measuring physiologically relevant ions in the endosomes. These multifunctional probes may then give the status of the virus uncoating, and simultaneously monitor ionic conditions inside endosomes. With these different combinations and multifunctional probes, we could investigate the different cellular environments and their effects on the uncoating event while visualizing the expulsion of the fluorescent probe (4) from the pockets. As discussed already with the Au102-MI markers, also here the unique properties of Au could be utilized. Here we could expose the virus capsid to local heat even more specifically to the cite of the uncoating and investigate the procedure even further.

Properties of the fluorescent and the gold cluster probes could be exploited in correlated light and electron microscopy (Sjollema *et al.* 2012). The site-specific and direct binding of the probes would overcome the background noise problem that the conventional antibody labelling has as a defect. With the correlated light and electron microscopy the entry of the EV-B viruses could be investigated in more detail. The probes could be modified as one single probe having both the fluorescent and the gold cluster in the same end of the probe or they could be used as a mixture by binding both fluorescent probes (4) and gold cluster probes (3) to the target virus.

5.3 CVB1 shows strain specific differences in infecting non-polarized cells

We studied the infectious entry routes of the CVB1-ATCC strain and two different clinical isolates, CVB1-CDC7 and CVB1-CDC11. We showed that there are strain specific differences in how CVB1 infects non-polarized cells (III). Already, CVB1 has revealed strain specific differences in the initiated immunogenicity in peripheral blood mononuclear cells as well as in isolated human pancreatic islets (Anagandula *et al.* 2014; Hämäläinen *et al.* 2014). We wanted to further investigate CVB1 strains used in the earlier studies.

5.3.1 CVB1 infection kinetics

As described, CVB1-CDC7 and CVB1-CDC11 differ in their production of cytokine and interferon responses as well as in growth kinetics and in intensity of the cytopathic effect (Anagandula *et al.* 2014; Hämäläinen *et al.* 2014). Furthermore, Hämäläinen *et al.* (2014) suggested that even though CVB1-CDC7 yields new viral progeny faster in HeLa MZ cells, CVB1-CDC11 might replicate more efficiently in plasmacytoid dendritic cells. Thus, we investigated the infection kinetics of CVB1-CDC7, CVB1-CDC11, and CVB-ATCC in non-polarized A549 cells.

First, the uncoating time table was studied with a neutral red (NR) assay. The assay revealed that CVB1-ATCC uncoating takes place from 45 min to 1 h

p.i. and continues until 4 h p.i. (III, Fig. 1D, i). Interestingly, CVB1-CDC11 began uncoating at 15 min p.i. (III, Fig. 1D, iii), while CVB1-CDC7 also uncoated early but with much lower efficiency (III, Fig. 1D, ii). The timing of CVB1-ATCC uncoating is rather similar to what has been shown with E1 and CVA9 (Pietiäinen *et al.* 2004; Siljamäki *et al.* 2013; Huttunen *et al.* 2014). Strikingly, CVB1-CDC11 resembles EVs that uncoat early, e.g. the poliovirus, which has been shown to uncoat at 10 min p.i., however not directly from the plasma membrane (Brandenburg *et al.* 2007; Coyne *et al.* 2007a; Bergelson 2008). Nevertheless, the localization of the uncoating must be carefully considered.

In addition to uncoating, the kinetics of active replication of CVB-ATCC strain was studied by immunofluorescence (III, Fig. 1C). The intensity of dsRNA antibody labeling was quantified at different time points of the infection (III, Fig. 1B). Here, CVB1-ATCC showed some dsRNA structures as soon as 3 h p.i. and increasing more clearly at 4 h p.i. (III, Fig. 1B). Overall, CVB1-ATCC appeared to follow similar kinetics to its close relatives E1 and CVA9 shown earlier (Marjomäki *et al.* 2002; Pietiäinen *et al.* 2004; Siljamäki *et al.* 2013; Huttunen *et al.* 2014). Similar studies of infection kinetics are ongoing with the two clinical isolates of CVB1.

5.3.2 CVB1 strains enter via macropinocytosis

First we studied several cellular factors involved in various entry pathways. Well-known pharmacological inhibitors were used to downregulate these factors (Table 3). It has been previously shown for EV-B viruses E1 and CVA9 that they internalize via macropinocytosis (Marjomäki *et al.* 2015).

The effect of chemical inhibitors on viral infection was studied by immunofluorescence labeling of capsid proteins. Ethyl-isopropyl amiloride (EIPA), NSC23766 and a bisindolylmaleimide (BIM), inhibitors of Na^+/H^+ exchanger, Rac1, and PKC, caused a statistically significant decrease in CVB1-ATCC, CVB1-CDC7, and CVB1-CDC11 infection, indicating use of macropinocytic entry by these viruses. Nocodazole had a mild inhibitory effect on CVB1-ATCC and CVB1-CDC7 but not on CVB1-CDC11, suggesting that microtubules may slightly promote the efficiency of replication of some isolates. Wortmannin and Dyngo-4a had a mild effect on CVB1-ATCC but no effect on the clinical isolates, suggesting that a clathrin-mediated pathway is not used. Pak1 inhibition by IPA-3 showed no significant decrease in any strains. This has also been observed with CVA9 (Huttunen *et al.* 2014). Bafilomycin A1 had no significant effect on any of the CVB1 strains (III, Fig. 2A).

TABLE 3 Pharmagological inhibitors used to study coxsackievirus B1 (CVB1) entry in to non-polarized A549 cells. All three strains of CVB1 were included (CVB1-ATCC, CVB1-CDC7 and ATCC-CDC11). The dependence of the target molecule is stated with a plus sign (+) and independence with a minus sign (-). The minor effect is stated a plus/minus sign (+/-). Proteinkinase C (PKC), phosphoinositide-3-kinase (PI3K), bisindolylmaleimide (BIM), ethyl-isopropyl amiloride (EIPA).

Target	Dependence			Inhibitor
	ATCC	CDC7	CDC11	
PKC	+	+	+	BIM
Dynamin	-	-	-	Dyngo-4a
Rac1	+	+	+	NSC23766
Pak1	-	+/-	-	IPA-3
Na^+/H^+ exchanger	+	+	+	EIPA
PI3K	+/-	-	-	Wortmannin
Microtubules	+/-	+/-	-	Nocodazole
Acidification	-	-	-	Bafilomycin A1

PLCs are known to be important factors in E1, CVA9, and CVB3 early infection (Upla *et al.* 2004; Karjalainen *et al.* 2008; Bozym *et al.* 2010; Krieger *et al.* 2013; Huttunen *et al.* 2014). In turn, PLCs activate PKCs at the plasma membrane. It has been previously shown that there is an increase in PKCα levels due to receptor clustering of E1 infections. In addition, specific inhibitions of PKCα prevent virus internalization (Upla *et al.* 2004; Karjalainen *et al.* 2008). Coyne *et al.* (2007) showed that PKC inhibition blocks CVB3 infection in the tight junctions of polarized cells, thus blocking the early macropinocytosis step of the entry. However, Delorme-Axford *et al.* (2013) suggested that the PKC inhibitor effect also occurs post entry. Here, we observed a significant decrease in infection due to PKC inhibition (III, Fig. 2A). These results, together with previous literature, suggest that all of the CVB1 strains need to be internalized for successful infection.

Other important factors for macropinocytosis are Rac1 and Na^+/H^+ exchangers. One of the important roles of Rac1 is the remodeling of actin (Bosco *et al.* 2009). The Na^+/H^+ exchanger, in turn, regulates the pH equilibrium inside cellular structures. The inhibitor of the Na^+/H^+ exchanger, EIPA, is also known to have mechanisms e.g. disturbing the Rac1 function and inhibiting virus replication (Gazina *et al.* 2005; Harrison *et al.* 2008; Koivusalo *et al.* 2010). Previously, we demonstrated that both of these factors are involved in E1 and CVA9 entry. The inhibition of Rac1 and Na^+/H^+ exchangers halts viral entry into cytoplasmic vesicles (Karjalainen *et al.* 2008; Heikkilä *et al.* 2009; Krieger *et al.* 2013; Huttunen *et al.* 2014). These factors are also known to be important regulators of CVB3 infection (Coyne and Bergelson 2006; Delorme-Axford *et al.* 2013) However, Rac1 inhibition stopped CVB3 infection in the tight junctions of

Caco-2 cells (Coyne and Bergelson 2006). In conclusion, all EV-Bs show great similarity in their entry, although some small differences are expected and may also be due to different cell lines used for the study.

In addition to the factors mentioned above, PI3K activation has often been associated with a clathrin-independent pathway (Basquin *et al.* 2013). But, as it has been previously shown with E1 and CVA9, here, only a mild inhibitory effect on CVB1-ATCC, and no effect on CVB1-CDC7 and CVB1-CDC11, was observed. Interestingly, wortmannin treatment caused a statistically significant increase in CVB1-CDC7 and CVB1-CDC11 infection. In our previous studies, we observed a similar increase with CVA9 (Huttunen *et al.* 2014). These results may suggest that the PI3K pathway plays a down-regulating role in virus replication. A similar observation was made for a dsDNA virus, gamma 2 herpesvirus (Peng *et al.* 2010). It is also known through a siRNA screen that activation of one group of cellular regulators on an endocytic route can exert an opposing, down-regulative effect on other endocytic routes (Pelkmans *et al.* 2001).

In conclusion, by inhibiting these well-known factors of endocytosis, our results strongly indicate that all three CVB1 strains internalize into cells via macropinocytosis. As described, CVB1 strains show remarkable similarities to other extensively studied EV-B group viruses, E1, CVA9 and CVB3.

5.3.3 CVB1s do not enter the acidifying canonical endocytic pathway

As pharmagological inhibitors suggested macropinocytic entry for CVB1s and because it has been extensively studied with E1 and CVA9 already (Upla *et al.* 2004; Karjalainen *et al.* 2008, 2011; Huttunen *et al.* 2014), we wanted to further study whether these viruses stay outside of the acidifying endosomal pathway. Thus, we followed the infection of CVB1-ATCC, CVB1-CDC7, and CVB1-CDC11 by immunofluorescence at different time points (III, Fig. 3). We observed only background values for colocalization with the early endosome marker (EEA1) or with the late endosomal marker (LAMP1). Additionally, colocalization with the known marker of the clathrin-dependent pathway, transferrin, was quantified and showed no significant colocalization with CVB1-CDC7 nor CVB1-CDC11. Colocalization with CVB1-ATCC is still to be studied. These results strongly suggest that CVB1 does not use the canonical endocytic pathway.

We then investigated whether pH played a role in viral infection or uncoating. Vacuolar ATPase is needed for the formation of endosomal carrier vesicles. The vacuolar ATPase generates the acidic luminal environment of endosomes and lysosomes (Claque *et al.* 1994). In earlier studies, we demonstrated with in -situ endosomal pH measurements that Bafilomycin A1 increases the endosomal pH (Rintanen *et al.* 2012). Here, we showed that inhibition of the vacuolar ATPase pump did not affect the infectivity of any of the strains (III, Fig. 2A). These results indicate that endosomal acidification is not important for CVB1 infection. Acidity independence is already known with other EVs (Gromeier and Wetz 1990; Perez and Carrasco 1993; Brandenburg *et*

al. 2007; Patel *et al.* 2009). Furthermore, independence of acidity strongly suggests that CVB1 entry is not associated with a clathrin-dependent pathway.

5.3.4 Biogenesis of multivesicular bodies is needed for effective infection

Next, we studied whether CVB1 strains require MVBs for successful infection. Generally, MVBs are needed in cargo transport destined to degradation. However, earlier studies have shown that E1 and CVA9 enter and are highly dependent on novel, non-acidic MVBs (Karjalainen *et al.* 2011; Huttunen *et al.* 2014). Thus, we wanted to explore the importance of ESCRT-driven MVBs with CVB1. ESCRT machinery is needed for the formation of intraluminal vesicles (ILVs). The machinery consists of four ESCRT complexes: ESCRT-0, -I, -II and -III (Gruenberg and Stenmark 2004). It is possible to disturb the ESCRT function by overexpressing or downregulating two important proteins involved in ESCRT machinery, the hepatocyte growth factor regulated tyrosine kinase substrate (Hrs) and VPS4, respectively.

We used the dominant negative mutant to downregulate VPS4 functioning (DN-VPS4). VPS4 is needed for the release of the ESCRT-III component from the endosomal-limiting membrane and further promotes the formation of ILVs (Raiborg *et al.* 2008; Henne *et al.* 2011). Thus, we transfected HeLa MZ cells with VPS4-E235Q-GFP plasmid and studied the effect on virus infection by immunofluorescence (III, Fig. 4). As expected, VPS4 had a strong, statistically significant effect on CVB1-ATCC and CVB1-CDC11 (III, Fig. 4A, i, iii). However, CVB1-CDC7 infection was not significantly decreased (III, Fig. 4A ii).

In addition to VPS4, we studied the significance of Hrs. Hrs is a subunit of ESCRT-0 which binds to the ubiquitinated receptor molecule and recruits other ESCRT components on the endosomal limiting membrane. We overexpressed Hrs by transfecting HeLa MZ cells with wt-Hrs. CVB1 was detected by immunofluorescence (III, Fig. 4A). Hrs overexpression showed a statistically significant decrease in CVB1-ATCC and CVB1-CDC11 infection (III, Fig. 4A, i, iii), whereas CVB1-CDC7 was only mildly affected (Fig. 4A, ii). The localization of CVB1-ATCC capsid labels was studied in more detail during ESCRT perturbation and showed that the virus was stuck in vesicular-like structures (III, Fig. 4B).

The results indicate that CVB1-ATCC and CVB1-CDC11 seem to follow similar infection pathways as other EV-B viruses. Studied extensively with E1 and CVA9, CVB1-ATCC and CVB1-CDC11 also showed dependence on the biogenesis of ESCRT driven MVBs. Interestingly, CVB1-CDC7 infection was not affected by disturbing the ESCRT function, suggesting that it is not efficiently targeted to MVBs. However, this remains to be shown by immunofluorescence or TEM. Furthermore, these results suggest that CVB1-CDC7 cannot uncoat and infect as efficiently as CVB1-ATCC and CVB1-CDC11, perhaps because the association to MVBs is lacking. In other words, ESCRT driven MVBs may be necessary for efficient EV-B infection.

6 CONCLUDING REMARKS

The main conclusions of this thesis are:

I A successful, robust, site-specific labeling technique of E1 and CVB3 capsid was demonstrated. Atomically precise Au102p(pMBA)$_{44}$ nanoclusters were functionalized with specifically designed linker molecule. Cysteines on E1 and CVB3 capsids were labeled with direct, covalent conjugation of functionalized Au nanoclusters. Moreover, Au conjugation did not compromise the infectivity of the virus.

II A novel probe targeted to E1 and CVA9 hydrophobic pockets was developed. The probe was bound to a fluorescent molecule and a Au102(pMBA)$_{44}$ nanocluster. Successful conjugation was analyzed by STD-NMR which also revealed dynamic binding properties of the probe. The Au-probe virus conjugations were visualized by TEM. The fluorescent probes allowed direct virus tracking inside cells via confocal microscopy. The fluorescent probe was released from the virus capsid, likely due to the uncoating of the virus.

III The entry of the CVB1 strains studied is dependent on macropinocytosis regulators PKC as well as Rac1 and Na^+/H^+ exchangers. These viruses are also absent from the acidifying endosomes and do not require low pH for infection. The kinetics of infection for the field isolates showed early uncoating for CVB1-CDC7 which resulted in lower efficiency of infection, while CVB1-CDC11 showed higher dependency of ESCRT driven MVBs and more efficient uncoating. The results highlight the importance of MVBs in promoting efficient infection for CVB1 viruses, as previously observed with other EVBs.

Acknowledgements

This work was carried out during 2013-2016 at the University of Jyväskylä, at the Department of Biological and Environmental Sciences and NanoScience Center, in the Division of Cell and Molecular Biology. The thesis was supported by Tekes-FiDiPro project for development of novel vaccine strategies. I would like to acknowledge all the people involved in my PhD studies.

First of all, I am extremely grateful to my supervisor Docent Varpu Marjomäki. Thank you for all the kindness, support and guidance during these years. Thank you for all the amazing possibilities to do science both in Finland and abroad. I am grateful also for all the unforgettable moments outside of science. I feel privileged to have been part of the Marjomäki lab.

I would also like to acknowledge the reviewers of this thesis, Professor Renate Fuchs and Docent Tero Ahola. In addition, I am extremely grateful for Professor Dieter Blaas kindly accepting the invitation to serve as an opponent in the public examination of my thesis. I would like to extent my gratitude the members of my thesis follow-up group: Professor Hannu Häkkinen and Professor Heikki Hyöty. In addition, I would like to thank PhD Francois Maree for all the kindness and support during my visit in Pretoria, South Africa, as well as for all the valuable comments during my PhD studies. I also want to acknowledge Professor Jacques Theron for the comments during my PhD studies.

The work would have not been possible without the right kind of people. Thus, I would like to acknowledge the brilliant collaboration inside the NanoScience center. Thank you Hannu, Tanja, Kirsi, Sami, Mika & Jaakko. Additionally, I would like to acknowledge the collaboration with University of Tampere, especially Babak, Heikki and Anni.

Next, I would like to thank all my wonderful fellow scientists. First, the previous people in Marjomäki lab: Moona, Lassi, Maria, Marie, Anni, and Artur. It was a pleasure to work with you and share all the funny moments such as Seili, Milan, paintball, dancing, Switzerland, Copenhagen, Seili again, parties…and what not. Then the current members: Paula, Mira and Visa. I have no words to express how grateful I am for you – you are the best colleagues one could have hoped for. Thank you for endless support and for all the laughs. There were times that your support carried me through the days. I would also like to acknowledge all the trainees, master's students, and other group members during the years.

Then not to forget all the other colleagues at the corridors: Alli, Leena, Laura, Elina D., Elina M., Kai and Lina. Thank you! I would also like to acknowledge the amazing technicians Arja Mansikkaviita, Alli Liukkonen, and Petri Papponen, for their invaluable help and advices during the years.

Next, I would like to express my gratitude to my family. They have always provided me with the greatest support and love that one can ask for. Especially, thank you Mom. I would also like to thank Jyri and Nisa for adopting me for the last year of my studies. Then to my Muurame-family, Riitta

and Pertti, thank you for all the love and care during the years. Last but not least, the Martikainen-family. I am deeply grateful for your support during the years.

Next, I would like to thank all my friends for giving me a life outside of science. Especially Aino, thank you for the endless hours of making the world a better place. We are more than friends, we are sisters. Then my other friends especially Sari, Ultsu, Monica, Sarvivuori-people and Emppis-people. Thank you!

Finally, I want to express my deepest gratitude to my husband Jaakko. Even though during the last 1.5 years we have been more apart than together (geographically), I feel like you never left my side. Thank you for your endless love and support, and for making the life little less serious. You are my rock and the love of my life. I cannot wait to start the new journey of our lives. Thank you.

YHTEENVETO (RÉSUMÉ IN FINNISH)

Uudenlaisten markkereiden kehittäminen enterovirus B-ryhmän virusten kapsidin aukeamisen ja infektion tutkimiseen

Virukset ovat biologisia partikkeleita, joiden lisääntyminen on riippuvaista isäntäsolun toiminnasta. Virusten rakenne muodostuu proteiinikuoresta sekä sen sisällä olevasta perimäaineksesta, joka on joko DNA:ta tai RNA:ta. Riippuen virustyypistä, proteiinikuorta voi ympäröidä myös lipidivaippa. Proteiinikuoren muoto vaihtelee symmetrisistä monitahokkaista sauvamaisiin partikkeleihin. Kooltaan virukset ovat hyvin pieniä, 15 – 400 nanometrin suuruisia. Virukset lajitellaan niiden fylogeneettisten yhteyksien perusteella eri ryhmiin. Yhteisenä tekijänä kaikilla viruksilla on perimäaineksen kuljettaminen solun sisään, joka lopulta johtaa uusien infektiivisen viruspartikkeleiden tuottoon.

Enterovirukset ovat pienimpiä ihmisiä infektoivista viruksista. Niiden proteiinikuori on muodoltaan ikosaedri ja se sulkee sisäänsä positiivisesti varautuneen RNA-genomin. Pääosin ne aiheuttavat tavallista nuhakuumetta, sydänlihastulehdusta, aivokalvontulehdusta sekä enterorokkoa. Enterovirusinfektio on myös linkitetty yhdeksi tyypin 1 diabetesta aiheuttavaksi ympäristötekijäksi. Vaikka enterovirukset ovat yhteiskunnalle merkityksellisiä viruksia, kaupallisia rokotteita on olemassa vain muutamaa enterovirusta vastaan. Myöskään perinteiset viruksen seurantamenetelmät eivät ole tarpeeksi tehokkaita viruksen infektiivisen reitin tarkkaan seuraamiseen solussa tai kudoksessa. Nykypäivänä erilaiset seurantamenetelmät perustuvat pääosin vasta-aineleimauksiin, jotka kuvannetaan erilaisin mikroskooppisin keinoin. Vasta-aineleimauksen huonona puolena on epätarkka sitoutuminen näytteeseen sekä heikko kiinnittyminen antigeeniin. Uusia menetelmiä kehitelläänkin virusten tarkempaan ja tehokkaamman leimaamiseen ja detektoimiseen. Nykyaikaisemmat menetelmät mahdollistaisivat myös uuden informaation keräämisen virusten infektiivisiltä reiteiltä, ja näin myös uusien virusinfektiota estävien lääkkeiden kehittämisen.

Tämä väitöskirjaa koostuu kolmesta osatyöstä. Kahdessa ensimmäisessä työssä keskityttiin uudenlaisten virusta leimaavien markkereiden kehittämiseen enteroviruksia echovirus 1 (E1), coxsackievirus B3 (CVB3) sekä coxsackievirus A9 (CVA9) vastaan. Kolmannessa osatyössä tarkasteltiin prototyypi-coxsackievirus B1:n (CVB1) ja sen kahden eri kliinisen serotyypin infektiivistä reittiä soluissa.

Ensimmäisessä osatyössä kiinnitimmee E1- ja CVB3-viruksen ulkokuoren kysteiineihin kovalenttisesti kultananopartikkeleita. Työssä käytetty kultananopartikkelin kiderakenne on tarkkaan määritetty, ja sen tiedetään sisältävän 102 kulta-atomia. Kultananopartikkelin kultaydintä suojaa 44 orgaanista molekyyliä. Näihin molekyyleihin kiinnitettiin kuuden hiilen mittainen käsivarsi, joka lopulta kiinnittyi kovalenttisesti viruksen kapsidiin. Onnistunut sitoutuminen kuvannettiin elektronimikroskooppisin menetelmin.

Toisen osatyön tarkoituksena oli kohdentaa markkerin kiinnittyminen viruksen kapsidin hydrofobiseen taskuun. Tätä varten kehitettiin markkerimolekyyli, johon kiinnitettiin myös edellisessä osatyössä mainittu kultananopartikkeli tai fluoresoiva proteiini. Markkerimolekyyli oli johdannainen tunnetusta virusinfektiota estävästä molekyylistä, Pleconarilista. Koska aikaisemmassa kirjallisuudessa oli näytetty Pleconarilin estävän virusinfektiota ja stabilisoivan viruskuoren rakennetta, tutkimme tarkemmin markkereiden vaikutusta viruksen infektioon. Solukokeet näyttivät, että markkerit hidastivat hieman virusinfektiota, mutta eivät aiheuttauneet eroa lopullisessa infektoivien partikkeleiden määrässä. Lämpöstabiilisuuskokeissa nähtiin myös, että uudet markkerit hieman stabiloivat viruksen kuoren kestävyytta, mutta eivät kuitenkaan niin paljoa kuin alkuperäinen Pleconaril.

Elektronimikroskooppisen tarkastelun avulla pystyimme varmistamaan kultananopartikkeleiden kiinnittymisen. Tarkempi analyysi osoitti, että kultananopartikkelit olivat kiinnittyneet samoille kohdille kuin missä hydrofobisten taskujen suuaukot tyypillisesti sijaitsivat. Tämän lisäksi onnistuimme kuvantamaan fluoreseoivalla markkerila leimattua virusta elävissä soluissa infection aikana. Havaitsimme myös markkerin irtoamista viruksesta endosomeissa infektion aikana, mikä viittaa siihen, että voisimme seurata markkerin irtoamista viruksen avautumisen seurauksena.

Väitöskirjan viimeisessa osatyössä keskityimme tutkimaan CVB1:n soluun sisäänmenoreittiä. Tämän lisäksi tutkimme sisäänmenoon vaikuttavia solun säätelijämolekyylejä sekä solun sisäisiä rakenteita, joihin viruksen kertyvät. Tutkimuksessa käytimme CVB1:n kolmea erilaista alatyyppiä. Nämä tyypit osoittautuivat olevan hyvin erilaisia genomin vapautumisaikataulultaan. Mielenkiintoista oli myös, että virus joka vapautti genominsa kaikista heikoimmalla tehokkuudella, ei ollut riippuvainen monirakkulaendosomien muodostumisesta. Näyttää siis siltä, että enterovirukset tarvitsevat monirakkulaendosomien muodostumista tehokkaan infektion saavuttamiseksi. Yleisesti tarkastellen CVB1-virusten infektiivinen reitti vaikutti hyvin samankaltaiselta kuin mitä on osoitettu aiemmin muille enterovirus B-ryhmän viruksille E1 ja CVA9.

REFERENCES

Ackerson C.J., Powell R.D. & Hainfeld J.F. 2010. Site-Specific Biomolecule Labeling with Gold Clusters. *Methods Enzymology* 10: 54–56.

Agrez M. V., Shafren D.R., Gu X., Cox K., Sheppard D. & Barry R.D. 1997. Integrin αvβ6 Enhances Coxsackievirus B1 Lytic Infection of Human Colon Cancer Cells. *Virology* 239: 71–77.

Ahmad Z.A., Yeap S.K., Ali A.M., Ho W.Y., Alitheen N.B.M. & Hamid M. 2012. scFv Antibody: Principles and Clinical Application. *Clinical and Developmental Immunology* 2012: 1–15.

Anagandula M., Richardson S.J., Oberste M.S., Sioofy-Khojine A.-B., Hyöty H., Morgan N.G., Korsgren O. & Frisk G. 2014. Infection of human islets of langerhans with two strains of coxsackie B virus serotype 1: Assessment of virus replication, degree of cell death and induction of genes involved in the innate immunity pathway. *Journal of Medical Virology* 86: 1402–1411.

Basquin C., Malarde V., Mellor P., Anderson D.H., Meas-Yedid V., Olivo-Marin J.-C., Dautry-Varsat A. & Sauvonnet N. 2013. The signalling factor PI3K is a specific regulator of the clathrin-independent dynamin-dependent endocytosis of IL-2 receptors. *Journal of Cell Science* 126: 1099–1108.

Belov G.A., Altan-Bonnet N., Kovtunovych G., Jackson C.L., Lippincott-Schwartz J. & Ehrenfeld E. 2007. Hijacking Components of the Cellular Secretory Pathway for Replication of Poliovirus RNA. *Journal of Virology* 81: 558–567.

Benie A.J., Moser R., Bäuml E., Blaas D. & Peters T. 2003. Virus-ligand interactions: Identification and characterization of ligand binding by NMR spectroscopy. *Journal of the American Chemical Society* 125: 14–15.

Bergelson J.M. 2008. New (fluorescent) light on poliovirus entry. *Trends in Microbiology* 16: 44–47.

Bergelson J. 2010. *Receptors* Ehrenfeld E., Domingo E. & Roos R.P. (eds.). Wiley. The Picornaviruses. p. 73-86

Bergelson J.M., Cunningham J. a, Droguett G., Kurt-Jones E. a, Krithivas a, Hong J.S., Horwitz M.S., Crowell R.L. & Finberg R.W. 1997. Isolation of a common receptor for Coxsackie B viruses and adenoviruses 2 and 5. *Science (New York, N.Y.)* 275: 1320–1323.

Bergelson J.M., Shepley M.P., Chan B.M., Hemler M.E. & Finberg R.W. 1992. Identification of the integrin VLA-2 as a receptor for echovirus 1. *Science (New York, N.Y.)* 255: 1718–1720.

Best M.D. 2009. Click chemistry and bioorthogonal reactions: Unprecedented selectivity in the labeling of biological molecules. *Biochemistry* 48: 6571–6584.

Bhunia A., Bhattacharjya S. & Chatterjee S. 2012. Applications of saturation transfer difference NMR in biological systems. *Drug Discovery Today* 17: 505–513.

Blum A.S., Soto C.M., Wilson C.D., Cole J.D., Kim M., Gnade B., Chatterji A., Ochoa W.F., Lin T., Johnson J.E. & Ratna B.R. 2004. Cowpea mosaic virus as a scaffold for 3-D patterning of gold nanoparticles. *Nano Letters* 4: 867–870.

Bolten R., Egger D., Gosert R., Schaub G., Landmann L., Bienz K., Bolten R., Gosert R., Schaub G. & Landmann L. 1998. Intracellular localization of poliovirus plus- and minus-strand RNA visualized by strand-specific fluorescent In situ hybridization. *Journal of General Virology* 72: 8578–8585.

Bordería A. V, Isakov O., Moratorio G., Henningsson R., Agüera-González S., Organtini L., Gnädig N.F., Blanc H., Alcover A., Hafenstein S., Fontes M., Shomron N. & Vignuzzi M. 2015. Group Selection and Contribution of Minority Variants during Virus Adaptation Determines Virus Fitness and Phenotype Coyne C.B. (ed.). *PLOS Pathogens* 11: e1004838.

Bosco E.E., Mulloy J.C. & Zheng Y. 2009. Rac1 GTPase: A 'Rac' of all trades. *Cellular and Molecular Life Sciences* 66: 370–374.

Bozym R.A., Morosky S.A., Kim K.S., Cherry S. & Coyne C.B. 2010. Release of Intracellular Calcium Stores Facilitates Coxsackievirus Entry into Polarized Endothelial Cells Hope T.J. (ed.). *PLoS Pathogens* 6: e1001135.

Brandenburg B., Lee L.Y., Lakadamyali M., Rust M.J., Zhuang X. & Hogle J.M. 2007. Imaging poliovirus entry in live cells. *PLoS Biology* 5: 1543–1555.

Bruchez Jr. M., Moronne M., Gin P., Weiss S. & Alivisatos A.P. 1998. Semiconductor Nanocrystals as Fluorescent Biological Labels. *Science* 281: 2013–2016.

Chan W.C.W. & Nie S. 1998. Quantum Dot Bioconjugates for Ultrasensitive Nonisotopic Detection. *Science* 281: 2016–2018.

Chu Y., Oum Y.H. & Carrico I.S. 2016. Surface modification via strain-promoted click reaction facilitates targeted lentiviral transduction. *Virology* 487: 95–103.

Claque M.J., Urbe S., Aniento F. & Gruenberg J. 1994. Vacuolar ATPase Activity Is Required for Endosomal Carrier Vesicle Formation. *The Journal of Biological Chemistry* 269: 21–24.

Cohen C.J., Shieh J.T., Pickles R.J., Okegawa T., Hsieh J.T. & Bergelson J.M. 2001. The coxsackievirus and adenovirus receptor is a transmembrane component of the tight junction. *Proceedings of the National Academy of Sciences of the United States of America* 98: 15191–15196.

Colibus L. De, Wang X., Spyrou J. a B., Kelly J., Ren J., Grimes J., Puerstinger G., Stonehouse N., Walter T.S., Hu Z., Wang J., Li X., Peng W., Rowlands D.J., Fry E.E., Rao Z. & Stuart D.I. 2014. More-powerful virus inhibitors from structure-based analysis of HEV71 capsid-binding molecules. *Nature structural & molecular biology* 21: 282–288.

Coppieters K.T., Wiberg A. & Herrath M.G. von. 2012. Viral infections and molecular mimicry in type 1 diabetes. *Apmis* 120: 941–949.

Coyne C.B. & Bergelson J.M. 2006. Virus-induced Abl and Fyn kinase signals permit coxsackievirus entry through epithelial tight junctions. *Cell* 124: 119–131.

Coyne C.B., Kim K.S. & Bergelson J.M. 2007a. Poliovirus entry into human brain microvascular cells requires receptor-induced activation of SHP-2. *The EMBO journal* 26: 4016–4028.

Coyne C.B., Shen L., Turner J.R. & Bergelson J.M. 2007b. Coxsackievirus Entry across Epithelial Tight Junctions Requires Occludin and the Small GTPases Rab34 and Rab5. *Cell Host and Microbe* 2: 181–192.

Delorme-Axford E., Sadovsky Y. & Coyne C.B. 2013. Lipid raft- and SRC family kinase-dependent entry of coxsackievirus B into human placental trophoblasts. *Journal of virology* 87: 8569–8581.

Dharmawardhane S., Schürmann A., Sells M. a, Chernoff J., Schmid S.L. & Bokoch G.M. 2000. Regulation of macropinocytosis by p21-activated kinase-1. *Molecular biology of the cell* 11: 3341–3352.

Dragnea B., Chen C., Kwak E.S., Stein B. & Kao C.C. 2003. Gold nanoparticles as spectroscopic enhancers for in vitro studies on single viruses. *Journal of the American Chemical Society* 125: 6374–6375.

Elices M.J. & Hemler M.E. 1989. The human integrin VLA-2 is a collagen receptor on some cells and a collagen/laminin receptor on others. *Proceedings of the National Academy of Sciences of the United States of America* 86: 9906–9910.

Everts M., Saini V., Leddon J.L., Kok R.J., Stoff-Khalili M., Preuss M.A., Millican C.L., Perkins G., Brown J.M., Bagaria H., Nikles D.E., Johnson D.T., Zharov V.P. & Curiel D.T. 2006. Covalently Linked Au Nanoparticles to a Viral Vector: Potential for Combined Photothermal and Gene Cancer Therapy. *Nano Letters* 6: 587–591.

Filman D.J., Syed R., Chow M., Macadam A.J., Minor P.D. & Hogle J.M. 1989. Structural factors that control conformational transitions and serotype specificity in type 3 poliovirus. *The EMBO journal* 8: 1567–1579.

Frisk G. & Diderholm H. 2000. Tissue Culture of Isolated Human Pancreatic Islets Infected With Different Strains of Coxsackievirus B4: Assessment of Virus Replication and Effects on Islet Morphology and Insulin Release. *International Journal of Experimental Diabetes Research* 1: 165–175.

Fritschy J.-M. & Härtig W. 2001. Immunofluorescence. In: *Encyclopedia of Life Sciences*, John Wiley & Sons, Ltd, Chichester.

Gamble D.R., Kinsley M.L., Fitzgerald M.G., Bolton F.R.C.P.R. & Taylorjj K.W. 1969. Viral Antibodies in Diabetes Mellitus. *British Medical Journal* 3: 627–630.

Gazina E. V., Harrison D.N., Jefferies M., Tan H., Williams D., Anderson D.A. & Petrou S. 2005. Ion transport blockers inhibit human rhinovirus 2 release. *Antiviral Research* 67: 98–106.

Ghosh A., Basak S., Wunsch B.H., Kumar R. & Stellacci F. 2011. Effect of composition on the catalytic properties of mixed-ligand-coated gold nanoparticles. *Angewandte Chemie - International Edition* 50: 7900–7905.

Giranda V.L., Russo G.R., Felock P.J., Bailey T.R., Draper T., Aldous D.J., Guiles J., Dutko F.J., Diana G.D., Pevear D.C. & McMillan M. 1995. Structures of four methyltetrazole-containing antiviral compounds in human rhinovirus

serotype 14. *Acta crystallographica. Section D, Biological crystallography* 51: 496–503.

Groarke J.M. & Pevear D.C. 1999. Attenuated virulence of pleconaril-resistant coxsackievirus B3 variants. *The Journal of infectious diseases* 179: 1538–1541.

Gromeier M. & Wetz K. 1990. Kinetics of poliovirus uncoating in HeLa cells in a nonacidic environment. *Journal of Virology* 64: 3590–3597.

Gruenberg J. & Stenmark H. 2004. The biogenesis of multivesicular endosomes. *Nature reviews. Molecular cell biology* 5: 317–323.

Harrison D.N., Gazina E. V, Purcell D.F., Anderson D.A. & Petrou S. 2008. Amiloride Derivatives Inhibit Coxsackievirus B3 RNA Replication. *Journal of Virology* 82: 1465–1473.

Heikkilä O., Susi P., Stanway G. & Hyypiä T. 2009. Integrin αVβ6 is a high-affinity receptor for coxsackievirus A9. *Journal of General Virology* 90: 197–204.

Henne W.M., Buchkovich N.J. & Emr S.D. 2011. The ESCRT Pathway. *Developmental Cell* 21: 77–91.

Huttunen M., Waris M., Kajander R., Hyypiä T. & Marjomäki V. 2014. Coxsackievirus A9 Infects Cells via Nonacidic Multivesicular Bodies. *Journal of Virology* 88: 5138–5151.

Hynes R.O. 2002. Integrins: Bidirectional, allosteric signaling machines. *Cell* 110: 673–687.

Häkkinen H. 2008. Atomic and electronic structure of gold clusters: understanding flakes, cages and superatoms from simple concepts. *Chemical Society Reviews* 37: 1847.

Hämäläinen S., Nurminen N., Ahlfors H., Oikarinen S., Sioofy-Khojine A.-B., Frisk G., Oberste M.S., Lahesmaa R., Pesu M. & Hyöty H. 2014. Coxsackievirus B1 reveals strain specific differences in plasmacytoid dendritic cell mediated immunogenicity. *Journal of Medical Virology* 86: 1412–1420.

Ismail-Cassim N., Chezzi C. & Newman J.F.E. 1990. Inhibition of the uncoating of bovine enterovirus by short chain fatty acids. *Journal of General Virology* 71: 2283–2289.

Jackson A.M., Myerson J.W. & Stellacci F. 2004. Spontaneous assembly of subnanometre-ordered domains in the ligand shell of monolayer-protected nanoparticles. *Nature Materials* 3: 330–336.

Jadzinsky P.D., Calero G., Ackerson C.J., Bushnell D.A. & Kornberg R.D. 2007. Structure of a thiol monolayer-protected gold nanoparticle at 1.1 A resolution. *Science (New York, N.Y.)* 318: 430–433.

Jenson A.B., Rosenberg H.S. & Notkins A.L. 1980. Pancreatic islet-cell damage in children with fatal viral infections. *Lancet* 2: 354–358.

Jiménez-Clavero M.A., Douglas A., Lavery T., Garcia-Ranea J.A. & Ley V. 2000. Immune recognition of swine vesicular disease virus structural proteins: novel antigenic regions that are not exposed in the capsid. *Virology* 270: 76–83.

Joo K. Il, Fang Y., Liu Y., Xiao L., Gu Z., Tai A., Lee C.L., Tang Y. & Wang P. 2011. Enhanced real-time monitoring of adeno-associated virus trafficking by virus-quantum dot conjugates. *ACS Nano* 5: 3523–3535.

Kalveram B., Lihoradova O., Indran S. V, Head J.A. & Ikegami T. 2013. Using Click Chemistry to Measure the Effect of Viral Infection on Host-Cell RNA Synthesis. *Journal of Visualized Experiments*: e50809.

Karjalainen M., Kakkonen E., Upla P., Paloranta H., Kankaanpää P., Liberali P., Renkema G.H., Hyypiä T., Heino J. & Marjomäki V. 2008. A Raft-derived, Pak1-regulated Entry Participates in 2 1 Integrin-dependent Sorting to Caveosomes. *Molecular Biology of the Cell* 19: 2857–2869.

Karjalainen M., Rintanen N., Lehkonen M., Kallio K., Mäki A., Hellström K., Siljamäki V., Upla P. & Marjomäki V. 2011. Echovirus 1 infection depends on biogenesis of novel multivesicular bodies. *Cellular Microbiology* 13: 1975–1995.

Katpally U., Fu T.-M., Freed D.C., Casimiro D.R. & Smith T.J. 2009. Antibodies to the buried N terminus of rhinovirus VP4 exhibit cross-serotypic neutralization. *Journal of virology* 83: 7040–7048.

Kim H., Carney R.P., Reguera J., Ong Q.K., Liu X. & Stellacci F. 2012. Synthesis and characterization of Janus gold nanoparticles. *Advanced Materials* 24: 3857–3863.

Koivusalo M., Welch C., Hayashi H., Scott C.C., Kim M., Alexander T., Touret N., Hahn K.M. & Grinstein S. 2010. Amiloride inhibits macropinocytosis by lowering submembranous pH and preventing Rac1 and Cdc42 signaling. *Journal of Cell Biology* 188: 547–563.

Krieger S.E., Kim C., Zhang L., Marjomäki V. & Bergelson J.M. 2013. Echovirus 1 entry into polarized Caco-2 cells depends on dynamin, cholesterol, and cellular factors associated with macropinocytosis. *Journal of virology* 87: 8884–8895.

Krogvold, L., Skog, O., Sundström, G., Edwin, B., Buanes, T., Hanssen, K. F., ... & Dahl-Jørgensen K. 2015. Function of Isolated Pancreatic Islets From Patients at Onset of Type 1 Diabetes: Insulin Secretion Can Be Restored After Some Days in a Nondiabetogenic Environment In Vitro Results From the DiViD Study. *Diabetes* 64,: 2506–2.

Lahtinen T., Hulkko E., Sokołowska K., Tero T.-R., Saarnio V., Lindgren J., Pettersson M., Häkkinen H. & Lehtovaara L. 2016. Covalently linked multimers of gold nanoclusters Au 102 (p-MBA) 44 and Au ~250 (p-MBA) n. *Nanoscale*.

Laiho J.E., Oikarinen S., Oikarinen M., Larsson P.G., Stone V.M., Hober D., Oberste S., Flodström-Tullberg M., Isola J. & Hyöty H. 2015. Application of bioinformatics in probe design enables detection of enteroviruses on different taxonomic levels by advanced in situ hybridization technology. *Journal of Clinical Virology* 69: 165–171.

Laitinen O.H., Honkanen H., Pakkanen O., Oikarinen S., Hankaniemi M.M., Huhtala H., Ruokoranta T., Lecouturier V., Andre P., Harju R., Virtanen S.M., Lehtonen J., Almond J.W., Simell T., Simell O., Ilonen J., Veijola R., Knip M. & Hyöty H. 2014. Coxsackievirus B1 Is Associated With Induction

of beta-Cell Autoimmunity That Portends Type 1 Diabetes. *Diabetes* 63: 446–455.

Lentz K.N., Smith a D., Geisler S.C., Cox S., Buontempo P., Skelton a, DeMartino J., Rozhon E., Schwartz J., Girijavallabhan V., O'Connell J. & Arnold E. 1997. Structure of poliovirus type 2 Lansing complexed with antiviral agent SCH48973: comparison of the structural and biological properties of three poliovirus serotypes. *Structure (London, England : 1993)* 5: 961–978.

Levi-Kalisman Y., Jadzinsky P.D., Kalisman N., Tsunoyama H., Tsukuda T., Bushnell D.A. & Kornberg R.D. 2011. Synthesis and characterization of Au102(p-MBA)44 nanoparticles. *Journal of the American Chemical Society* 133: 2976–2982.

Lewis J.K., Bothner B., Smith T.J. & Siuzdak G. 1998. Antiviral agent blocks breathing of the common cold virus. *Proceedings of the National Academy of Sciences of the United States of America* 95: 6774–6778.

Li Q., Yafal a G., Lee Y.M., Hogle J. & Chow M. 1994. Poliovirus neutralization by antibodies to internal epitopes of VP4 and VP1 results from reversible exposure of these sequences at physiological temperature. *Journal of Virology* 68: 3965–3970.

Lin J., Lee L.Y., Roivainen M., Filman D.J., Hogle J.M. & Belnap D.M. 2012. Structure of the Fab-Labeled 'Breathing' State of Native Poliovirus. *Journal of Virology* 86: 5959–5962.

Lipman N.S., Jackson L.R., Weis-Garcia F. & Trudel L.J. 2005. Monoclonal versus polyclonal antibodies: distinguishing characteristics, applications, and information resources. *ILAR journal / National Research Council, Institute of Laboratory Animal Resources* 46: 258–268.

Litman G.W., Rast J.P., Shamblott M.J., Haire R.N., Hulst M., Roess W., Litman R.T., Hinds-Frey K.R., Zilch A. & Amemiya C.T. 1993. Phylogenetic diversification of immunoglobulin genes and the antibody repertoire. *Molecular biology and evolution* 10: 60–72.

Liu Y., Sheng J., Fokine a., Meng G., Shin W.-H., Long F., Kuhn R.J., Kihara D. & Rossmann M.G. 2015. Structure and inhibition of EV-D68, a virus that causes respiratory illness in children. *Science* 347: 71–74.

Liu S.-L., Wang Z.-G., Zhang Z.-L. & Pang D.-W. 2016. Tracking single viruses infecting their host cells using quantum dots. *Chemical Society Reviews* 45: 1211–1224.

Liu X., Yu M., Kim H., Mameli M. & Stellacci F. 2012a. Determination of monolayer-protected gold nanoparticle ligand-shell morphology using NMR. *Nature Communications* 3: 1–9.

Liu S.L., Zhang Z.L., Tian Z.Q., Zhao H.S., Liu H., Sun E.Z., Xiao G.F., Zhang W., Wang H.Z. & Pang D.W. 2012b. Effectively and efficiently dissecting the infection of influenza virus by quantum-dot-based single-particle tracking. *ACS Nano* 6: 141–150.

Macleod A.M., Mitchell D.R., Palmer N.J., Poël H. Van De, Conrath K., Andrews M., Leyssen P. & Neyts J. 2013. Identification of a series of

compounds with potent antiviral activity for the treatment of enterovirus infections. *ACS Medicinal Chemistry Letters* 4: 585–589.

Marjomäki V., Pietiäinen V., Matilainen H., Upla P., Ivaska J., Nissinen L., Reunanen H., Huttunen P., Hyypiä T. & Heino J. 2002. Internalization of Echovirus 1 in Caveolae. *Journal of Virology* 76: 1856–1865.

Marjomäki V., Turkki P. & Huttunen M. 2015. Infectious entry pathway of enterovirus B species. *Viruses* 7: 6387–6399.

Mayer M. & Meyer B. 1999. Characterization of ligand binding by saturation transfer difference NMR spectroscopy. *Angewandte Chemie - International Edition* 38: 1784–1788.

McCafferty J., Griffiths a D., Winter G. & Chiswell D.J. 1990. Phage antibodies: filamentous phage displaying antibody variable domains. *Nature* 348: 552–554.

Merilahti P., Karelehto E. & Susi P. 2016. Role of Heparan Sulfate in Cellular Infection of Integrin-Binding Coxsackievirus A9 and Human Parechovirus 1 Isolates. *PLoS ONE* 11: 1–13.

Milstone A.M., Petrella J., Sanchez M.D., Mahmud M., Whitbeck J.C. & Bergelson J.M. 2005. Interaction with coxsackievirus and adenovirus receptor, but not with decay-accelerating factor (DAF), induces A-particle formation in a DAF-binding coxsackievirus B3 isolate. *J. Virol.* 79: 655–660.

Myllynen M., Kazmertsuk A. & Marjomäki V. 2016. A Novel Open and Infectious Form of Echovirus 1 López S. (ed.). *Journal of Virology* 90: 6759–6770.

Nieba L., Honegger A., Krebber C. & Pluckthun A. 1997. Disrupting the hydrophobic patches at the antibody variable/constant domain interface: improved in vivo folding and physical characterization of an engineered scFv fragment. *Protein Engineering Design and Selection* 10: 435–444.

Oikarinen M., Tauriainen S., Honkanen T., Vuori K., Karhunen P., Vasama-Nolvi C., Oikarinen S., Verbeke C., Blair G.E., Rantala I., Ilonen J., Simell O., Knip M. & Hyöty H. 2008. Analysis of pancreas tissue in a child positive for islet cell antibodies. *Diabetologia* 51: 1796–1802.

Oliveira M., Zhao R., Lee W., Kremer M., Minor I., Rueckert R., Diana G., Pevear D., Dutko F. & Mckinlay M. 1993. The structure of human rhinovirus 16. *Structure* 1: 51–68.

Patel K.P., Coyne C.B. & Bergelson J.M. 2009. Dynamin- and lipid raft-dependent entry of decay-accelerating factor (DAF)-binding and non-DAF-binding coxsackieviruses into nonpolarized cells. *Journal of virology* 83: 11064–11077.

Patolsky F., Zheng G., Hayden O., Lakadamyali M., Zhuang X. & Lieber C.M. 2004. Electrical detection of single viruses. *Proceedings of the National Academy of Sciences of the United States of America* 101: 14017–14022.

Paul A. V, Boom H.J. van, Filippov D. & Wimmer E. 1998. Protein-primed RNA synthesis by purified poliovirus RNA polymerase. *Nature* 393: 280–284.

Paul A.L. De, Mukdsi J.H., Petiti J.P., Gutiérrez S., Quintar A.A., Maldonado C.A. & Torres A.I. 2012. Immunoelectron Microscopy: A Reliable Tool for

the Analysis of Cellular Processes. *Applications of Immunocytochemistry*: 66–96.

Pelkmans L., Kartenbeck J. & Helenius a. 2001. Caveolar endocytosis of simian virus 40 reveals a new two-step vesicular-transport pathway to the ER. *Nature cell biology* 3: 473–483.

Peng L., Wu T.T., Tchieu J.H., Feng J., Brown H.J., Feng J., Li X., Qi J., Deng H., Vivanco I., Melinghoff I.K., Jamieson C. & Sun R. 2010. Inhibition of the phosphatidylinositol 3-kinase-Akt pathway enhances gamma-2 herpesvirus lytic replication and facilitates reactivation from latency. *Journal of General Virology* 91: 463–469.

Perez L. & Carrasco L. 1993. Entry of polivirus into cells does not require a low-pH step. *Journal of Virology* 67: 4543–4548.

Pevear D.C., Tull T.M., Seipel M.E. & Groarke J.M. 1999. Activity of pleconaril against enteroviruses. *Antimicrobial Agents and Chemotherapy* 43: 2109–2115.

Pietiäinen V., Marjomäki V., Upla P., Pelkmans L., Helenius A. & Hyypiä T. 2004. Echovirus 1 Endocytosis into Caveosomes Requires Lipid Rafts, Dynamin II, and Signaling Events. *Molecular Biology of the Cell* 15: 4911–4925.

Plevka P., Perera R., Yap M.L., Cardosa J., Kuhn R.J. & Rossmann M.G. 2013. Structure of human enterovirus 71 in complex with a capsid-binding inhibitor. *Proceedings of the National Academy of Sciences of the United States of America* 110: 5463–5467.

Poonthiyil V., Nagesh P.T., Husain M., Golovko V.B. & Fairbanks A.J. 2015. Gold Nanoparticles Decorated with Sialic Acid Terminated Bi-antennary N-Glycans for the Detection of Influenza Virus at Nanomolar Concentrations. *ChemistryOpen* 4: 708–716.

Pulli T., Lankinen H., Roivainen M. & Hyypiä T. 1998. Antigenic sites of coxsackievirus A9. *Virology* 240: 202–212.

Raiborg C., Malerød L., Pedersen N.M. & Stenmark H. 2008. Differential functions of Hrs and ESCRT proteins in endocytic membrane trafficking. *Experimental Cell Research* 314: 801–813.

Reisdorph N., Thomas J.J., Katpally U., Chase E., Harris K., Siuzdak G. & Smith T.J. 2003. Human rhinovirus capsid dynamics is controlled by canyon flexibility. *Virology* 314: 34–44.

Ridley A.J. 2006. Rho GTPases and actin dynamics in membrane protrusions and vesicle trafficking. *Trends in Cell Biology* 16: 522–529.

Rincón V., Rodríguez-Huete A., López-Argüello S., Ibarra-Molero B., Sanchez-Ruiz J.M., Harmsen M.M. & Mateu M.G. 2014. Identification of the Structural Basis of Thermal Lability of a Virus Provides a Rationale for Improved Vaccines. *Structure* 22: 1560–1570.

Rintanen N., Karjalainen M., Alanko J., Paavolainen L., Mäki A., Nissinen L., Lehkonen M., Kallio K., Cheng R.H., Upla P., Ivaska J. & Marjomäki V. 2012. Calpains promote 2 1 integrin turnover in nonrecycling integrin pathway. *Molecular Biology of the Cell* 23: 448–463.

Roivainen M., Piirainen L., Hovi T., Virtanen I., Riikonen T., Heino J. & Hyypiä T. 1994. Entry of coxsackievirus A9 into host cells: specific interactions with alpha v beta 3 integrin, the vitronectin receptor. *Virology* 203: 357–365.

Roivainen M., Rasilainen S., Ylipaasto P., Nissinen R., Ustinov J., Bouwens L., Eizirik D.L., Hovi T. & Otonkoski T. 2000. Mechanisms of Coxsackievirus-Induced Damage to Human Pancreaticβ -Cells 1. *The Journal of Clinical Endocrinology & Metabolism* 85: 432–440.

Roivainen M., Ylipaasto P., Savolainen C., Galama J., Hovi T. & Otonkoski T. 2002. Functional impairment and killing of human beta cells by enteroviruses: The capacity is shared by a wide range of serotypes, but the extent is a characteristic of individual virus strains. *Diabetologia* 45: 693–702.

Rotbart H. a. 1991. Nucleic acid detection systems for enteroviruses. *Clinical Microbiology Reviews* 4: 156–168.

Roth J. 1982. Applications of Immunocolloids in Light Microscopy. *Journal of Histochemistry and Cytochemistry* 30: 691–696.

Roy A. & Post C.B. 2012. Long-distance correlations of rhinovirus capsid dynamics contribute to uncoating and antiviral activity. *Proceedings of the National Academy of Sciences* 109: 5271–5276.

Ruokola P., Dadu E., Kazmertsuk A., Häkkänen H., Marjomäki V. & Ihalainen J. a. 2014. Raman Spectroscopic Signatures of Echovirus 1 Uncoating. *Journal of Virology* 88: 8504–8513.

Salorinne K., Lahtinen T., Malola S., Koivisto J. & Häkkinen H. 2014. Solvation chemistry of water-soluble thiol-protected gold nanocluster Au102 from DOSY NMR spectroscopy and DFT calculations. *Nanoscale* 6: 7823–7826.

Schaar H.M. van der, Melia C.E., Bruggen J.A.C. van, Strating J.R.P.M., Geenen M.E.D. van, Koster A.J., Bárcena M. & Kuppeveld F.J.M. van. 2016. Illuminating the Sites of Enterovirus Replication in Living Cells by Using a Split-GFP-Tagged Viral Protein Coyne C.B. (ed.). *mSphere* 1: e00104-16.

Schmidtke M., Schnittler U., Jahn B., Dahse H.-M. & Stelzner A. 2001. A rapid assay for evaluation of antiviral activity against coxsackie virus B3, influenza virus A, and herpes simplex virus type 1. *Journal of Virological Methods* 95: 133–143.

Schmidtke M., Wutzler P., Zieger R., Riabova O.B. & Makarov V.A. 2009. New pleconaril and [(biphenyloxy)propyl]isoxazole derivatives with substitutions in the central ring exhibit antiviral activity against pleconaril-resistant coxsackievirus B3. *Antiviral Research* 81: 56–63.

Shafren D.R., Bates R.C., Agrez M. V, Herd R.L., Burns G.F. & Barry R.D. 1995. Coxsackieviruses B1, B3, and B5 use decay accelerating factor as a receptor for cell attachment. *Journal of Virology* 69: 3873–3877.

Shibata D.K., Arnheim N. & Maritn J. 1988. Paraffin-Embedded Tissue Using the Polymerase. *The Journal of Experimental Medicine* 167: 0–5.

Siljamäki E., Rintanen N., Kirsi M., Upla P., Wang W., Karjalainen M., Ikonen E. & Marjomäki V. 2013. Cholesterol Dependence of Collagen and Echovirus 1 Trafficking along the Novel α2β1 Integrin Internalization Pathway Gullberg D. (ed.). *PLoS ONE* 8: e55465.

Sjollema K.A., Schnell U., Kuipers J., Kalicharan R. & Giepmans B.N.G. 2012. *Correlated Light Microscopy and Electron Microscopy*. Elsevier.

Smyth M.S. 2002. Picornavirus uncoating. *Molecular Pathology* 55: 214–219.

Smyth M., Pettitt T., Symonds a. & Martin J. 2003. Identification of the pocket factors in a picornavirus. *Archives of Virology* 148: 1225–1233.

Soonsawad P., Paavolainen L., Upla P., Weerachatyanukul W., Rintanen N., Espinoza J., McNerney G., Marjomäki V. & Cheng R.H. 2014. Permeability Changes of Integrin-Containing Multivesicular Structures Triggered by Picornavirus Entry Pecheur E.-I. (ed.). *PLoS ONE* 9: e108948.

Takada Y., Ye X. & Simon S. 2007. The integrins. *Genome biology* 8: 215.

Tan T.T.T., Khaw C. & Ng M.M.L. 2010. Challenges and recent advances in live cell bioimaging. *Microscopy: Science, Technology, Applications and Education*: 1495–1505.

Tan C.W., Lai J.K.F., Sam I.-C. & Chan Y.F. 2014. Recent developments in antiviral agents against enterovirus 71 infection. *Journal of biomedical science* 21: 14.

Thibaut H.J., Palma A.M. De & Neyts J. 2012. Combating enterovirus replication: State-of-the-art on antiviral research. *Biochemical Pharmacology* 83: 185–192.

Tokarz R., Firth C., Madhi S.A., Howie S.R.C., Wu W., Sall A.A., Haq S., Briese T. & Ian Lipkin W. 2012. Worldwide emergence of multiple clades of enterovirus 68. *Journal of General Virology* 93: 1952–1958.

Triantafilou K. & Triantafilou M. 2003. Lipid raft microdomains: Key sites for Coxsackievirus A9 infectious cycle. *Virology* 317: 128–135.

Triantafilou M., Triantafilou K., Wilson K.M., Takada Y., Fernandez N. & Stanway G. 1999. Involvement of beta2-microglobulin and integrin alpha(v)beta3 molecules in the coxsackievirus A9 infectious cycle. *Journal of General Virology* 80: 2591–2600.

Tsang S.K., Danthi P., Chow M. & Hogle J.M. 2000. Stabilization of poliovirus by capsid-binding antiviral drugs is due to entropic effects. *Journal of molecular biology* 296: 335–340.

Tsoi K.M., Dai Q., Alman B.A. & Chan W.C.W. 2013. Are quantum dots toxic? Exploring the discrepancy between cell culture and animal studies. *Accounts of Chemical Research* 46: 662–671.

Tuthill T.J., Groppelli E., Hogle J.M. & Rowlands D.J. 2010. Picornaviruses. In: *Current Topics in Microbiology and Immunology*, pp. 43–89.

Upla P., Marjomäki V., Kankaanpää P., Ivaska J., Hyypiä T., van der Goot F. G. & Heino J. 2004. Clustering Induces a Lateral Redistribution of 2 1 Integrin from Membrane Rafts to Caveolae and Subsequent Protein Kinase C-dependent Internalization. *Molecular Biology of the Cell* 15: 625–636.

Upla P., Marjomäki V., Nissinen L., Nylund C., Waris M., Hyypiä T. & Heino J. 2008. Calpain 1 and 2 Are Required for RNA Replication of Echovirus 1. *Journal of Virology* 82: 1581–1590.

Walter M., Akola J., Lopez-Acevedo O., Jadzinsky P.D., Calero G., Ackerson C.J., Whetten R.L., Gronbeck H. & Häkkinen H. 2008. A unified view of

ligand-protected gold clusters as superatom complexes. *Proceedings of the National Academy of Sciences* 105: 9157–9162.

Walter T.S., Ren J., Tuthill T.J., Rowlands D.J., Stuart D.I. & Fry E.E. 2012. A plate-based high-throughput assay for virus stability and vaccine formulation. *Journal of Virological Methods* 185: 166–170.

Wang Q., Chan T.R., Hilgraf R., Fokin V. V., Sharpless K.B. & Finn M.G. 2003. Bioconjugation by copper(I)-catalyzed azide-alkyne [3 + 2] cycloaddition. *Journal of the American Chemical Society* 125: 3192–3193.

Wang Z. & Ma L. 2009. Gold nanoparticle probes. *Coordination Chemistry Reviews* 253: 1607–1618.

Wang I.H., Suomalainen M., Andriasyan V., Kilcher S., Mercer J., Neef A., Luedtke N.W. & Greber U.F. 2013. Tracking viral genomes in host cells at single-molecule resolution. *Cell Host and Microbe* 14: 468–480.

Ward T., Powell R.M., Pipkin P.A., Evans D.J., Minor P.D. & Almond J.W. 1998. Role for beta2-microglobulin in echovirus infection of rhabdomyosarcoma cells. *Journal of virology* 72: 5360–5365.

Williams C.H., Kajander T., Hyypiä T., Jackson T., Sheppard D. & Stanway G. 2004. Integrin alphavbeta6 Is an RGD-Dependent Receptor for Coxsackievirus A9. *Journal of Virology* 78: 6967–6973.

Wimmer E. & Paul A. V. 2010. *The Making of a Picornavirus Genome* Ehrenfeld E., Domingo E. & Roos R.P. (eds.). Wiley. The picornaviruses p. 33-55

Vollmer F., Arnold S. & Keng D. 2008. Single virus detection from the reactive shift of a whispering-gallery mode. *Proceedings of the National Academy of Sciences of the United States of America* 105: 20701–20704.

Wörn A. & Plückthun A. 1999. Different equilibrium stability behavior of scFv fragments: Identification, classification, and improvement by protein engineering. *Biochemistry* 38: 8739–8750.

Xing L. 2004. Structural and Functional Analysis of Integrin 2I Domain Interaction with Echovirus 1. *Journal of Biological Chemistry* 279: 11632–11638.

Xu H., Hao X., Wang S., Wang Z., Cai M., Jiang J., Qin Q., Zhang M. & Wang H. 2015. Real-time Imaging of Rabies Virus Entry into Living Vero cells. *Scientific Reports* 5: 11753.

Ylipaasto P., Klingel K., Lindberg A.M., Otonkoski T., Kandolf R., Hovi T. & Roivainen M. 2004. Enterovirus infection in human pancreatic islet cells, islet tropism in vivo and receptor involvement in cultured islet beta cells. *Diabetologia* 47: 225–239.

Zhang Y., Simpson A. a, Ledford R.M., Bator C.M., Chakravarty S., Skochko G. a, Demenczuk T.M., Watanyar A., Pevear D.C. & Rossmann M.G. 2004. Structural and Virological Studies of the Stages of Virus Replication That Are Affected by Antirhinovirus Compounds. *Journal of Virology* 78: 11061–11069.

Zhu J.G., Ozdemir S.K., He L., Chen D.R. & Yang L. 2011. Single virus and nanoparticle size spectrometry by whispering-gallery-mode microcavities. *Optics Express* 19: 16195–16206.

ORIGINAL PAPERS

I

SITE-SPECIFIC TARGETING OF ENTEROVIRUS CAPSID BY FUNCTIONALIZED MONIDISPERSE GOLD NANOCLUSTERS

by

Varpu Marjomäki, Tanja Lahtinen, Mari Martikainen, Jaakko Koivisto, Sami Malola, Kirsi Salorinne, Mika Pettersson and Hannu Häkkinen

Proceedings of the National Academy of Sciences 111(4):1277-81

Site-specific targeting of enterovirus capsid by functionalized monodisperse gold nanoclusters

Varpu Marjomäki[a,b], Tanja Lahtinen[b,c], Mari Martikainen[a,b], Jaakko Koivisto[b,c], Sami Malola[b,d], Kirsi Salorinne[b,c], Mika Pettersson[b,c], and Hannu Häkkinen[b,c,d,1]

Departments of [a]Biology and Environmental Science, [c]Chemistry, and [d]Physics, and [b]Nanoscience Center, University of Jyväskylä, FI-40014 Jyväskylä, Finland

Edited* by Roger D. Kornberg, Stanford University School of Medicine, Stanford, CA, and approved December 18, 2013 (received for review June 9, 2013)

Development of precise protocols for accurate site-specific conjugation of monodisperse inorganic nanoparticles to biological material is one of the challenges in contemporary bionanoscience and nanomedicine. We report here a successful site-specific covalent conjugation of functionalized atomically monodisperse gold clusters with 1.5-nm metal cores to viral surfaces. Water-soluble Au_{102}(*para*-mercaptobenzoic acid)$_{44}$ clusters, functionalized by maleimide linkers to target cysteines of viral capsid proteins, were synthesized and conjugated to enteroviruses echovirus 1 and coxsackievirus B3. Quantitative analysis of transmission electron microscopy images and the known virus structures showed high affinity and mutual ordering of the bound gold clusters on the viral surface and a clear correlation between the clusters and the targeted cysteine sites close to the viral surface. Infectivity of the viruses was not compromised by loading of several tens of gold clusters per virus. These advances allow for future investigations of the structure–function relations of enteroviruses and enterovirus-related virus-like particles, including their entry mechanisms into cells and uncoating in cellular endosomes.

monolayer-protected cluster | biolabeling | virus tracking

Enteroviruses belong to a large family of picornaviridae, which are about 30- to 35-nm icosahedral bionanoparticles consisting of a protein capsid without a lipid envelope (1). These nonenveloped viruses contain numerous clinically important human pathogens belonging to coxsackie viruses, echoviruses, and polioviruses. They cause a wide range of acute diseases, from mild rash to viral meningitis, heart muscle failure, and paralysis. Certain enteroviruses, especially from the coxsackie virus group, have also recently been associated with chronic diseases such as diabetes (2). It is thus of great importance to understand the pathogenesis of virus infection in vitro and in vivo, and reliable means of tracking the virus in tissues and cells are crucially needed.

Recent applications to study viruses and their distribution in cells and tissues have usually involved the use of fluorescent markers for optical imaging or colloidal gold markers for enhancing image contrast in electron microscopy (3, 4). However, long-term stability of the markers may be compromised by uncontrolled processes such as photobleaching. Furthermore, as the markers link to viruses indirectly via antibodies, the antibody–antigen interactions may not be strong enough to withstand harsh conditions, e.g., under the attack of protein-degrading enzymes in low pH within cellular acidic vesicles or in the gut. Therefore, reliable tracking continues to be a challenge, and more direct and robust tracking strategies are desirable. Here we report a success in using designed covalently bound functionalized linkers that connect atomistically well-defined monodisperse gold clusters with 1.5-nm metal cores to cysteine sites on the surface of enteroviruses echovirus 1 (EV1) and coxsackievirus B3 (CVB3). We observe that the clusters enhance the icosahedral topology of the viruses in transmission electron microscopy (TEM) imaging. Moreover, conjugation of the gold clusters to the virus does not compromise infectivity of the virus even with tens of clusters attached to one virus.

Results and Discussion

Our synthesis and targeting strategy combined two steps: (*i*) utilization of water-soluble monodisperse gold clusters, namely the structurally known (5) and theoretically well-understood (6) $Au_{102}(pMBA)_{44}$ cluster (pMBA stands for *para*-mercaptobenzoic acid) and (*ii*) the use of maleimide as the functional molecule on the gold marker to target the cysteine residues of the viral surface as the covalent binding site, schematically shown in Fig. 1. The water-soluble monodisperse $Au_{102}(pMBA)_{44}$ clusters were synthesized by a method described by Kornberg and coworkers (7) using *para*-mercaptobenzoic acid as the protective ligand layer. This one-step synthesis provided 2.8-nm-sized particles with 1.5-nm metal cores, which were characterized and confirmed to be monodisperse by TEM (*SI Appendix*, Fig. S1), NMR (*SI Appendix*, Fig. S2), and UV-visible (UV-vis) spectroscopy (*SI Appendix*, Fig. S3) as well as gel electrophoresis (*SI Appendix*, Fig. S4). The *para*-mercaptobenzoic acid ligand of the $Au_{102}(pMBA)_{44}$ cluster provides a convenient carboxylic acid functionality, which was used in ester bond condensation with a terminal alcohol. In our case, a six-carbon alcohol with terminal maleimide functionality provided the needed length to function as the linker molecule. Therefore, a modified Steglich esterification reaction of *N*-(6-hydroxyhexyl)maleimide (NMR spectrum in *SI Appendix*, Fig. S5) with $Au_{102}(pMBA)_{44}$ cluster was used to synthesize the water-soluble maleimide functionalized gold clusters of $Au_{102}(pMBA)_{44-m}$(*N*-(6-hexyl 4-mercaptobenzoate)maleimide)$_m$, hereafter called Au102-MI. The success of the functionalization was confirmed by gel electrophoresis (*SI Appendix*, Fig. S4), UV-vis (*SI Appendix*, Fig. S3), and IR spectroscopy (*SI Appendix*, Fig. S6). The amount of linker molecules

Significance

Development of precise protocols for accurate site-specific conjugation of monodisperse inorganic nanoparticles to large biomolecules and bionanoparticles is one of the challenges in contemporary bionanoscience and nanomedicine, providing new tools for bioimaging and tracking in biological systems. Here we report a success in labeling enteroviruses by atomically precise thiol-stabilized gold clusters with 1.5-nm metal cores that bind, via a covalent link, to cysteines that are close to the viral surface. It is shown that the infectivity of the viruses is not compromised by this labeling procedure. These advances allow for future investigations of the structure–function relations of enteroviruses and enterovirus-related virus-like particles, including their entry mechanisms into cells and uncoating in cellular endosomes.

Author contributions: V.M. and H.H. designed research; V.M., T.L., M.M., J.K., S.M., and K.S. performed research; M.M., J.K., S.M., and K.S. analyzed data; and V.M., T.L., M.M., J.K., S.M., K.S., M.P., and H.H. wrote the paper.

The authors declare no conflict of interest.

*This Direct Submission article had a prearranged editor.

[1]To whom correspondence should be addressed. E-mail: hannu.hakkinen@jyu.fi.

This article contains supporting information online at www.pnas.org/lookup/suppl/doi:10.1073/pnas.1310973111/-/DCSupplemental.

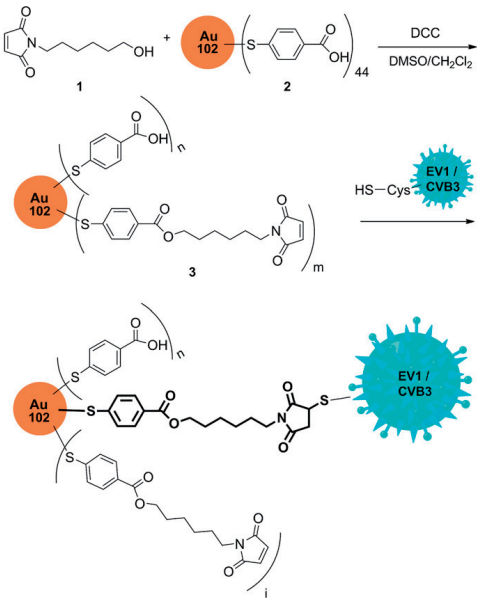

Fig. 1. Synthesis of the maleimide functionalized $Au_{102}(pMBA)_{44}$ clusters and site-specific conjugation to enteroviruses. (*Top*) Maleimide-functionalized linker molecules (molecule 1) are reacted with $Au_{102}(pMBA)_{44}$ clusters (molecule 2). (*Middle*) The linker binds covalently to the cluster via an ester bond. The functionalized gold clusters (molecule 3) are conjugated with EV1 and CVB3 to target the free thiols of the cysteines close to the viral surface. (*Bottom*) Michael addition leads to the gold cluster–virus complex. This schematic figure is not in scale; the diameter of the $Au_{102}(pMBA)_{44}$ is 2.8 nm, the length of *N*-(6-hydroxyhexyl)maleimide linker is 1.1 nm, and the diameters of EV1 and CVB3 are about 30 nm.

per cluster (m) cannot be currently accurately controlled, but it was kept sufficiently low so that the functionalized clusters remained water soluble. The functionalized clusters were then conjugated to free thiols of surface cysteines of EV1 and CVB3 via the Michael addition reaction.

Visualization of purified enteroviruses by TEM showed typically virus particles of roughly 30-nm diameter after negative staining with phosphotungstic acid (PTA). Incubation with nonfunctionalized $Au_{102}(pMBA)_{44}$ showed virtually no association of the clusters with virus particles (Fig. 2*C* and *SI Appendix*, Fig. S7). There was no clear change in the association between incubation times between 15 min and 2 d, suggesting that nonfunctionalized clusters could not actively associate with the virus particles even after longer incubations. In contrast, visualization of the samples where EV1 or CVB3 had been incubated with functionalized Au102-MI gold clusters showed abundant loading of clusters (see Fig. 2 *A*, *B*, and *D* and *SI Appendix*, Fig. S8). It is apparent from those figures that many viruses bind tens of gold clusters, there is intrinsic order between the clusters at the viral surface, and the clusters reflect the icosahedral shapes of the virus particles (highlighted specifically in *SI Appendix*, Fig. S9). To remove excess Au102-MI clusters unbound to viruses, virus preparations were subjected to column purification based on size exclusion chromatography after 1–2 d of incubation. Virus-positive fractions were verified by adding aliquots from the fractions on green monkey kidney (GMK) cells and monitoring the infectivity. TEM analysis showed that these virus preparations were largely free of unbound Au102-MI and contained mostly virus–cluster conjugates (*SI Appendix*, Figs. S10 and S11). Similar virus preparation with nonfunctionalized gold clusters showed only pure virus particles, which confirms that the nonfunctionalized gold clusters could not conjugate to viruses during 1–2 d of incubation at 37 °C (*SI Appendix*, Fig. S12).

EV1 and CVB3 are relatively simple nonenveloped viruses whose structures are known from single-crystal X-ray diffraction (8, 9). Their capsid contains 60 identical units of viral proteins VP1–VP4, and the units are packed in the icosahedral geometry. Of interest to possible covalent linking through the Michael addition reaction are the few outermost cysteine layers (*SI Appendix*, Figs. S13 and S14). Using a 2-nm-diameter sphere to probe the topography of the viral surface, the shortest distances from the thiol end of cysteine residues to the viral surface of EV1 are 0.78 nm, 0.88 nm, and 1.24 nm for cys256, cys209, and cys73, respectively. For CVB3, the corresponding values are 0.31 nm, 0.72 nm, and 1.15 nm for cys234, cys134, and cys73, respectively. These values should be compared with the approximate length of 1.1 nm of the *N*-(6 hydroxyhexyl)maleimide linker. The spatial ordering of the clusters in two representative virus–cluster conjugates (EV1 and CVB3) is analyzed in Fig. 3. A clear correlation of the cluster positions to the known sites of the cysteines listed above is found, to the extent that the most likely orientation of the virus particle with respect to the TEM grid can be deduced, and several features of pentagonal and trigonal rotational symmetries of the viral surface can be identified.

The spatial distribution and cysteine–cysteine distance distributions are different in EV1 and CVB3. The fact that the cluster–cluster distributions reflect well these differences (Fig. 3) is the most convincing evidence of cysteine-specific binding of the functionalized clusters to both virus types. It is also important to consider the open environments adjacent to the sulfur of the cysteines, which has been analyzed in *SI Appendix*, Figs. S15 and S16 (the details of this analysis method are discussed in *SI Appendix*). The analysis shows that the most accessible cysteines are cys73 of EV1 and cys234 of CVB3. Because binding of the clusters to other cysteines is observed as well for both EV1 and CVB3, the targeting is likely to be mediated by the natural dynamics of the viral surface, opening momentarily "channels" for thiol accessibility and facilitating the Michael reaction. This kinetic effect may also explain the rather long incubation times (a few hours to 1 d; see *SI Appendix*, Fig. S8) needed for achieving samples where most viruses are loaded with gold clusters. These observations are in line with previous results on poliovirus by other groups that showed dynamic access of exogenously added antibodies against polypeptides located inside the virus capsid (10), connected to a "breathing" mechanism. This natural breathing dynamics of the viruses (10, 11) may play an important role also for the conjugation of the Au102-MI and is a topic of further investigations.

We also addressed the issue of whether binding of tens of Au102-MI clusters to the viral surface affected the infectivity of viruses. We studied infectivity by end-point titration in GMK cells. Quantitative data on infectivity were obtained from end-point titration resulting in the number of infective virus particles in the virus preparations. Comparison of the virus preparations with or without the functionalized gold clusters showed that 1–2 d of incubation of virus with gold clusters at 37 °C did not lower the infectivity in GMK cells (Fig. 4). To assess a typical labeling outcome, we counted, for example for CVB3, more than 400 virus particles from randomly picked TEM images. This resulted in 79.3% of viruses being decorated with functionalized gold clusters after 48 h of incubation (356 out of 430 virus particles). Therefore, even if there are roughly 20% of viruses that are not conjugated with gold clusters, these results imply that gold

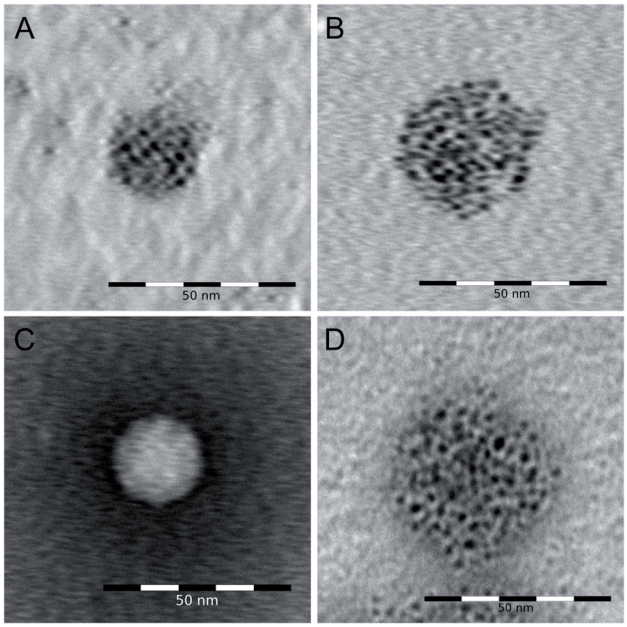

Fig. 2. TEM images of CVB3 viruses (*A*–*C*) treated with functionalized and nonfunctionalized gold clusters. (*A*) After incubation for 2 d with Au102-MI clusters without column purification, (*B*) after column purification, (*C*) control with conventional negative staining of virus sample incubated with nonfunctionalized $Au_{102}(pMBA)_{44}$, and (*D*) EV1 incubated with Au102-MI for 1 d. Negative staining has been used also in *D*, resulting in the dark gray halo around the cluster. TEM magnification: (*A*) 2×10^5, (*B*) 2×10^5, (*C*) 1.5×10^5, and (*D*) 1×10^5. Note that the Au102-MI conjugated viruses appear larger than the nonconjugated virus. This results from two factors. On one hand, the particles of PTA salt are able to enter the grooves of the virus capsid in *C*. On the other hand, only the linker arm of the maleimide group can penetrate into the virus capsid, but the metal nanocluster part will remain outside. This makes the cluster–virus conjugates appear larger in *A*, *B*, and *D*.

cluster conjugation keeps the viruses more stable, closer to the values of fresh virus taken directly from the freezer.

Linking colloidal gold nanoparticles and phosphine-functionalized gold nanoclusters to biomolecules has been a topic of wide interest since the 1980s (12–14). More recently, gold–cysteine interactions have been used for rigid labeling of proteins and DNA (15–17) and as facilitators for gold self-assembly at viral scaffolds for sensing and nanoelectronics (18, 19). Our work

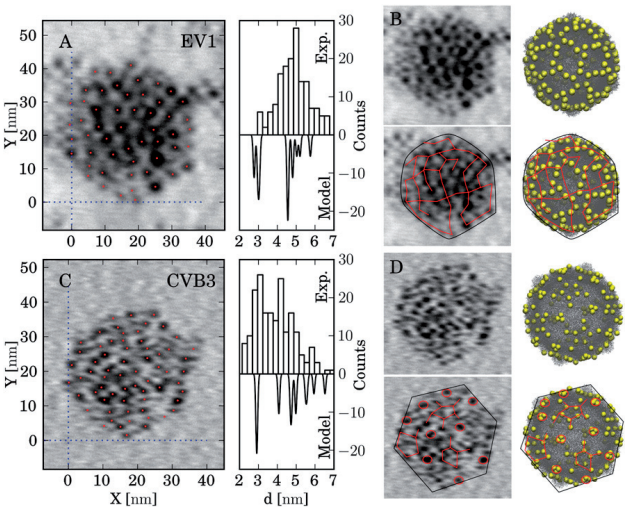

Fig. 3. Quantitative and positions analysis of the Au102-MI clusters in the TEM images of cluster–virus conjugates. (*A*) Cluster–cluster distances compared with the thiol–thiol distances of cysteine residues in the known structure of EV1. In the panels on the right, "Exp." shows the experimental data for the distribution of the cluster centers (marked by red dots on the left) and "Model" shows the calculated distance distribution of the thiol binding sites in the cysteines close to the viral surface. (*B*) Identification of binding patterns of the gold clusters in EV1, compared with thiol positions denoted by yellow spheres. (*C*) The same as *A* but for CVB3. (*D*) The same as *B* but for CVB3. In all of the analysis, three cysteine shells closest and most accessible to the viral surface are used (cys256, cys209, and cys73 for EV1 and cys134, cys234, and cys73 for CVB3). More details of the analysis are given in *SI Appendix*. TEM magnification: (*A* and *B*) 2.5×10^5 and (*C* and D) 2×10^5.

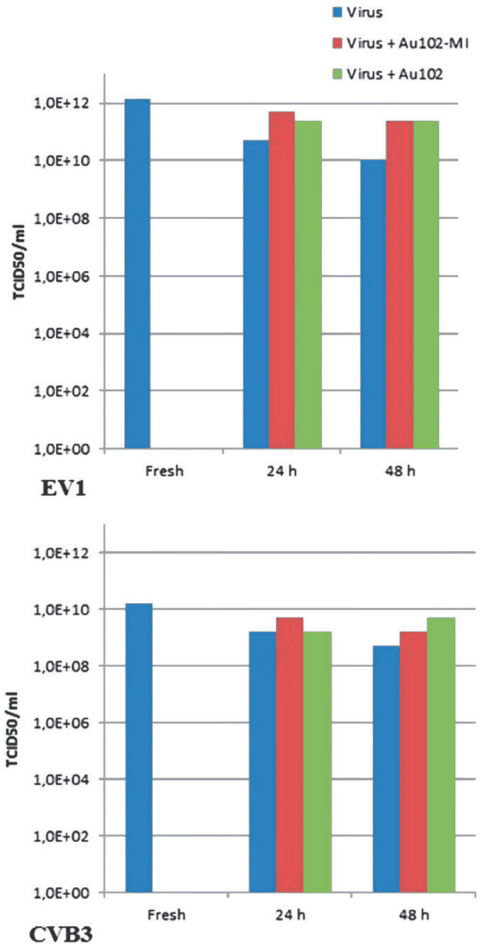

Fig. 4. The amount of infective (*Upper*) EV1 and (*Lower*) CVB3 quantified by the endpoint dilution assay. EV1 or CVB3 was treated with Au102-MI gold clusters and control clusters for 24 or 48 h at 37 °C and serially diluted on GMK cells to evaluate the infectivity of the virus preparations. Control virus was either fresh virus directly from the stock or virus that was incubated at 37 °C without gold clusters. The results are calculated as 50% tissue culture infective dose (TCID50).

demonstrates a unique procedure for achieving robust, direct, site-specific labeling of enteroviruses for future structural studies of virus uncoating, for electron microscopy investigations of virus entry and pathways into cells in vitro and in vivo. In addition, when enterovirus-based virus-like particles (VLPs) or attenuated viruses are used as vaccines, covalently bound gold nanoclusters allow visualization of their entry to various cells and tissues. The covalent binding of clusters creates more robust tags on the virus capsid compared with many other currently used markers that bind by weaker interactions (e.g., via antibodies or protein A). The stronger binding will allow also biodistribution studies where one needs to track viruses along the normal infective route, e.g., through intestine to target tissues.

There are very few data yet available to understand enterovirus uncoating and genome release in cellular structures. Gold nanoclusters will allow for a better visualization of viruses in complex endosomal structures, which may help in understanding the biochemical and structural factors leading to successful opening of the virus to release the genome. With simultaneous labeling of virus receptor (e.g., α2β1 integrin for EV1), one may evaluate the spatial location of the virus in relation to the receptor or the limiting membrane of the endosome. In addition, gold nanoclusters allow potentially detailed (*i*) spectroscopic measurements of nanoclusters moving in relation to each other upon adding biochemical factors that lead to virus opening or (*ii*) manipulation of virus structure and function by using the fact that the clusters are strong absorbers of near-infrared radiation and generators of "local heat" upon deexcitation. Future work to refine the synthesis of maleimide linkers with tunable-length arms and impose fewer linkers per gold cluster by using ligand-exchange kinetics (20, 21), combined with control of concentration of clusters and time of incubation with viruses, may yield improved control of targeting desired cysteine groups at the surface of enteroviruses, e.g., close to positions that are currently thought of as critical for virus uncoating based on in vitro studies (22–24).

Materials and Methods

All materials were commercial unless otherwise mentioned and were used without further purification. *N*-(6-hydroxyhexyl)maleimide (25) and $Au_{102}(pMBA)_{44}$ (7) were prepared according to literature procedures. NMR spectra were recorded with Bruker Avance 500 MHz or Bruker Avance 400 MHz spectrometers at 298 K, and the chemical shifts were calibrated to the residual proton resonances of the deuterated solvent. Mass spectra were measured with a Micromass LCT ESI-TOF instrument. Gel electrophoresis visualization was run on an 18% polyacrylamide gel (19:1, acrylamide:bisacrylamide) using 1× TBE buffer in a Bio-Rad Mini-Protean Tetra System gel electrophoresis apparatus at 120 V.

Synthesis of *N*-(6-hydroxyhexyl)maleimide. A stirred solution of 6-aminohexanol (380 mg, 3.24 mmol) in saturated aqueous sodium bicarbonate (17 mL) was cooled to 0 °C in an ice bath. *N*-(methoxylcarbonyl)maleimide (500 mg, 3.22 mmol) was added in small portions, and the resulting solution was stirred at 0 °C for 30 min. The ice bath was then removed, and the solution was allowed to warm to room temperature over 20 min. The aqueous layer was extracted with chloroform (4 × 20 mL), and the combined organic layers were dried over $MgSO_4$. Rotary evaporation gave a white solid, which was purified by column chromatography on siliga gel, eluting with dichloromethane-ethylacetate (3:2, vol/vol) to give 0.38 g (60%) of *N*-(6-hydroxyhexyl)maleimide as a white solid. The NMR parameters were as follows: ^{1}H NMR ($CDCl_3$, 500 MHz) δ 6.65 (s, 2H), 3.57 (t, J = 6.55 Hz), 3.47 (t, J = 7.23 Hz, 2H), 1.87 (br s, 1H), 1.58–1.48 (m, 4H), 1.34 (m, 2H), 1.26 (m, 2H) ppm. ^{13}C NMR ($CDCl_3$, 126 MHz) δ 170.3, 134.0, 62.5, 37.6, 32.4, 28.3, 26.3, 25.1 ppm. ESI-MS $[M+Na]^+$: *m/z* 220.

Synthesis of $Au_{102}(pMBA)_{44}$. The thiolate monolayer protected monodisperse $Au_{102}(pMBA)_{44}$ clusters were prepared according to previously published synthesis procedure using *p*-mercaptobenzoic acid (*p*MBA) as the protecting ligand. The purity and monodispersity of the prepared $Au_{102}(pMBA)_{44}$ clusters were determined by ^{1}H NMR (400 MHz, D_2O-NaOH) and UV-vis spectroscopy, gel electrophoresis, and transmission electron microscopy.

Synthesis of Au102-MI. A solution of *N*-(6-hydroxyhexyl)maleimide (0.74 mg, 3.73 μmol) in dry dichloromethane (DCM) (1 mL) was added to a presonicated $Au_{102}(pMBA)_{44}$ (2 mg, 0.0745 μmol) in dry DMSO (5 mL) in a 50-mL conical. The mixture was vigorously stirred for 20 min. A solution of *N*,*N*′ dicyclohexylcarbodiimide (0.77 mg, 3.73 μmol) in dry DCM (1 mL) was then added dropwise to the cooled mixture while stirring. The stirring was continued overnight, and the solution was then centrifuged at 3500 rpm for 5 min (Heraeus Labofuge 400, Thermo Scientific). The supernatant was transferred to a new 50-mL conical, and the maleimide-functionalized gold clusters were precipitated from the solution by adding solid NH_4OAc (73 mg, 0.947 mmol) and methanol (20 mL). The contents were mixed by shaking the conical and

then centrifuged at 3500 rpm for 10 min. The precipitates were collected, dried in air, and dissolved in ultrapure water. The product and the success of the *N*-(6-hydroxyhexyl)maleimide functionalization of the $Au_{102}(pMBA)_{44}$ cluster was analyzed by gel electrophoresis visualization on an 18% polyacrylamide gel, UV-vis, and IR.

Viruses. EV1 (Farouk strain) and CVB3 (Nancy strain) were obtained from ATCC. The viruses were propagated in GMK cells and purified using sucrose gradient as described (26). The infectivity of the purified virus was determined by end-point titration. The purity and RNA and protein content were determined by spectroscopic analysis and protein measurement using the Zlotnik method. Column purification of virus–gold clusters preparations was done using the Sephadex G-25 columns (NAP-5) according to the manufacturer's protocol (GE Healthcare). Briefly, 150 μL of the virus–gold suspension was added on top of the column, which was previously balanced with salt solution (137 mM NaCl, pH 7.0). After administering 350 μL of the salt solution, 5 × 100 μL fractions were eluted by adding salt solution in 100-μL increments. A small amount of gold eluted from the column concomitantly with the virus, while the bulk of the unbound gold was left on top of the column and did not elute during extensive washing. Gold clusters were recorded from the eluates with absorbance at 405 nm (OD_{405}), and the amount of infective virus particles in the eluates was measured by end-point titration.

Virus–Gold Conjugation. EV1 or CVB3 purified by sucrose density gradient fractionation was used for gold conjugation. Gold clusters (45 μM, either Au102-MI or control Au102) were added to the virus samples in equal amounts (based on OD_{405} values). Binding was performed in the presence of 137 mM NaCl for various time periods at 37 °C.

Virus Infectivity Measurement by the 50% Tissue Culture Infective Dose. The endpoint dilution assay quantifies the amount of virus required to kill 50% of the infected hosts, here GMK cells. First, GMK cells (5×10^4 cells/mL) are plated the previous day, and serial 10-fold dilutions of the virus samples are added. After 3 d of incubation, the percentage of cell death (i.e., infected cells) is manually observed after crystal violet staining (10-min staining with crystal violet containing 10% formaline, followed by a wash with water to detach dead cells), which reveals intact (noninfected) cells, and recorded for each virus dilution. The 50% tissue culture infective dose (TCID50) is calculated by comparing the number of infected and uninfected wells of four replicates of the same virus concentration. The concentration at which half the wells would statistically be infected is extrapolated (TCID50).

TEM Analysis. Virions were visualized by TEM using negative staining. First, 3 μl (containing about 1×10^{10} virus particles) of the virus was bound on formvar-coated grids, which were glow-discharged using an EMS/SC7620 Mini sputter coater. After a 15-s incubation, excess sample was blotted away by carefully touching the drop with a blotting paper (Whatman 3MM). Negative stain (5 μl of 1% PTA solution) was added on the grid, and after 1 min, excess dye was blotted away as before. After air drying, samples were visualized using a TEM JEOL JEM1400. The images were recorded by using a bottom-mounted Quemesa CCD camera with 4008 × 2664 pixel resolution. Particle centers in Fig. 3 were identified using ImageJ (27).

Spectroscopy. IR spectra were measured with a Nicolet Magna-IR 760 FTIR spectrometer using 2-cm^{-1} resolution and averaging 200 scans. UV-vis spectra were measured with a Perkin-Elmer Lambda 850 spectrometer using 2-nm resolution.

ACKNOWLEDGMENTS. We thank H. Ojaniemi for preliminary synthetic work, A. Honkimaa for preliminary conjugation experiments on EV1 with nonfunctionalized gold clusters, and S. Mustalahti for helping in TEM imaging. V.M. wishes to thank S. Hafenstein and her group for helpful discussions on EV1 structure. This research is supported by the Academy of Finland (Grant 257125 to V.M. and Grant 128341 to H.H.) and the Finnish National Graduate School on Computational Chemistry and Spectroscopy (LASKEMO) (J.K.).

1. Tuthill TJ, Groppelli E, Hogle JM, Rowlands DJ (2010) *Current Topics in Microbiology and Immunology*, ed Johnson JE (Springer, Berlin).
2. Hober D, Sauter P (2010) Pathogenesis of type 1 diabetes mellitus: Interplay between enterovirus and host. *Nat Rev Endocrinol* 6(5):279–289.
3. Kankaanpää P, et al. (2012) BioImageXD: An open, general-purpose and high-throughput image-processing platform. *Nat Methods* 9(7):683–689.
4. Karjalainen M, et al. (2011) Echovirus 1 infection depends on biogenesis of novel multivesicular bodies. *Cell Microbiol* 13(12):1975–1995.
5. Jadzinsky PD, Calero G, Ackerson CJ, Bushnell DA, Kornberg RD (2007) Structure of a thiol monolayer-protected gold nanoparticle at 1.1 Å resolution. *Science* 318(5849):430–433.
6. Walter M, et al. (2008) A unified view of ligand-protected gold clusters as superatom complexes. *Proc Natl Acad Sci USA* 105(27):9157–9162.
7. Levi-Kalisman Y, et al. (2011) Synthesis and characterization of Au102(p-MBA)44 nanoparticles. *J Am Chem Soc* 133(9):2976–2982.
8. Filman DJ, Wien MW, Cunningham JA, Bergelson JM, Hogle JM (1998) Structure determination of echovirus 1. *Acta Crystallogr D Biol Crystallogr* 54(Pt 6 Pt 2):1261–1272.
9. Yoder JD, Cifuente JO, Pan J, Bergelson JM, Hafenstein S (2012) The crystal structure of a coxsackievirus B3-RD variant and a refined 9-angstrom cryo-electron microscopy reconstruction of the virus complexed with decay-accelerating factor (DAF) provide a new footprint of DAF on the virus surface. *J Virol* 86(23):12571–12581.
10. Lin J, et al. (2012) Structure of the Fab-labeled "breathing" state of native poliovirus. *J Virol* 86(10):5959–5962.
11. Lewis JK, Bothner B, Smith TJ, Siuzdak G (1998) Antiviral agent blocks breathing of the common cold virus. *Proc Natl Acad Sci USA* 95(12):6774–6778.
12. Hainfeld JF, Furuya FR (1992) A 1.4-nm gold cluster covalently attached to antibodies improves immunolabeling. *J Histochem Cytochem* 40(2):177–184.
13. Hainfeld JF (1987) A small gold-conjugated antibody label: Improved resolution for electron microscopy. *Science* 236(4800):450–453.
14. Hainfeld JF (1988) Gold cluster-labelled antibodies. *Nature* 333(6170):281–282.
15. Ackerson CJ, Powell RD, Hainfeld JF (2010) Chapter nine - Site-specific biomolecule labeling with gold clusters. *Methods Enzymol* 481:195–230.
16. Ackerson CJ, Sykes MT, Kornberg RD (2005) Defined DNA/nanoparticle conjugates. *Proc Natl Acad Sci USA* 102(38):13383–13385.
17. Sexton JZ, Ackerson CJ (2010) Determination of rigidity of protein bound Au144 clusters by electron cryomicroscopy. *J Phys Chem C* 114:16037–16042.
18. Blum AS, et al. (2004) Cowpea Mosaic Virus as a scaffold for 3-D patterning of gold nanoparticles. *Nano Lett* 4:867–870.
19. Kostiainen MA, et al. (2013) Electrostatic assembly of binary nanoparticle superlattices using protein cages. *Nat Nanotechnol* 8(1):52–56.
20. Heinecke CL, et al. (2012) Structural and theoretical basis for ligand exchange on thiolate monolayer protected gold nanoclusters. *J Am Chem Soc* 134(32): 13316–13322.
21. Devries GA, et al. (2007) Divalent metal nanoparticles. *Science* 315(5810):358–361.
22. Levy HC, Bostina M, Filman DJ, Hogle JM (2010) Catching a virus in the act of RNA release: A novel poliovirus uncoating intermediate characterized by cryo-electron microscopy. *J Virol* 84(9):4426–4441.
23. Bostina M, Levy H, Filman DJ, Hogle JM (2011) Poliovirus RNA is released from the capsid near a twofold symmetry axis. *J Virol* 85(2):776–783.
24. Smyth MS, Martin JH (2002) Picornavirus uncoating. *Mol Pathol* 55(4):214–219.
25. Keller KA, Guo J, Punna S, Finn MG (2005) A thermally-cleavable linker for solid-phase synthesis. *Tetrahedron Lett* 46:1181–1184.
26. Abraham G, Colonno RJ (1984) Many rhinovirus serotypes share the same cellular receptor. *J Virol* 51(2):340–345.
27. Schneider CA, Rasband WS, Eliceiri KW (2012) NIH Image to ImageJ: 25 years of image analysis. *Nat Methods* 9(7):671–675.

II

HYDROPHOBIC POCKET TARGETING PROBES FOR ENTEROVIRUSES

by

Mari Martikainen, Kirsi Salorinne, Tanja Lahtinen, Sami Malola, Perttu Permi, Hannu Häkkinen and Varpu Marjomäki

Nanoscale 7(41):17457-67

Nanoscale

PAPER

Cite this: *Nanoscale*, 2015, **7**, 17457

Hydrophobic pocket targeting probes for enteroviruses†

Mari Martikainen,[a,b] Kirsi Salorinne,[b,c] Tanja Lahtinen,[b,c] Sami Malola,[b,d] Perttu Permi,[a,b,c,e] Hannu Häkkinen*[b,c,d] and Varpu Marjomäki*[a,b]

Visualization and tracking of viruses without compromising their functionality is crucial in order to understand virus targeting to cells and tissues, and to understand the subsequent subcellular steps leading to virus uncoating and replication. Enteroviruses are important human pathogens causing a vast number of acute infections, and are also suggested to contribute to the development of chronic diseases like type I diabetes. Here, we demonstrate a novel method to target site-specifically the hydrophobic pocket of enteroviruses. A probe, a derivative of Pleconaril, was developed and conjugated to various labels that enabled the visualization of enteroviruses under light and electron microscopes. The probe mildly stabilized the virus particle by increasing the melting temperature by 1–3 degrees, and caused a delay in the uncoating of the virus in the cellular endosomes, but could not however inhibit the receptor binding, cellular entry or infectivity of the virus. The hydrophobic pocket binding moiety of the probe was shown to bind to echovirus 1 particle by STD and tr-NOESY NMR methods. Furthermore, binding to echovirus 1 and Coxsackievirus A9, and to a lesser extent to Coxsackie virus B3 was verified by using a gold nanocluster labeled probe by TEM analysis. Molecular modelling suggested that the probe fits the hydrophobic pockets of EV1 and CVA9, but not of CVB3 as expected, correlating well with the variations in the infectivity and stability of the virus particles. EV1 conjugated to the fluorescent dye labeled probe was efficiently internalized into the cells. The virus–fluorescent probe conjugate accumulated in the cytoplasmic endosomes and caused infection starting from 6 hours onwards. Remarkably, before and during the time of replication, the fluorescent probe was seen to leak from the virus-positive endosomes and thus separate from the capsid proteins that were left in the endosomes. These results suggest that, like the physiological hydrophobic content, the probe may be released upon virus uncoating. Our results collectively thus show that the gold and fluorescently labeled probes may be used to track and visualize the studied enteroviruses during the early phases of infection opening new avenues to follow virus uncoating in cells.

Received 22nd June 2015,
Accepted 15th September 2015

DOI: 10.1039/c5nr04139b

www.rsc.org/nanoscale

Introduction

Enterovirus genus belongs to the family of *Picornaviridae* containing numerous clinically important human pathogens and causing a variety of diseases from common cold and mild rashes to viral meningitis and paralysis.[1] Some viruses, especially in the Coxsackie group, have also been associated with chronic diseases such as type 1 diabetes.[2] Moreover, members of enteroviruses, like human enterovirus 71, have recently been causing serious acute infections and are a great threat to public health.[3]

Enteroviruses have an icosahedron shaped protein capsid consisting of 60 copies of each of the structural proteins (VPs 1 to 4). The non-enveloped capsid encloses the 7.5 kb long single-stranded positive-sense RNA genome. VP1 proteins surround the five-fold axis, VP2 and VP3 alternate around the two- and three-fold axes, while VP4 is a shorter internal protein.[4] Within the capsid protein VP1, there is a hydrophobic pocket which is occupied by a pocket factor (natural lipid).[5] The pocket entrance is located at the end of the canyon-like depression surrounding the five-fold axis. The pocket factors have been anticipated to play a role in the

[a]*Department of Biological and Environmental Science, University of Jyväskylä, FI-40014 Jyväskylä, Finland. E-mail: varpu.s.marjomaki@jyu.fi; Tel: +358-40-5634422*
[b]*Nanoscience Center, University of Jyväskylä, FI-40014 Jyväskylä, Finland*
[c]*Department of Chemistry University of Jyväskylä, FI-40014 Jyväskylä, Finland. E-mail: hannu.j.hakkinen@jyu.fi; Tel: +358-400-247973*
[d]*Departmen of Physics, University of Jyväskylä, FI-40014 Jyväskylä, Finland*
[e]*Institute of Biotechnology, University of Helsinki, FI-00014 Helsinki, Finland*

†Electronic supplementary information (ESI) available: Details of the synthesis of the probes, UV-Vis absorption spectra of the probe (**2**), PAGE separation and the absorption spectra of the gold labeled probe (**3**), details of the NMR experiments, determination of the cytotoxicity of the studied molecules, TEM micrographs of the gold labeled probe (**3**) with enteroviruses, live cell imaging of the fluorescent probe (**4**) in cells, and additional details of modeling of the hydrophobic pockets. See DOI: 10.1039/c5nr04139b

capsid stability since their expulsion seems to be needed for the genome release.[6–8] Replacement of the pocket factor with a compound having a much higher binding affinity could be an efficient antiviral tool acting on the virus capsid. This has been demonstrated with viruses whose receptor binding occurs in the canyon region of the capsid, triggering the uncoating process.[6,9]

Although enteroviruses have a huge impact on human health, their pathogenicity is not fully understood. Still, little is known about the subcellular structures that mediate infection of non-enveloped enteroviruses. In recent applications, detection of the virus from tissues and cells is usually based on indirect antibody labelling methods *e.g.* immunofluorescence, immunohistochemistry and electron microscopy methods. In addition, the nucleic acid of the infectious virus can be detected with specific probes coupled with *in situ*-hybridization and different PCR methods.[13] However, all these methods bring challenges in terms of background and sensitivity.[14,15] Novel, covalently bound probes are needed to facilitate live experiments in animals or visualizing specific domains for high-resolution microscopy. We previously demonstrated the production and specificity of a cysteine targeted gold cluster probe against enteroviruses.[16]

None of the indirect labeling methods or stable covalent probes mentioned above are able to bring crucial dynamic information about virus uncoating inside the cellular structures – the key event leading to successful infection in cells and tissues. Our understanding on the actual site of virus uncoating comes from recent structural studies of purified enteroviruses, such as poliovirus and Coxsackievirus A7 (CVA7),[17] revealing that the actual site of capsid opening is at the 2-fold axis. These and other studies also suggest that enteroviruses are differently sensitive to receptor interactions. For poliovirus, receptor binding starts the uncoating process, whereas for both Coxsackie virus A9 (CVA9) and echovirus 1 (EV1), receptor binding stabilizes the virus structure.[18] Thus the capsid opening for many enteroviruses must rely on cellular cues that trigger the virus opening after virus entry to the cytoplasmic endosomes. Therefore, it is important to have reliable techniques to follow the uncoating of the virus *in vivo* and *in vitro* in order to elucidate the cellular factors leading to the release of their genome.

Presently there are no direct tools to follow virus uncoating by microscopy in cells and animal models. Despite its supposedly important role for virus uncoating, there is no understanding of the mechanistic role of the hydrophobic pocket for this process. This is mainly due to the fact that no probes are presently available to follow the function of the hydrophobic pocket. Pleconaril, one of the designated WIN compounds, is one of the most studied capsid binding inhibitors.[10–12] However, the efficacy of Pleconaril as an inhibitor is not exceedingly high for many enteroviruses suggesting that slight modifications of the molecule could provide a more dynamic imaging tool for binding without compromising viral infectivity.

Here, we created a novel dynamic probe to enable virus labeling through the hydrophobic pocket both for live fluorescence imaging, as well as, for ultrastructural studies. We show that the probe does bind to selected members of the enterovirus B group, which become mildly stabilized due to binding, and can be followed through the early steps of virus infection.

Materials and methods

Cells and viruses

Viruses EV1 (Farouk strain), CVB3 (Nancy strain) and CVA9 (Griggs strain) were obtained from the American Type Culture Collection (ATCC). All viruses were propagated in the GMK cells (ATCC) and purified in a 10 to 40% sucrose gradient as described earlier.[19,20] Infectivity of the purified virus was determined by the $TCID_{50}$ assay, and the purity and RNA and protein content were determined by spectroscopic analysis and protein measurement was by using the Zlotnik method.

The human lung carcinoma A549 cell line was obtained from ATCC and they were maintained in Dulbecco's modified Eagle's medium (DMEM) containing 10% fetal bovine serum (FBS) supplemented with penicillin and streptomycin (P/S) and Glutamax. The green monkey kidney (GMK) cells were obtained from ATCC and maintained in Minimum Essential Medium Eagle containing 10% FBS, P/S and Glutamax.

CPE-inhibition- and $TCID_{50}$ per ml assay

The cytopathic effect (CPE)-inhibitory assays were performed using an overall scheme similar to that described earlier.[21] To summarize, the experiments were carried out using 2 day-old A549 cells (8×10^4 cells per well) in 96-well cell culture plates. The cell culture media was changed to fresh DMEM (1% FBS). The cells were infected with MOI 5 and the amount of virus was kept constant in each well. The viruses were pre-incubated for 1 h at 37 °C with the studied compounds before the assay. For CPE-assay, 100 μM concentrations of the studied compounds were used during pre-incubation with the virus, and then diluted ten-fold when added onto the cells. For 50% inhibitory concentration (IC_{50}) quantifications the compounds were tested in various concentrations from 0.6 to 200 μM in 2-fold dilutions. The IC_{50} value for the gold probe (**3**) was quantified using concentrations from 0.2 to 14 μM, and for the fluorescent probe (**4**) from 3.5 to 500 μM. The infected cells without the test compounds and the non-infected cells served as virus only control (vc) and cell control (cc), respectively. After 24 h infection, crystal violet formalin solution was used to fix and stain the cells. The dye was extracted and the optical density was quantified spectrophotometrically at 570 nm with a Victor™ X4 2030 Multilabel Reader (Perkin Elmer). The CPE values were calculated using the following equation: % CPE = 100 − ([[OD virus + compound − OD vc]/OD cc] × 100). Virus only controls were set to 100% CPE and cells only to 0%. The IC_{50} values were calculated by regression analysis.

The 50% tissue culture infective dose ($TCID_{50}$) was calculated as previously described.[22] Briefly, the GMK cells were

grown in 96-well plates to subconfluency. The viruses were pre-incubated for 1 h at 37 °C with the studied compounds before the assay. After the pre-incubation samples were added to the first wells and then serially diluted using 1 log dilutions. After 72 h of incubation, the cells were stained using crystal violet formalin solution for 10 min at room temperature. The detached cells were washed off with water and the remaining cells were counted as viable and non-infected. The $TCID_{50}$ per ml values were calculated by using the Reed–Muench formula.

PaSTRy assay

The thermostabilities of purified EV1, CVA9 and CVB3 were evaluated by Particle Stability Thermal Release Assay performed as previously described.[23] Briefly, the reactions were carried out in thin-walled PCR plates (Agilent) containing 1 μg of EV1, CVA9 or CVB3, 100 μM of the probe (**2**), derivative (**1**) or Pleconaril and 10 × SYBR Green II (Invitrogen) in PBS, pH = 7.4. The viruses were pre-incubated for 1 h at 37 °C with the studied compounds before the thermostability assay. The release of viral genome was detected with the SYBR Green II dye in a Bio-Rad C1000 thermal cycler by raising the temperature gradually from 20 °C to 90 °C, with fluorescence recorded in quadruple at 0.5 °C intervals. The Bio-Rad CFX Manager 2.1 software was used to define the melting temperature (T_m) of each sample. In detail, the T_m was measured from the inflection point (dI/dT) of the fluorescence intensity (I) as functions of temperature (T) from the derivative plot.

Immunofluorescence labelling and confocal microscopy

For immunofluorescence assay a saturated amount (500 μM, 50 000 × molar excess of the ligand over the hydrophobic pocket) of the fluorescent probe (**4**) was first bound to 12.9 μg of EV1 for 1 h at 37 °C in 2 mM $MgCl_2$ PBS. The unbound dye was dialyzed three times against 500 ml of PBS supplemented with 2 mM $MgCl_2$ using 50 000-molecular-mass-cutoff Spectra/Por Micro Float-A-Lyzer cellulose ester membranes (Spectrum Laboratories). For the cell experiments A549 cells were grown on coverslips to subconfluency. An EV1–fluorescent probe conjugate was first bound to the cells for 1 h on ice in DMEM (1% FBS), after which the cells were washed with PBS containing 0.5 % bovine serum albumin, and after incubation at 37 °C (in 1% DMEM) they were fixed at RT with 4% paraformaldehyde (PFA) for 30 min. The fixed samples were permeabilized with 0.2% Triton X-100 for 5 min, and labeled with polyclonal rabbit antiserum against EV1 (produced as described in ref. 24) and anti-rabbit secondary antibody Alexa Fluor 488 (Invitrogen). The cells were mounted on ProLong Gold antifade reagent 4′-6-diamidino-2-phenylindole (Invitrogen) and examined with an Olympus microscope IX81 with a Fluo-View-1000 confocal setup.

In addition, a live imaging experiment was performed in which the A549 cells were infected similarly as described above with the EV1–fluorescent probe conjugate. The cells were imaged at different time points (30 min, 4 h, 12 h and 24 h) before fixation. Finally the cells were fixed, permeabilized and labeled as described above.

TEM

The binding of the gold probe (**3**) to different viruses' hydrophobic pockets was visualized with a transmission electron microscope (TEM) JEM-1400 (JEOL). First 14 μM of the gold probe (**3**) was incubated with 12.9 μg of the virus for 1 h at 37 °C in PBS. In addition, high-molecular weight EV1–gold conjugate was separated from the small unconjugated gold using a 1 ml Sephacryl (Sephacryl S-300 high resolution, GE Healthcare) column according to the manufacturer's instructions. The Butvar-coated copper grids were glow discharged (EMS/SC7620 mini-sputter coater), and the samples were added on the grids for 15 s after which the excess sample was blotted away with a blotting paper (Whatman 3MM). The virions were visualized by gentle negative staining with 1% (wt/vol) phosphotungstic acid (PTA). The stain was added for 30 s, and the excess dye was blotted away as before. The samples were air dried overnight and imaged with TEM.

Results

Probe design, structure and synthesis

"WIN compounds" – named after the developer Sterling-Winthrop – are a family of antiviral drugs designed to target the early events (attachment, entry and uncoating) of viral replication (Scheme 1).[2,11,25] WIN compounds have been shown to bind specifically into the interior hydrophobic pocket located at the VP1 protein of enterovirus capsid replacing the naturally occurring lipid.[26–29] Therefore, the WIN framework, which is best known for Pleconaril (WIN 63843), was chosen as the basis for the design of a probe that would target the hydrophobic pocket of the virus capsid and bind *via* non-covalent interactions. Our previous data (unpublished) on the best known WIN compound Pleconaril (WIN 63843), however, showed only a minor effect on EV1 infectivity despite the suspected binding ability to the hydrophobic pocket of the virus. Therefore, Pleconaril was chosen for further modification to develop a probe that would label the hydrophobic pocket with good enough affinity, but without compromising the infectivity of the virus.

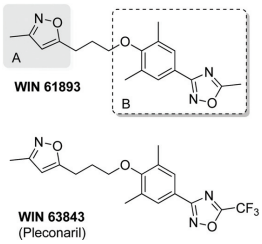

Scheme 1 Molecular structures of two representatives WIN compounds highlighting the different structural units A and B.

The WIN framework in its simplicity consists of two rigid aromatic planar ring systems of isoxazole (unit A) and phenyloxadiazole (unit B) that are connected by a flexible propyloxy unit (Scheme 1). Based on earlier studies[10,11,25,28] the phenyloxadiazole ring system binds to the deeper end of the viral hydrophobic pocket and, consequently, the isoxazole ring located at the open end of the pocket was therefore chosen as the site for a linker unit that would reach out to the surface of the virus particle. This was accomplished by incorporating a carboxylic acid functionality at the 3-position of the isoxazole ring, to which a C-11 alkyl chain with a terminal hydroxyl group was then attached *via* an amide linkage (Scheme 2). Here, the amide group was also intended as an anchoring group that would hold the probe in place in the hydrophobic pocket. The optimal length provided by the C11-alkyl chain was determined by molecular modeling to be long enough for the linker unit to reach out from the mouth of the hydrophobic pocket to the viral capsid surface. The hydroxyl group at the end of the linker arm provided further linking to gold clusters or fluorescent dye labels *via* an ester bond formation (Scheme 2).

The synthesis of the probe (**2**) was accomplished by an amide coupling reaction of the carboxylic acid derivative[30] (**1**) with 11-amino-1-undecanol in dichloromethane in the presence of *N*-(3-dimethylaminopropyl)-*N*′-ethylcarbodiimide (EDC) coupling reagent and a catalytic amount of 1-hydroxybenzotriazole (HOBt) in good yield (Scheme 2). Subsequent Steglich esterification reaction with a *p*-mercaptobenzoic acid (pMBA) protected $Au_{102}(pMBA)_{44}$ cluster[31,32] or an azadioxatriangulenium dye molecule[33,34] in DCM in the presence of dicyclohexylcarbodiimide (DCC) and a catalytic amount of *N*,*N*-dimethylaminopyridine (DMAP) afforded the gold (**3**) and fluorescent dye (**4**) labeled probes (see the ESI† for details).

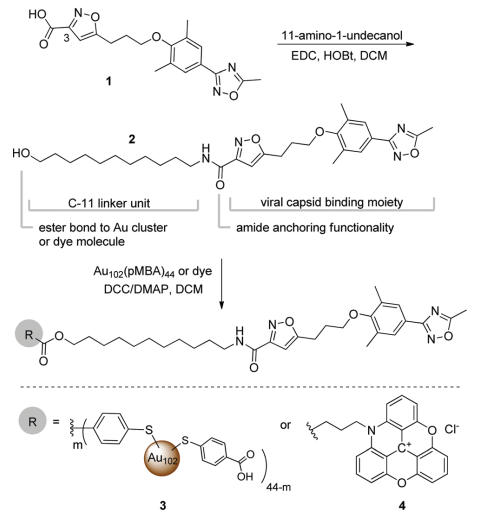

Scheme 2 Synthesis and molecular structures of the probes (**2**), and the gold (**3**) and dye (**4**) labels of the probe. C11-linker unit, viral capsid binding moiety, amide anchoring functionality and terminal hydroxyl group for further reactions with gold clusters or dye molecules *via* ester bond formation are highlighted. EDC = *N*-(3-dimethylaminopropyl)-*N*′-ethylcarbodiimide, HOBt = 1-hydroxybenzotriazole, DCC = dicyclocarbodiimide, DMAP = *N*,*N*-dimethylaminopyridine and DCM = dichloromethane.

Probe does not compromise the infectivity of enteroviruses

As the produced probes were based on an antiviral molecule that was however slightly modified, we wanted to study the toxicity of the probe (**2**) and derivative (**1**) to cells and whether they affected virus infectivity. All the assays were also carried out with Pleconaril for comparison. First, we studied the effects of each derivative and Pleconaril on cell viability without the virus. A 3-(4,5-dimethylthiazol-2-yl)-2,5-diphenyltetrazolium bromide (MTT) assay verified that the studied compounds or Pleconaril did not cause any significant cell death (Fig. S5D†).

In order to test the effects of the derivative (**1**), probe (**2**), gold probe (**3**), fluorescent probe (**4**) and Pleconaril on virus infectivity we applied several well characterized approaches. Firstly, we used the $TCID_{50}$ assay in which 50% tissue culture infective dose is quantified with and without the studied compounds. In this assay, the infection is followed to the end (end-point-dilution) so that the assay reveals the last dilution, which still contains infective particles. In the assay, the $TCID_{50}$ value is finally calculated from the dilutions. Strikingly, the assay revealed that the infectivity of the virus with the studied compounds was not affected (Fig. 1A and S5†). The infectivity was typically in the order of 10^{10} to 10^{11} $TCID_{50}$ per ml.

Next we studied the effect of the compounds on a shorter time scale, with a 24 h cytopathic effect (CPE) inhibition assay, which is also an established method to evaluate virus infectivity.[21] In this method the antiviral effect of the compound is quantified using a crystal violet uptake of the live cells. The quantification is performed with an optical plate reader and the cell viability is calculated from the optical reading values. This assay verified that there was a delay in infection rather than total inhibition of the infection (Fig. 1B): after 24 h, the probe (**2**) inhibited the infection of EV1 by 65%, that of CVA9 by 67% and that of CVB3 by 18%. Pleconaril seemed to have the strongest inhibitory effect on all viruses, whereas the studied derivatives showed a smaller effect at these earlier time points suggesting that the modification and derivatization of the Pleconaril core changed the activity only slightly. In addition, with CPE assay we quantified the half maximal inhibitory concentrations (IC_{50} (μM)) for each compound (Fig. S5A†). All the compounds showed the least effect on CVB3 as expected, since previously Pleconaril has been shown not to fit the Nancy strain of CVB3.[10] Consequently the IC_{50} values of CVB3 were considerably higher than that of EV1 or CVA9. This assay is based on a 24 h time point, which is why it differs from the end-point-titration result and shows more

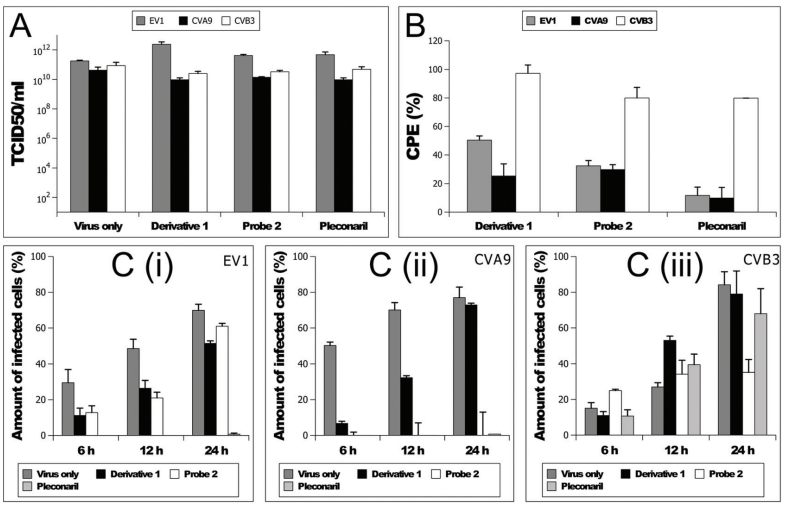

Fig. 1 Effects on virus infectivity. The concentration of studied compounds was 100 μM in all experiments. (A) Amount of infective particles ($TCID_{50}$ per ml) was calculated with end-point titration assay. Experiment was performed three times, and the means are shown (±standard errors (SE)). (B) Effects of short term infectivity were studied with 24 h CPE inhibition assay. In B the controls containing virus only the values were set to 100% CPE and with cells only to 0%. The results are shown as mean values from three different independent experiments (±SE). (C) The inhibiting effect was studied further on EV1 (i), CVA9 (ii) and CVB3 (iii) by quantifying the amount of infected cells at different time points.

similarity with the CPE result that similarly relies on a 24 h time point. Thus the IC_{50} measurement is not as reliable as a method to compare the real inhibitory effects between the different compounds used.

As the total number of infective particles revealed by end-point-dilution was not changed in the preparations with the probe (**2**), we wanted to study this delay in more detail with additional assays. Namely, confocal microscope immunofluorescence studies were performed to evaluate the kinetics of the infective pathways (Fig. 1C). We performed the infection by first binding the viruses on ice, then washing the unbound viruses at 0 °C before allowing the virus to enter the cell at 37 °C. This ensured the entry of the viruses into the cells *via* receptor binding and not by fluid phase uptake of the virus. First of all, there were no apparent differences in the amount of virus internalized in the cells with or without the probe suggesting that it did not interfere with receptor binding. The infected cells were evaluated after different time periods of 6 h, 12 h and 24 h post infection (p.i.). After these time periods, the cells were fixed and labeled using antibodies against the major capsid proteins. This allowed us to visualize the viruses first in cytoplasmic endosomes, and then, typically after 3 h or more, the massive production of new capsid proteins in the cytoplasm was seen as a widespread cytoplasmic stain that verified the start of replication. This way we were able to count the number of infected cells after various time periods and treatments. This capsid labeling may show the number of infected cells more sensitively than the previously described CPE assay. The analysis clearly revealed that the start of infection was delayed: normally, the number of infected cells increased quickly after 4 to 6 h p.i. Now, in the presence of the probe (**2**) or derivative (**1**) the same number of infected cells as in the control infection after 12 h was observed after 24 h with EV1 or CVA9. Thus, the virus treated with the probe seemed to remain longer in the endosomes and produced new viral proteins with a slower pace, but was still as infective as the native virus. All the methods described above showed an effect with EV1 and CVA9 but not with CVB3.

We also used a different method to measure cell viability at various time points with native viruses or viruses treated with studied compounds. This method is based on measuring ATP levels in cells. This measurement verified the results that were revealed by the more conventional infectivity tests: after a short period of incubation with cells, the studied compounds slowed down the CPE, but, after longer time periods, the viability was also lost in the viruses treated with the same compounds (Fig. S6†).

Probe increases mildly the stability of the viruses

One of the effects of antiviral drugs, and especially that of the drugs targeting the hydrophobic pocket, has been suggested to act *via* stabilization of the hydrophobic pocket.[35] If the drug molecule replaces the fatty acid in the hydrophobic pocket and remains there for a longer period of time, it could stabilize the

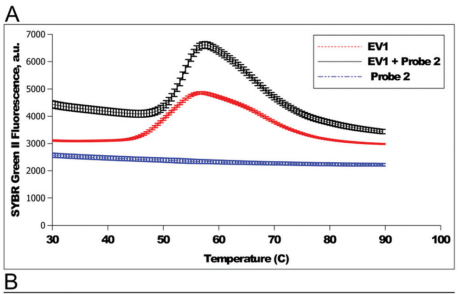

B

Tm (°C)	Virus only	Probe 2	Derivative 1	Pleconaril
EV1	50.5 (± 0.33)	53.5 (± 0.14)	55.0 (± 0.13)	56.0 (± 0.00)
CVA9	50.0 (± 0.14)	51.0 (± 0.14)	55.0 (± 0.00)	55.5 (± 0.00)
CVB3	44.5 (± 0.14)	44.5 (± 0.00)	44.5 (± 0.00)	47.5 (± 0.00)

Fig. 2 PaSTRy of EV1, CVA9 and CVB3 with derivative (**1**), probe (**2**) and Pleconaril. (A) Fluorescence curves of EV1 with and without the probe (**2**). Release of the RNA is detected as SYBR Green II Fluorescence. (B) T_m of all viruses and compounds (±SE from four independent experiments).

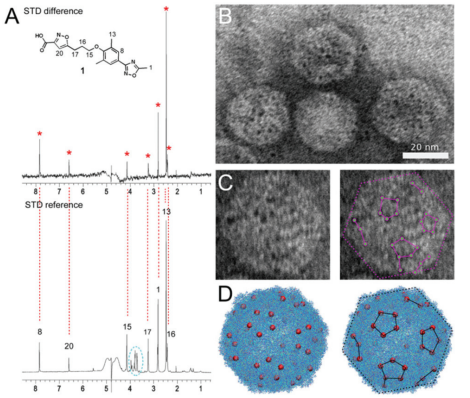

Fig. 3 Binding of the probe into the hydrophobic pocket. (A) STD NMR experiment of EV1 virus particle and derivative (**1**) in D_2O at 37 °C: The upper STD spectrum showing the signals of derivative (**1**) as a result of binding to EV1 (red asterisk) and the lower reference spectrum (with off-resonance irradiation only) of EV1 and derivative (**1**). Chemical shifts marked with cyan color are impurities in the virus sample. In (B) and (C) TEM images of column purified EV1–gold probe conjugates are shown. In (D) a model structure of EV1 with red spheres denoting the positions of the hydrophobic pocket entrances is shown. Orientation of the model structure is arranged to agree with the experimentally observed shape of the virus and the positions of gold probe (**3**) that are drawn in purple and in black.

virus particle by not allowing the dynamic changes to occur in the active areas during the uncoating event of the virus. This would also be seen as an increase in the stability upon warming the virus particles to non-physiological high temperatures.

Therefore, we studied the thermal stability of virus capsids with Particle Stability Thermal Release Assay (PaSTRy), where the release of viral RNA is promoted with gradual heating and detected with an SYBR Green II dye. PaSTRy was developed to investigate the dynamics of viral uncoating and viral stability.[23] We studied the stabilizing effects of compounds (**1**) and (**2**) always using Pleconaril as a comparison. The melting temperature (T_m) at which the purified virus releases its genome was determined for each virus (Fig. 2). These were 50.5 °C, 50 °C and 44.5 °C for EV1, CVA9 and CVB3, respectively. CVB3 was the most unstable during heating as it showed remarkable 5 degree difference compared to the other enteroviruses. The PaSTRy showed an increase in the stability of the viruses treated with the derivative (**1**), by increasing 2.5 and 4 degrees of the melting temperature for EV1 and CVA9, respectively. For the CVB3 derivative (**1**) had a negligible change in the melting temperature, yet, the probe (**2**) showed only a little effect on the thermal stability of all the studied viruses.

Probe binds to enteroviruses

In order to study the binding of the probe into the enterovirus hydrophobic pocket in solution, saturation transfer difference (STD)[36] NMR studies were performed. Due to the poor solubility of probe (**2**) in aqueous solution, the derivative (**1**) was used instead as a model compound to simulate the viral capsid binding moiety of the probe. A 5000-fold excess of derivative (**1**) over the hydrophobic binding sites of EV1 virus particle in 2 mM $MgCl_2$-PBS buffer in D_2O was used to record the STD NMR spectra with 1–3.5 s saturation times. The STD difference spectra showed distinct signals belonging to the derivative (**1**), which indicated binding to EV1 virus particle (Fig. 3A). A similar binding was also observed with a complementary transfer NOESY experiment, furthermore demonstrating the successful binding of the derivative (**1**) to EV1 virus capsid in aqueous solution (Fig. S4†).

The requirement and basis of an STD NMR experiment relies on the weak binding of the ligand to the virus particle.[37,38] Therefore, due to the rapid exchange between the bound and the free ligand, magnetization from the virus particle is transferred to the bound ligand and can only be detected when the bound ligand is released back to the solution. Hence, the STD NMR measurement gives both evidence of the derivative (**1**) binding to the virus particle, as well as, demonstrates the dynamic nature of the binding process.

Gold cluster and fluorescent dye conjugates bind to virus capsids

The binding of the gold cluster probe (**3**) to the virus capsid was monitored by TEM (Fig. 3B, C and S7†). The gold probe (**3**) was mixed with purified viruses in PBS containing 2 mM $MgCl_2$ at 37 °C to allow conjugation with the virus particles. We performed 1 h incubation to evaluate the extent of binding. The

gold–virus conjugate was placed on a TEM grid with or without negative staining and the binding was monitored directly under a microscope. TEM revealed that gold cluster probes bound to EV1 and CVA9 capsids forming pentamer-like symmetries (Fig. 3B, C and S7A, B†). The gold probes (**3**) usually occupied only a small fraction of the total 60 hydrophobic pockets. In order to remove the excess gold from the preparations, we used Sephacryl S-300 column purification based on size exclusion. After the column purification we could still see similar binding of scattered gold clusters to EV1 virus confirming that the binding of the gold probes (**3**) to virus was strong enough to withstand short elution of the virus conjugate preparation with buffer. TEM analysis of CVB3 (Fig. S7C†) did not show a similar kind of binding in pentamer-like symmetries than EV1 and CVA9, as expected.

In addition to TEM analysis, we studied whether the addition of the gold cluster probe (**3**) had any effect on the infectivity of the viruses. Similar to what was observed with compounds (**1**) and (**2**), the gold probe (**3**) delayed the infection rather than inhibit it altogether (Fig. S5C†). There was no difference in the number of infected virus particles based on the end-point-titration assay (Fig. S5B†).

Additionally, we used the fluorescent probe (**4**) in order to follow the enteroviruses in cells (Fig. 4A). Conjugation of the fluorescent probe (**4**) to the virus particles was done similarly as described above with the gold probe (**3**). The fluorescent probe–virus mixture was extensively dialyzed before adding on cells in order to avoid the loosely bound fluorescent probe (**4**) with viruses. In addition, we fixed the cells and labeled the viruses with antibodies against capsid proteins in order to follow the viruses with another method as well in case the dye would come off the virus at some point. The antibody labeling of the viruses verified that the virus was indeed present in the virus–fluorescent probe conjugate and no loose dye was entering the endosomes. Also, separate control experiments with the fluorescent probe (**4**) without the virus verified that the dye did not accumulate in endosomes without the virus (Fig. S8†). During the first hours of virus entry into the cells, the virus capsid label and the fluorescent probe (**4**) were only present in the cytoplasmic vesicles colocalizing together well, as expected.

We have shown earlier that EV1 and CVA9 capsids remain in the endosomes, whereas typically at 3 h p.i. and later, virus replication is observed as the resulting high cytoplasmic accumulation of newly made capsid proteins.[39,40] For both native viruses and virus–fluorescent probe conjugates, the number of infected cells increased rapidly after 6, 12 and 24 h. However, as observed with the other infectivity methods, the virus–fluorescent probe conjugates remained for a longer time in the vesicles before the start of replication. The quantitation of the infected cells after different time points showed that the virus–fluorescent dye conjugates always showed 30% less infected cells at every time point (Fig. 4B).

The fluorescent probe (**4**) comes off the virus by dissociating most probably due to the opening of the virus (Fig. 4C). This is a gradual process, which happens in endosomes as the

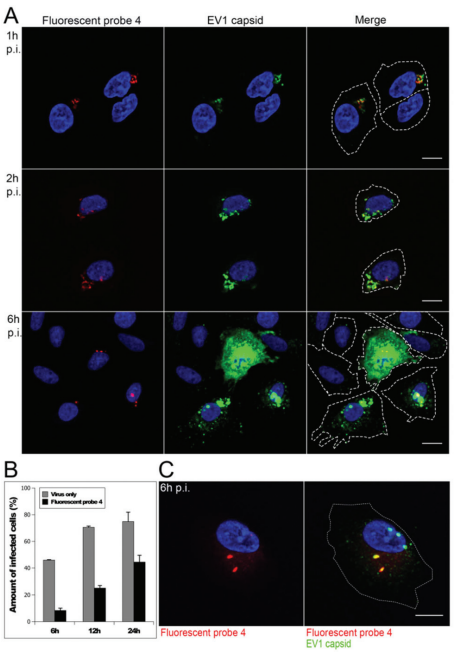

Fig. 4 Fluorescent probe (**4**) conjugated to EV1 and internalized into cells. (A) The internalization of the virus–fluorescent probe conjugate was followed from 1 h to 6 h. Fluorescent probe (**4**) was seen in the same vesicular structures than EV1 capsid label (green). Scale bars 10 μm. (B) The amount of infected cells was calculated at different time points p.i. from confocal microscope images. (C) Fluorescent probe (**4**) leaked from the endosomes to cell cytoplasm after 6 h of infection. Scale bar 10 μm.

virus capsids themselves do not leak from the endosomes to the cytoplasm. Thus, the dissociated fluorescent probe (**4**) is first located inside the endosomes, and then leaks through the endosomal membrane as time passes. Even though the leaking from the endosomes starts from 6 h onwards, these are the real rate limiting steps in the viral infection, and the possible delay in the uncoating and/or release will greatly postpone the outcome of the infection. The release of the viral genome from the endosomes is one important rate limiting step in enterovirus infection, and any delay in uncoating may lower the probability.

Live imaging of the fluorescent probe (**4**) conjugated to EV1 in cells showed high values of the fluorescent probe in endosomes, but clearly lower amounts after longer incubation times suggesting that a separation of the dye from the virus had occurred (Fig. S9†). The loose dye was observed in the cytoplasm nearby the endosomes after 6 and 8 h but the level of the fluorescent signal was already very faint after 12 to 24 h

(Fig. S10†). This further demonstrates the dynamic nature of the fluorescent probe (**4**) binding.

Modeling of the hydrophobic pocket

In order to understand the differences between the interactions of probe (**2**) with EV1, CVA9 and CVB3 we examined the structures of their hydrophobic pockets and analyzed the solvent accessible volumes using their crystal structures[4,18,41] (for details of the analysis method, see the ESI†). The overall structure of the pocket and arrangement of the surrounding protein chains in EV1 and CVA9 are similar while that of CVB3 is different (Fig. 5). There is a direct "main entrance" into the pocket in all of the three viruses and in addition a narrower "side entrance". The main entrance into the pocket is the most open in EV1 with an opening of at least 6 Å for the whole pocket (Fig. S11†). Thus, there is enough space for the probe (**2**) to enter into the pocket fully. For CVA9 there is a narrow 1 Å gap in the main entrance at the center of the pocket (Fig. S11B†), but otherwise the surface is well open and the pocket is large enough for the probe, especially if the dynamic effects of the capsid might open the small closure in the way in. Most importantly, the direct entrance to the pocket in CVB3 is significantly more closed at the center of the pocket.

The structure of the side entrance is also favoring EV1, and especially CVA9, in possible binding of probe molecules (Fig. 5A and B). First, the average width of the side route is the narrowest in CVB3 for all of the three viruses (Fig. 5C). Second, the side entrance is the farthest from the actual pocket in CVB3 as compared to EV1 and CVA9. Both these factors indicate that replacing the fatty acid and binding of the probe in CVB3 are more difficult than in EV1 and CVA9. By looking at the general structure of the pocket, the binding properties of the probe molecules on EV1 and CVA9 are expected to be very similar. Analyzing the binding properties of EV1 and CVA9 more closely reveals that the aromatic rings of the probe (**2**) molecule have reasonably good possibilities to bind to the pocket in both viruses, but the possibilities for anchoring the amide functional group (shown in Scheme 2) into the bottom of the main entrance are much better in CVA9 compared to EV1. The minor static structural differences in the dimensions of the entrances of EV1 and CVA9 are most probably becoming negligible as the dynamics of the virus capsids are taken into account.

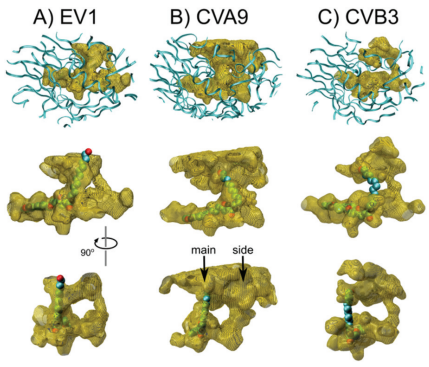

Fig. 5 Space-filling models of the hydrophobic pocket with the nearby protein chains shown (top panels), with probe (**2**) inserted inside for EV1, CVA9 and CVB3 (center and bottom panels). The center and bottom illustrations show the same pocket with about 90 degree rotation.

Discussion

We have developed a novel probe targeting the hydrophobic pockets of selected enteroviruses but without compromising the infectivity of the virus. As far as we know, this is the first study to specifically label and visualize the pocket by using both gold nanoclusters and a fluorescent dye as visualizing tags. Probes that have been recently designed for enteroviruses have been suggested to act as antiviral agents.[3,10,29,42] However, probes that replace the natural hydrophobic moiety, but do not compromise the infectivity and uncoating of the virus, could also act as potential markers and tools to study the function of the hydrophobic pocket.

The probe developed here is a derivative of Pleconaril, which was originally designed to fit the pocket and stabilize the capsid and thus act as an antiviral.[12] The results observed here with the new derivatives of Pleconaril suggest that the derivatization has probably changed the binding ability of the modified Pleconaril moiety as they all showed a very similar change on virus infection compared to original Pleconaril: a delayed infection but no lowering of the final infectivity. Pleconaril was first designed against rhinoviruses, for which it shows a good inhibitory effect on virus replication, but also several other enteroviruses, such as CVB1, CVB5, and CVA9 have been shown to be sensitive to Pleconaril.[10] Since then, several modifications of Pleconaril have been designed showing varying antiviral effects, and thus suggesting variations in the pocket structure.[43] Here, the derivative (**1**) was synthesized by modifying the structure of WIN 61893 to (1) provide a link to gold clusters or a fluorescent dye, and to (2) provide an anchoring group that would hold the probe in place at the open end of the hydrophobic pocket *via* hydrogen bonding. The stability of the virus-conjugations with gold clusters and a fluorescent dye was verified by column purification of the unbound gold and extensive dialysis of the unbound dye.

In our study we tested three different enteroviruses belonging to the same HEV B subgroup of enteroviruses, namely EV1, CVA9 and CVB3 Nancy strain. Pleconaril was already shown earlier not to fit into the hydrophobic pocket of the Nancy strain of CVB3 due to amino acid substitutions of Ile1092 to Leu or Ile1092 to Met.[10,43] This was also observed as high IC_{50} values in *in vitro* studies and as low protective efficacy in mouse models.[10] CVB3 Nancy strain thus acted as a good nega-

tive control in our study, as it did not show good binding of the gold probe (**3**) to this virus in TEM. In concordance with this, our probes (**1** & **2**) based on Pleconaril could not change the melting temperature of the Nancy strain.

TEM results of EV1 and CVA9 suggested that only some of the 60 possible hydrophobic pockets may be replaced by our probe at any given time. Presently, there is no information on how well the hydrophobic pockets are occupied by fatty acids. The most thorough study was performed on bovine enterovirus with mass spectrometry of the fatty acids found in the virus structure.[6] That study showed some variation in the repertoire of the used fatty acids, the palmitic acid being the most used fatty acid suggesting that it is the best length for the pocket structure. Yet, there is no direct information whether all the pockets are normally occupied by fatty acids and whether all of them or only some pockets close to the uncoating site are emptied during uncoating. There is a consensus in the field that the occupancy of the pockets by the pocket factors has a definite role in capsid stabilization.[6,8,44] Without any direct proof and only a few tools to study the pocket factors, the function and significance of the pocket has remained elusive so far.

Importantly, our TEM results suggested that some exchange between our probe and the natural fatty acid in the pocket might occur, as this exchange did not lead to an empty virus. However, whether the sites that more easily exchange the fatty acid with our probe are close to the hotspot of the uncoating, remains to be studied. Another alternative is of course that some pockets are naturally empty and our probe would fit those empty sites more easily. The studies that we performed using STD and trNOESY NMR gave more understanding on the dynamic nature of the binding and release of the pocket factor. Namely, the NMR methods used in this study are based on dynamic binding and release of the probe from the virus. That is the only way the virus may magnetize the small probe that is then measured after release from the hydrophobic pocket in the experiment. The NMR results thus indicate that there is most likely some dynamic exchange of the pocket factor in the hydrophobic pocket. Previously, the binding of another Pleconaril derivative was also studied with this same method by Benie *et al.*[36] However, the specific binding of the tested drug, REPLA 394, to the hydrophobic pockets of the virus capsid was demonstrated using competition STD titration experiments with a more potent viral inhibitor (WIN 52084). Here, in our study, we were able to directly see the magnetization of the probe and could thus confirm its binding to the virus. Since the testing of all derivatives by STD NMR was impossible due to solubility issues, it is possible that some differences might occur in the binding affinity. However, considering the very similar behavior of all derivatives in their effects on infectivity, those differences may remain small.

The dynamic binding and release of the pocket factor may be one result of capsid breathing. Capsid breathing has been studied with different picornaviruses, *e.g.* poliovirus,[45] HRV14, HRV16,[7,46] swine vesicular disease virus[47] and CVA9. In addition, breathing has been detected with other ssRNA viruses such as some of the noda-[48] and tetraviruses.[49] It was shown for HRV14 by cryo EM, and further explored by MD simulation, that during the breathing procedure VP4 and N-terminus of VP1 extrude the capsid temporarily.[7] Similarly, cryo EM reconstruction of the poliovirus 1 has shown VP1 outside the capsid for the native virus close to the 2-fold axis where the uncoating has been shown to occur.[45] Thus, the capsid breathing is an important part of the virus dynamics and under specific circumstances may lead to the uncoating process of the virus, and further, to virus replication.[9,26,50] The capsid binding inhibitors have been shown to stabilize the virus particles. Mechanistically this may occur by decreasing the breathing of the virus capsid, which has been verified by mass spectroscopy (MC-MS and MALDI-MS).[26,50]

The stability of the enterovirus structure is reflected in its melting temperature. This method has been used more recently for virus capsid binding probes also.[3,51,52] While the extent of increase is difficult to extrapolate directly to the real inhibition of infection, it is a convenient way to monitor the effects of drugs on the viruses and compare the viruses with each other. The new (four 3-(4-pyridyl)-2-imidazolidinone derivatives) capsid inhibitor molecules were shown to increase the melting temperature of EV71 by 2–4 degrees and that of EVD68 with Pleconaril by 4 degrees.[3,51] This increase with EV71, however, was preceded by a lengthy 24 h to 72 h incubation with a high amount of inhibitor used (200 μM). For native enteroviruses the melting temperature vary between 44.5 and 58 degrees.[3] The foot and mouth disease virus has been shown to be more thermolabile.[53] This may be due to the lack of hydrophobic pocket altogether in FMDV, and argues for the importance of the pocket factor in enteroviruses. The enteroviruses are very robust viruses and can remain for a long time at room temperature or repeated freeze–thaw cycles without losing infectivity (data not shown). We observed with our probes that they increased the stability of the studied enteroviruses by increasing the melting temperature by 1 to 4.5 degrees (Fig. 4). However, this only delayed the infection cycle of EV1 and CVA9 roughly by 12 and 24 h, respectively, but did not inhibit the infection (Fig. 1).

Changes in the infectivity upon antiviral treatment have been studied using various methods, which make it difficult to compare the results between different studies. Schmidtke *et al.*[21] established a high-throughput CPE inhibitory assay for CVB3, influenza A virus and herpes simplex virus type 1. This method is based on a crystal violet uptake of the cells, and the results show a good correlation between the antiviral activity determined by CPE-inhibitory assays and more conventional plaque reduction assay. In addition, FACS analysis or qRT-PCR have also been used by others to evaluate infectivity.[52] However, various infection times between 24 h and 72 h have been used.[54,55] In addition to the method used, it is valid to consider for how long the infectivity is measured. Measurements after short periods of incubation with the antiviral may show temporarily high inhibition results, which however, may not be relevant anymore after 2 or 3 days of incubation. Here, we set out to explore three well established methods to

measure infectivity and also followed the outcome during several days of infection, namely CPE inhibition assay, $TCID_{50}$ assay and confocal microscopy, to evaluate the appearance of newly synthesized viral proteins. We saw some inhibition at first, but only a delay in the infection. This was also verified by an independent assay on cell viability that detects the cellular ATP levels (Fig. S6†).

Previous studies by others have shown very little effect of Pleconaril on poliovirus 1 (IC_{50} >300 μM) and EV71 (>300 μM).[55] However, better inhibition was observed in case of several enterovirus strains including EV5, CVA9, CVB1 and CVB5 (IC_{50} range of 0.001 to 1.05 μM) in the CPE assay.[10] Our results with CVA9 and EV1 suggest that despite the preliminary inhibition, virus infection is not really halted, only delayed. Most of the studied derivatives in the previous literature have been proven inactive against CVB3 (IC_{50} >6.1 μM), which is along the lines of our results. Recently more powerful virus inhibitors were developed against HEV71. One of the newest antivirals inhibited the HEV71 CPE with IC_{50} of 25 pM, which is the best recently reported inhibitor.[3]

Conclusions

Our results thus confirm that Pleconaril derivatives (**1–4**) studied here can be used to label hydrophobic pockets of enteroviruses EV1 and CVA9. This specified modification of Pleconaril framework combined with gold nanoclusters or a fluorescent dye afforded low effectiveness as antivirals without compromising the infectivity of the virus but, instead, provided a new imaging tool for these enteroviruses. Altogether, three different methods verified that our probes bound to the hydrophobic pocket of EV1. TEM showed that only some pockets were easily targeted by the gold probe. This may reflect the normal breathing of the virus and its activity in replacing the present pocket factor by the used probe. We cannot exclude the possibility that some pockets would not be normally empty and act as targets for our probe. The confocal observations of the fluorescent probe (**4**) showed high labeling of the cytoplasmic endosomes, and a high degree of colocalization of the fluorescent probe and the viruses labeled by an independent method by antibodies. The follow up of the virus–fluorescent probe conjugate showed decrease of labeling in the endosomes, and a temporary increase of cytoplasmic free labeling of the fluorescent probe (**4**), demonstrating that, indeed, this probe is dynamic and is able to detach from the virus. Being a hydrophobic dye and a probe, it can freely diffuse through the endosome and other cellular membranes and show a dynamic release probably upon the uncoating event of the virus, or also through a normal exchange of capsid breathing and spontaneous release. The delay in the dye release and in the viral infection suggests that slight stabilization of the virus due to the probe slows down the uncoating process. This may be taken into account and hopefully helps us to image the viruses in live assays with slower kinetics. The probes developed here thus offer us the opportunity to possibly study the functionality of the pocket in real life, in real uncoating events.

Acknowledgements

This research is supported by the Academy of Finland (VM: grant 257125, HH: grant 266492) and TEKES FiDiPro project NOVAC. The computational resources were provided by CSC – The Finnish IT Center for Science. We thank J. Koivisto for helping with spectroscopic characterization of the probes, M. Pettersson for discussions, and T. J. Sørensen and B. W. Laursen (University of Copenhagen) for providing the azadioxatriangulenium dye.

References

1 T. J. Tuthill, E. Groppelli, J. M. Hogle and D. J. Rowlands, *Curr. Top. Microbiol. Immunol.*, 2010, **343**, 43–89.
2 D. Hober and P. Sauter, *Nat. Rev. Endocrinol.*, 2010, **6**, 279–289.
3 L. De Colibus, X. Wang, J. a. B. Spyrou, J. Kelly, J. Ren, J. Grimes, G. Puerstinger, N. Stonehouse, T. S. Walter, Z. Hu, J. Wang, X. Li, W. Peng, D. J. Rowlands, E. E. Fry, Z. Rao and D. I. Stuart, *Nat. Struct. Mol. Biol.*, 2014, **21**, 282–288.
4 D. J. Filman, M. W. Wien, J. A. Cunningham, J. M. Bergelson and J. M. Hogle, *Acta Crystallogr., Sect. D: Biol. Crystallogr.*, 1998, **54**, 1261–1272.
5 D. J. Filman, R. Syed, M. Chow, A. J. Macadam, P. D. Minor and J. M. Hogle, *EMBO J.*, 1989, **8**, 1567–1579.
6 M. Smyth, T. Pettitt, a. Symonds and J. Martin, *Arch. Virol.*, 2003, **148**, 1225–1233.
7 J. K. Lewis, B. Bothner, T. J. Smith and G. Siuzdak, *Proc. Natl. Acad. Sci. U. S. A.*, 1998, **95**, 6774–6778.
8 M. Oliveira, R. Zhao, W. Lee, M. Kremer, I. Minor, R. Rueckert, G. Diana, D. Pevear, F. Dutko and M. Mckinlay, *Structure*, 1993, **1**, 51–68.
9 M. S. Smyth and J. H. Martin, *Mol. Pathol.*, 2002, **55**, 214–219.
10 D. C. Pevear, T. M. Tull, M. E. Seipel and J. M. Groarke, *Antimicrob. Agents Chemother.*, 1999, **43**, 2109–2115.
11 G. D. Diana, *Curr. Med. Chem.:Anti-Cancer Agents*, 2003, **2**, 1–12.
12 S. M. Abdel-Rahman and G. L. Kearns, *Antimicrob. Agents Chemother.*, 1998, **42**, 2706–2709.
13 M. Oikarinen, S. Tauriainen, S. Oikarinen, T. Honkanen, P. Collin, I. Rantala, M. Mäki, K. Kaukinen and H. Hyöty, *Diabetes*, 2012, **61**, 687–691.
14 P. Kankaanpää, L. Paavolainen, S. Tiitta, M. Karjalainen, J. Päivärinne, J. Nieminen, V. Marjomäki, J. Heino and D. J. White, *Nat. Methods*, 2012, **9**, 683–689.
15 M. Karjalainen, N. Rintanen, M. Lehkonen, K. Kallio, A. Mäki, K. Hellström, V. Siljamäki, P. Upla and V. Marjomäki, *Cell. Microbiol.*, 2011, **13**, 1975–1995.

16 V. Marjomäki, T. Lahtinen, M. Martikainen, J. Koivisto, S. Malola, K. Salorinne, M. Pettersson and H. Häkkinen, *Proc. Natl. Acad. Sci. U. S. A.*, 2014, **111**, 1277–1281.
17 J. J. T. Seitsonen, S. Shakeel, P. Susi, A. P. Pandurangan, R. S. Sinkovits, H. Hyvonen, P. Laurinmaki, J. Yla-Pelto, M. Topf, T. Hyypia and S. J. Butcher, *J. Virol.*, 2012, **86**, 7207–7215.
18 S. Shakeel, J. J. T. Seitsonen, T. Kajander, P. Laurinmäki, T. Hyypiä, P. Susi and S. J. Butcher, *J. Virol.*, 2013, **87**, 3943–3951.
19 G. Abraham and R. J. Colonno, *J. Virol.*, 1984, **51**, 340–345.
20 P. Ruokola, E. Dadu, A. Kazmertsuk, H. Häkkänen, V. Marjomäki and J. a. Ihalainen, *J. Virol.*, 2014, **88**, 8504–8513.
21 M. Schmidtke, U. Schnittler, B. Jahn, H. Dahse and a. Stelzner, *J. Virol. Methods*, 2001, **95**, 133–143.
22 J. Z. Porterfield and A. Zlotnick, *Virology*, 2010, **407**, 281–288.
23 T. S. Walter, J. Ren, T. J. Tuthill, D. J. Rowlands, D. I. Stuart and E. E. Fry, *J. Virol. Methods*, 2012, **185**, 166–170.
24 V. Marjomäki, V. Pietiäinen, H. Matilainen, P. Upla, J. Ivaska, L. Nissinen, H. Reunanen, P. Huttunen, T. Hyypiä and J. Heino, *J. Virol.*, 2002, **76**, 1856–1865.
25 A. M. De Palma, I. Vliegen, E. De Clercq and J. Neyts, *Med. Res. Rev.*, 2008, **28**, 823–884.
26 N. Reisdorph, J. J. Thomas, U. Katpally, E. Chase, K. Harris, G. Siuzdak and T. J. Smith, *Virology*, 2003, **314**, 34–44.
27 V. L. Giranda, G. R. Russo, P. J. Felock, T. R. Bailey, T. Draper, D. J. Aldous, J. Guiles, F. J. Dutko, G. D. Diana, D. C. Pevear and M. McMillan, *Acta Crystallogr., Sect. D: Biol. Crystallogr.*, 1995, **51**, 496–503.
28 Y. Zhang, A. a. Simpson, R. M. Ledford, C. M. Bator, S. Chakravarty, G. a. Skochko, T. M. Demenczuk, A. Watanyar, D. C. Pevear and M. G. Rossmann, *J. Virol.*, 2004, **78**, 11061–11069.
29 H. J. Thibaut, A. M. De Palma and J. Neyts, *Biochem. Pharmacol.*, 2012, **83**, 185–192.
30 K. Salorinne, T. Lahtinen, V. Marjomäki and H. Häkkinen, *CrystEngComm*, 2014, **16**, 9001–9009.
31 P. D. Jadzinsky, G. Calero, C. J. Ackerson, D. A. Bushnell and R. D. Kornberg, *Science*, 2007, **318**, 430–433.
32 K. Salorinne, T. Lahtinen, S. Malola, J. Koivisto and H. Häkkinen, *Nanoscale*, 2014, **6**, 7823–7826.
33 T. J. Sørensen, E. Thyrhaug, M. Szabelski, R. Luchowski, I. Gryczynski, Z. Gryczynski and B. W. Laursen, *Methods Appl. Fluoresc.*, 2013, **1**, 25001.
34 E. Thyrhaug, T. J. Sørensen, I. Gryczynski, Z. Gryczynski and B. W. Laursen, *J. Phys. Chem. A*, 2013, **117**, 2160–2168.
35 S. K. Tsang, P. Danthi, M. Chow and J. M. Hogle, *J. Mol. Biol.*, 2000, **296**, 335–340.
36 A. J. Benie, R. Moser, E. Bäuml, D. Blaas and T. Peters, *J. Am. Chem. Soc.*, 2003, **125**, 14–15.
37 A. Bhunia, S. Bhattacharjya and S. Chatterjee, *Drug Discovery Today*, 2012, **17**, 505–513.
38 C. Rademacher and T. Peters, *Top. Curr. Chem.*, 2008, **273**, 183–202.
39 M. Huttunen, M. Waris, R. Kajander, T. Hyypiä and V. Marjomäki, *J. Virol.*, 2014, **88**, 5138–5151.
40 P. Upla, V. Marjomäki, L. Nissinen, C. Nylund, M. Waris, T. Hyypiä and J. Heino, *J. Virol.*, 2008, **82**, 1581–1590.
41 J. D. Yoder, J. O. Cifuente, J. Pan, J. M. Bergelson and S. Hafenstein, *J. Virol.*, 2012, **86**, 12571–12581.
42 A. M. Macleod, D. R. Mitchell, N. J. Palmer, H. Van De Poël, K. Conrath, M. Andrews, P. Leyssen and J. Neyts, *ACS Med. Chem. Lett.*, 2013, **4**, 585–589.
43 M. Schmidtke, P. Wutzler, R. Zieger, O. B. Riabova and V. A. Makarov, *Antiviral Res.*, 2009, **81**, 56–63.
44 N. Ismail-Cassim, C. Chezzi and J. F. E. Newman, *J. Gen. Virol.*, 1990, **71**, 2283–2289.
45 Q. Li, a. G. Yafal, Y. M. Lee, J. Hogle and M. Chow, *J. Virol.*, 1994, **68**, 3965–3970.
46 U. Katpally, T.-M. Fu, D. C. Freed, D. R. Casimiro and T. J. Smith, *J. Virol.*, 2009, **83**, 7040–7048.
47 M. A. Jiménez-Clavero, A. Douglas, T. Lavery, J. A. Garcia-Ranea and V. Ley, *Virology*, 2000, **270**, 76–83.
48 B. Bothner, X. F. Dong, L. Bibbs, J. E. Johnson and G. Siuzdak, *J. Biol. Chem.*, 1998, **273**, 673–676.
49 B. Bothner, D. Taylor, B. Jun, K. K. Lee, G. Siuzdak, C. P. Schlutz and J. E. Johnson, *Virology*, 2005, **334**, 17–27.
50 Roy and C. B. Post, *Proc. Natl. Acad. Sci. U. S. A.*, 2012, **109**, 5271–5276.
51 Y. Liu, J. Sheng, a. Fokine, G. Meng, W.-H. Shin, F. Long, R. J. Kuhn, D. Kihara and M. G. Rossmann, *Science*, 2015, **347**, 71–74.
52 P. Plevka, R. Perera, M. L. Yap, J. Cardosa, R. J. Kuhn and M. G. Rossmann, *Proc. Natl. Acad. Sci. U. S. A.*, 2013, **110**, 5463–5467.
53 V. Rincón, A. Rodríguez-Huete, S. López-Argüello, B. Ibarra-Molero, J. M. Sanchez-Ruiz, M. M. Harmsen and M. G. Mateu, *Structure*, 2014, **22**, 1560–1570.
54 V. a. Makarov, O. B. Riabova, V. G. Granik, P. Wutzler and M. Schmidtke, *J. Antimicrob. Chemother.*, 2005, **55**, 483–488.
55 H. J. Thibaut, P. Leyssen, G. Puerstinger, A. Muigg, J. Neyts and A. M. De Palma, *Antiviral Res.*, 2011, **90**, 213–217.

III

CVB1 SHOWS STRAIN SPECIFIC DIFFERENCES INFECTING CELLS LEADING TO DIFFERENT OUTCOMES

by

Mari Martikainen, Amirbabak Sioofy-Khojine, Heikki Hyöty and Varpu Marjomäki

Manuscript

CVB1 shows strain specific differences infecting cells leading to different outcomes

Mari Martikainen*, Amirbabak Sioofy-Khojine[†], Heikki Hyöty[†], Varpu Marjomäki*[#]

*Department of Biological and Environmental Science, Nanoscience Center

University of Jyväskylä, PO Box 35, FI-40014 Jyväskylä, Finland

[†]School of Medicine

University of Tampere, Tampere, Finland

[#]To whom the correspond should be addressed. E-mail: varpu.s.marjomaki@jyu.fi

ABSTRACT

Coxsackievirus B1 (CVB1) is a member of the species B enteroviruses from the *Picornaviridae* family. CVB1 has been recently pinpointed as a risk factor for type I diabetes. However, there is no information on the infectious entry pathway of CVB1. Here, we have studied the entry of CVB1-ATCC prototype and two clinical isolates, strains CVB1-CDC7 and CVB1-CDC11. CVB1-ATCC showed start of uncoating 45 min p.i. in endosomes leading to efficient genome replication 4 h p.i. and viral protein production by 5 h p.i. Both isolates showed lower efficiency in uncoating in comparison to the prototype strain. However, CDC11 started the uncoating process already at 15 min p.i. which increased mildly until 4 h p.i. whereas CVB1-CDC7 uncoated in a low efficiency during the whole 4 h period. All studied CVB1 strains entered cytoplasmic endosomes that were not colocalizing with EEA1, transferrin or LAMP1, suggesting that they do not use the clathrin-dependent pathway. Inhibition of the cellular vacuolar ATPase pump had no effect on entry or infection, further suggesting that CVB1 strains do not enter acidic endosomes and are not dependent on acidic pH for uncoating. The drug experiments pinpointed Rac1 and Na^+/H^+ exchanger as important regulators of the entry for all of the strains but not dynamin, further suggesting that a macropinocytic-like pathway is used. Interestingly, inhibition of the Vacuolar ATPase pump, dynamin and PI3K showed an increase in CVB1-CDC7 and CVB1-CDC11 infection suggesting that these factors might be inhibitory to infection. Furthermore, the overexpression and downregulation of the ESCRT proteins Hrs and Vps4, respectively, had an inhibitory effect on all strains suggesting, that they enter ESCRT-driven multivesicular structures, and that their biogenesis is important for efficient uncoating and infection. The results altogether suggest that CVB1 strains follow a very similar macropinocytic entry pathway to non-acidic endosomes, which has already been suggested for two other members of the enterovirus B group: echovirus 1 (E1) and coxsackievirus A9 (CVA9). Clinical isolates CDC7 and 11 show interesting differences in the kinetics of entry giving insight to their differences in the cellular responses.

INTRODUCTION

Coxsackievirus B1 (CVB1) is a member of the species B Enteroviruses (EV-B) belonging to the family of *Picornaviridae.* EV-Bs are part of the Enterovirus genus, which consists of EV-Bs A to J and Rhinoviruses A to C. In addition to CVB1, EV-B species contains other coxsackieviruses from CVB2 to 6, coxsackievirus A9 (CVA9), over 30 serotypes of echoviruses and 20 other serotypes of EV-Bs. Enteroviruses are non-enveloped viruses with icosahedron-shaped capsids enclosed within 7 500 bp-long positive sense single-stranded RNA genome. The protein capsid is approximately 30 nm in diameter and consists of 60 protomers formed by the four viral proteins VP1-4. VP1, 2 and 3 are expressed on the outer surface of the capsid while VP4 is on the inner surface (1).

EV-B can cause diseases ranging from mild respiratory symptoms to more severe acute and chronic infections, such as aseptic meningitis, myocarditis and pancreatitis. Various studies have associated EV infection with type 1 diabetes (T1D) (2–4). EV RNA has been detected using *in situ* hybridization on post-mortem autopsy samples from patients who died of T1D or infants who died of coxsackievirus infection (5). In addition, enterovirus VP1 has been found in insulin containing islets by immunohistochemistry studies of T1D decreased organ donors (6). CVBs have been shown to be capable of infecting human pancreatic islets *in vitro* (7–9). Importantly, CVB1 has been shown to cause induction of islet beta-cell autoimmunity that possibly leads to the onset of T1D (10). Furthermore, CVB1 has been observed to cause insulitis and islet damage in samples collected from patients with fatal CVB1 infections (3). Furthermore, CVB1 has revealed strain specific difference in inducing immune response in purified human peripheral blood mononuclear cells and in isolated human pancreatic islet (11, 12). Two clinical isolates of CVB1, CVB1-CDC7 and CVB1-CDC11, were studied in their ability to induce pro-inflammatory and adaptive cytokines (11). CVB1-CDC11 showed to be highly immunogenic inducing high interferon α and interferon γ responses, while CVB1-CDC7 was weakly immunogenic showing no increase of these interferons. Moreover, immunoregulatory cytokine, interleukin-10, responses were also induced in similar matter (11). Anagandula et al. (2014) studied the differences of CVB1-CDC11 and CVB1-CDC7 in isolated human pancreatic islets. The

strongly immunogenic strain CVB1-CDC11 was more cytolytic in islet cells than CVB1-CDC7 (12). These results suggested that there may be some differences in the infection kinetics between CVB1 strains.

All CVB viruses have been shown to bind to the coxsackie and adenovirus receptor (CAR) that is mostly expressed in the tight junctions (TJ) of polarized cells and tissues (13). In polarized cells, viruses do not have free access to CAR due to its location, and therefore they need another receptor for the primary attachment. CVB1, CVB3 and CVB5 have been shown to use the decay-accelerating factor (DAF) as their primary receptor (14). After attachment, DAF plays an important role in transferring the virus from the apical surface to the tight junctions and initiating the cell signaling events (15). CAR has been shown to act in virus internalization and in inducing the conformational changes in the virus capsid that ultimately lead to the release of the viral RNA to start replication (16). Due to CAR expression in pancreas, brain and heart muscle tissues, the CVB group from EV-Bs have the potential to infect these tissues, thereby leading to acute and chronic diseases (13, 17).

We have previously shown that echovirus 1 (E1) and CVA9 infect cells via a specific entry pathway that seems to be generic for the enterovirus B group: these viruses internalize via a macropinocytic uptake into cytoplasmic endosomes that mature into non-acidic multivesicular bodies (MVBs) (18, 19). In these MVBs, viruses uncoat, leading to the release of their genome into the cytoplasm, and the replication and production of new viral particles. As both EV1 and CVA9 share several characteristics with CVB3 in their entry pathway (15, 20, 21), and there was no previous knowledge of the entry pathway of CVB1, we set out to study whether the clinically relevant CVB1 would also share these characteristics. Furthermore, as there was an interesting difference in the severity and immune response elicited by the field isolates CVB1-CDC7 and 11, we wanted to study if anything in the entry pathway would explain their differences.

We show here that the entry of CVB1 viruses bear great resemblance to the infectious entry pathway of the EV-B species EV1 and CVA9. Concerning the timeable of uncoating and replication however, the CDC7 isolate differs from the other by showing inefficient and early uncoating with less dependence on targeting to the multivesicular bodies that was shown to promote efficient infection also of E1 and CVA9.

MATERIALS AND METHODS

Cell culture, viruses and antibodies. Experiments were performed using human lung adenocarcinoma, human alveolar basal epithelial cell line A549, or human cervix adenocarcinoma cell line HeLa MZ (a kind gift from Marino Zerial, Max Planck Institute, Dresden). The cell lines were obtained from American type cell culture (ATCC) and maintained in Dulbecco's modified Eagle's medium (DMEM, Invitrogen) containing 5% or 10% fetal bovine serum (FBS) supplemented with Glutamax (Invitrogen) and penicillin and streptomycin (P/S). All of the cell culture solutions and supplements were obtained from Gibco ThermoFisher Scientific (USA).

CVB1-ATCC was obtained from ATCC and propagated in green monkey kidney (GMK) cells. CVB1-CDC7 and CVB1-CDC11 strains were clinical isolates collected originally from Argentina by Center of Disease and Control (CDC), Atlanta, GA. They were first propagated in HeLa MZ cells and then in GMKs. Virus was released from infected GMKs by freeze-thawing and concentrated by centrifugation (30 000 rpm for 3 h) into a 40% sucrose cushion as previously described (22). Infectivity of the produced virus stock was assayed with an end-point titration method to determine the 50% tissue culture infective dose (TCID50). For all infection studies, the culture medium was supplemented with 1% FBS. CVB1 was used in the multiplicity of infection (MOI) of 2 typically leading to 30 to 50% infection in A549 cells and 100% infection in HeLa MZ cells.

The following antibodies were used: polyclonal rabbit antiserum against CVB (kindly provided by Roivainen's lab), monoclonal antibodies (MAbs) against enteroviruses (clone 5-D8/1) NCL-ENTERO (Novocastra), dsRNA (J2, English & Scientific Consulting Kft.), early endosome antigen 1 (EEA1; BD Transduction Laboratories), Lysosomal-associated membrane protein 1 (Lamp1; Santa Cruz Biotechnology), and DAF binding CD55-FITC (Beckman Coulter), MAb detecting coxsackie and adenovirus receptor (CAR, clone RmcB, Millipore), mouse gammaglobulin (Jackson ImmunoResearch) and β-2-microglobulin (Santa Cruz Biotechnology). Alexa Fluor 488 (AF-488) and AF-555-labeled anti-mouse and anti-rabbit secondary antibodies prepared in goat, and the ProLong Gold Antifade reagent, were obtained from Invitrogen.

Single-step growth curve experiment. Confluent monolayers of A549 cells were infected with CVB1-ATCC using a MOI of 10. Excess virus was washed with HEPES-Hanks buffer followed by incubation in DMEM (supplemented with 2% BSA and P/S) at +37˚C. The new virus progeny was released by three times freeze-thawing. The supernatant was collected after centrifugation, and it was further purified using filters of 0.2µm pore size. Virus titers of time-course infections were identified using standard 50% tissue culture infectivity dose (TCID50) assays.

Immunofluorescence and confocal microscopy. For immunofluorescence experiments, A549 and HeLa MZ were grown on coverslips to subconfluency. CVB1 was bound to cells on ice for 60 min in DMEM (supplemented with 1% FBS) followed by washes with 0.5% bovine serum albumin (BSA)-phosphate buffered saline (PBS) and incubation in DMEM (1% FBS) at +37°C. CVB1-infected cells were fixed with 4% paraformaldehyde (PFA) for 30 min at room temperature (RT). Fixed cells were permeabilized with 0.2% Triton X-100 for 5 min at RT, labeled with selected antibodies diluted in 3% BSA-PBS, and mounted in ProLong Gold antifade reagent with 4’-6-diamidino-2-phenylindole. Labeled cells were examined using an Olympus microscope IX81 with a Fluo-View-1000 confocal setup.

Neutral red-CVB1 assay. Neutral red-CVB1 (NR-CVB1) was produced as described previously (23). In brief, monolayers of GMK cells were infected with CVB1 in the presence of 30 µg/ml of NR (Merck). NR-CVB1 virus was released after 20 h incubation by freeze-thawing three times and harvested by centrifugation. The supernatant, rich in NR-CVB1, was used as described above in the immunofluorescence protocol in the dark. At the indicated time points, cells were taken to RT and exposed to bright light for 10 min and transferred back to +37°C. As a control, NR-CVB1-infected cells were not exposed to light. After 8 h p.i., the cells were fixed and labeled for immunofluorescence, as described above. To evaluate the effects on infectivity, the amount of CVB1 VP1 expressing cells was quantified. The infectivity of the control samples kept in the dark was set as 100% while the infectivity of the light treated sample prior to infection was set to 0%.

Chemical inhibitors. A549 cells were incubated in DMEM (1% FBS) and 5-(N-ethyl-N-isopropyl) amiloride (EIPA, 100 µM, Sigma), NSC23766 (100 µM, Tocris Bioscience), IPA-3 (5 µM, Tocris Bioscience), Dyngo-4a (12.5 µM, ABCAM), Nocodazole (33 µM, Sigma), Bafilomycin A1 (50 nM,

Calbiochem), Bisindolylmaleimide (5 µM, AH Diagnostics) and Wortmannin (100 nM, Calbiochem). Using a 3-(4,5-dimethyl-2-thiazolyl)-2,5-diphenyl-2H-tetrazolium bromide (MTT) cell growth assay (Millipore) according to the manufacturer's instructions, it was confirmed that the concentrations used did not cause significant cytotoxicity in the A549 cells. The chemical inhibitors were added to cells 30 min prior to infection. After virus binding and washing, inhibitors were added again to cells so that they would be present during the entire infection cycle. At 8 h p.i., cells were fixed and labeled for immunofluorescence and the amount of infected cells was quantified by the high amount of newly synthesized cytoplasmic capsid proteins.

Transfections. Sub-confluent A549 cells were transfected with Lipofectamine-3000 reagent according to the manufacturer's instructions. The cells were used for CVB1 infection after 48 h of plasmid expression. The Hrs-WT-GFP was obtained from Sylvie Urbe (Cellular and Molecular Physiology, University of Liverpool, Liverpool, United Kingdom) and the VPS4-E235Q-GFP from Harald Stenmark (Department of Biochemistry, Institute of Cancer Research, the Norwegian Radium Hospital, Oslo, Norway).

Data analysis and processing of the microscopy data. To measure the intensity of dsRNA, an open source software platform, BioImageXD (24), was used. Altogether, 18 random wide-field images from three independent experiments were taken from all different time points and the total intensity of images was quantified using the following BioImageXD protocol. First, a lower threshold value was set to exclude all the unspecific labeling from the uninfected control images. Secondly, connected component labeling was set to remove objects with less voxels than four. Finally, the sum intensity of the segmented objects was analyzed.

Statistical testing. Unpaired t-test with Welch's correction was performed to evaluate the statistical significances of pairwise compared samples.

RESULTS

CVB1 strains differ in infection kinetics

We determined the infection kinetics of CVB1 strains including the time of uncoating and replication. First, single-step growth kinetics of CVB1-ATCC was studied in A549 cells (Fig. 1A). Cell monolayers were infected with CVB1 (MOI 10) and the virus yields were quantified at different time points using the $TCID_{50}$ method. The production of new viral progeny started 5 h p.i. (Fig. 1A).

Kinetics of active viral replication of CVB1 strains was studied by labeling the newly produced double-stranded RNA (dsRNA) which is the intermediate byproduct of picornavirus replication with monoclonal J2 antibody, and quantifying the intensity of the secondary fluorescent label (AF-555) at different time points of infection (Fig. 1B). CVB1-ATCC showed some dsRNA structures as soon as 3 h p.i.; however, their number and intensity increased more clearly at 4 h p.i. (Fig. 1C), thereby suggesting that replication started properly around that time. The intensity and volume of dsRNA structures was remarkably high around 6 h p.i. (Fig. 1C). At the replication starting point 3 to 4 h p.i., the CVB1 capsid signal was still mostly in cytoplasmic endosomes in the perinuclear region of the cell (Fig. 1C). After 6 h p.i., the production of newly synthesized virus capsid protein was evident by the strong diffuse cytoplasmic staining around the cytoplasm (Fig. 1C).

In order to study the kinetics of uncoating, we labeled the viruses with photosensitive Neutral red (NR) as described previously for poliovirus (23). Upon a short exposure to light, NR rapidly inactivated the RNA by causing irreversible cross-linking of the genome, thus inhibiting the virus infection process. Light treatment after virus uncoating no longer inactivated the virus and the infection proceeded normally (Fig. 1D). The cells were infected with CVB1-NR-ATCC, -CDC7 and -CDC11, and at various time points they were treated with light. Light treatments at 15 and 30 min p.i. blocked the NR-CVB1-ATCC infection almost entirely, suggesting that uncoating had not yet occurred in the endosomes (Fig. 1D, i). Light treatment at 45 min or 1 h p.i. resulted in ~40-50% CVB1-ATCC infection of the cell population demonstrating that uncoating had begun prior to the light treatment. Uncoating continued up to 4 h p.i. thereafter, showing progressive amounts of virus uncoating. The light

treatment of NR-CVB1-CDC11 at 15 min p.i resulted in 45% CVB1-CDC11 infection indicating that the uncoating process had started (Fig. 1D, iii). Light treatment at 4 h p.i. resulted in 60% of infection suggesting that the uncoating process still continued at later time points. CVB1-CDC7 showed low amount of uncoating infected cells were observed after 4 h p.i. light treatment (Fig. 1D, ii).

CVB1 strains follow a macropinocytic-like entry

In order to investigate what cellular regulators CVB1 uses in its entry, we used several drugs that disturb various entry pathways (Table 1). We and others have shown previously that other members of EV-B viruses internalize via macropinocytosis into cytosolic vesicles (25). Therefore, we tested various drugs linked with macropinocytosis but also others linked with the clathrin pathway.

It has shown previously that E1 and CVB3 are dependent on protein kinase Cs (PKCs). PKCs form a family of serine-threonine kinases which are involved in many cellular signalling pathways (15, 21, 26–28). Hence, we studied the importance of PKC using down regulative chemical Bisindolylmaleimide. The effect on virus infection was studied by quantifying the amount of cells expressing the newly formed CVB1 VP1 with immunofluorescence. Bisindolylmaleimide decreased the CVB1 infection in statistically significant manner (Fig. 3A). There were no clear differences between the strains.

Rac1 and Na^+/H^+ exchanger are both important regulatory factors of macropinocytotic entry. Rac1 is a Rho GTPase regulating the dynamics of actin (29), and Na^+/H^+ exchanger has an important function in regulating local sodium and proton concentrations (30). Earlier we have shown that both of these factors play an important role in E1 and CVA9 entry (18, 19, 28, 31). Therefore, NSC23766 (Rac1 inhibitor) and EIPA (Na^+/H^+ inhibitor) were used to downregulate these factors. (Fig. 2A). For all the strains, EIPA blocked the infection totally, leaving the CVB1-ATCC in the large vesicular structures in the cell periphery (Fig. 2B) ($p < 0.0001$). Also, NSC23766 decreased the infection in a statistically significant manner ($p < 0.0001$) and halted the CVB1-ATCC infection in the vesicular structures similar to EIPA, but to the perinuclear region on the cell periphery, although in smaller vesicles than seen with EIPA treatment (Fig. 2B). Altogether, these results suggest that both inhibitors allowed entry

CVB1-ATCC but stopped the infection at the endosomal step. Normally, newly produced viral proteins are detected as a cytoplasmic stain throughout the cell (Fig. 2B) This was not unexpected, as we have already found the same blockage of E1 and CVA9 entry in endosomes with these inhibitors for (19, 32).

We also studied the effect of phosphoinositide-3-kinase (PI3K) downregulation with the help of an other chemical inhibitor: Wortmannin. PI3Ks are signal transducer enzymes that function by phosphorylating the inositol ring of phosphatidylinositol (33). PI3K activation has often been associated with a clathrin-independent pathway (34). However, our earlier studies with E1 and CVA9 showed that the PI3K inhibition did not efficiently inhibit their infection. Similarly, here we found a minor inhibitory effect with CVB1-ATCC infection using Wortmannin ($p = 0.003$) (Fig. 2A, i), and no inhibitory effect with CVB1-CDC7 and CVB1-CDC11 suggesting that PI3K was not important in CVB1 entry (Fig. 2A, ii, iii). However, PI3K inhibition increased the CVB1-CDC7 and CVB1-CDC11 infection by 20-30% ($p = 0.0058$ and $p < 0.0001$, respectively).

As Rac1 was involved in CVB1 entry, we wanted to study the possible involvement of Pak1 in CVB1 entry as it is known to be regulated downstream to Rac1. Furthermore, it has been shown to regulate actin dynamics in some cases of macropinocytosis (35). However, the specific Pak1 inhibitor IPA-3 did not have any effect on the CVB1-ATCC and CVB1-CDC11 infection (Fig. 2A, i, iii). CVB1-CDC7 infection was mildly decreased by 18% ($p = 0.005$) with Pak1 inhibition (Fig. 2A, ii). The Pak1 independence has previously been seen with CVA9 (19), but not with E1 and CVB3 (25), suggesting that there are differences with respect to entry, even among closely related enterovirus species.

We also studied the involvement of dynamin using a specific small molecule inhibitor: Dyngo-4a. Dynamin is a GTPase, which has a substantial role in scission of the newly formed vesicles. The functionality of Dyngo-4a was first tested with transferrin uptake. Dyngo-4a inhibited successfully the recycling of transferring halting it in cytoplasmic vesicles close to the plasma membrane (data not shown). Dynamin inhibition showed no inhibitory effect on any of the CVB1 strains (Fig. 2A), suggesting that the vesicle scission caused by dynamin is not important in their entry pathway. However, downregulation of dynamin showed a mild, but statistically significant, increase in CVB1-

CDC7 and CVB1-CDC11 infection (Fig. 2A, ii, iii) ($p = 0.0077$ and $p = 0.0036$, respectively). In conclusion, as dynamin is required for clathrin mediated entry this result also further implies that endocytic uptake through the clathrin pathway was not used by the studied CVB1 strains.

CVB1 strains do not enter acidifying endosomes along the clathrin pathway

We wanted to determine whether the CVB1s were targeted to early or late endosomes, as the chemical inhibitors suggested macropinocytic entry. The infection was stopped at different time points from 15 min p.i. to 2 h p.i., followed by fixation and immunofluorescence labeling using the CVB1 capsid antibody and either early endosome antigen 1 antibody (anti-EEA1, Fig. 3A) or lysosomal-associated membrane protein 1 antibody (anti-LAMP1, Fig. 3C). The CVB1-ATCC infection for 15 min p.i. showed CVB1-ATCC in vesicular structures in the cell periphery. In addition, the vesicles after 2 h of infection were closer to the perinuclear region, as expected. Double labeling with the endosomal markers and anti VP1 showed no colocalization of the virus with early or late endosomal markers, thereby strongly suggesting that CVB1-ATCC does not use the canonical entry pathway. The association between the CVB1-CDC7 and CVB1-CDC11 strains to the endosomal markers is still to be studied in more detail. However, the preliminary colocalization studies with transferrin and EEA1 already suggest that these strains do not enter the acidic endosomal pathway (Fig. 3B)

Since the role of the early and late endosomes did not seem to be important in CVB1 infection, we investigated whether transition from peripheral to perinuclear endosomes via microtubules was necessary for successful infection. Therefore, we used the microtubule-depolymerizing agent Nocodazole in order to block the transfer of endosomes to the cell center. The A549 cells were treated with Nocodazole and infected with CVB1 for 8 h. The depolymerization effect was confirmed by labeling the microtubules with antibodies against beta-tubulin. Depolymerization of the microtubules did not show any decreasing effect on CVB1-CDC11 infection (Fig. 2A, iii). Whereas, Nocodazole treatment showed a mild, but statistically significant ($p = 0.0086$ and $p = 0.002$) decrease in CVB1-ATCC and CVB1-CDC7 infection by approximately 30% (Fig. 2A, i, ii). Even if the infection proceeded almost normally during microtubule depolymerization, the small reduction in infection still suggests that the transfer of CVB1-ATCC and CVB1-CDC11 to the perinuclear regions promotes the

infection. Also, that microtubules would also have a direct or indirect role in the biogenesis of endosomal vesicles bearing CVB1 cannot be excluded.

As microtubules seemed to have some significance role during the CVB1-ATCC and CVB1-CDC7 infection, we next tested whether the low pH played any role in the infection. We used the vacuolar ATPase pump inhibitor, Bafilomycin A1, in order to block acidification of the endosomes as described before (36). Previously, it has been shown with endosomal pH sensitive fluorescent-labeling that Bafilomycin A1 increases the pH, thus indicating the chemical inhibitor is functioning successfully (37). Vacuolar ATPase is involved in generating the acidic luminal environment of the endosomes and lysosomes. Moreover, it has a role in the formation of acidic endosomal vesicles (36). Quantification of infected cells showed clearly that Bafilomycin A1 had no inhibitory effect on any of the CVB1 strains (Fig. 2A). However, Bafilomycin A1 increased CVB1-CDC7 and CVB1-CDC11 infection drastically by 30-50% in statistically significant manner ($p < 0.0001$). This result was repeated in HeLa cells, in addition to A549 cells, with similar results (data not shown). Altogether, these results indicate that endosomal acidification is not important for CVB1 infection and further proves that CVB1 entry is not associated with canonical entry pathway.

Multivesicular bodies are needed for efficient uncoating and infection of CVB1

As biogenesis of MVBs has been indicated in our earlier studies to be necessary for E1 and CVA9 infectivity, we wanted to explore if this was also the case with CVB1 strains (19, 32, 38). The biogenesis of MVBs relies on endosomal sorting complexes required for transport (ESCRT) machinery that consists of four large ESCRT complexes, each comprised of several proteins: ESCRT-0, -I, -II and –III. By overexpressing or downregulating two of the important proteins, the hepatocyte growth factor regulated tyrosine kinase substrate (Hrs) and VPS4, respectively, we can disturb ESCRT function leading to the prevention of intraluminal vesicle (ILV) formation, and thus the formation of MVBs (39).

We transfected HeLa MZ cells to overexpress Hrs (wt-Hrs). Hrs is a subunit of ESCRT-0 complex binding to the ubiquitinated receptor molecules. In addition, it recruit other ESCRT components to the

site (38). Wt-Hrs-GFP and a control GFP plasmid were used for this purpose. 48 h post-expression cells were infected with CVB1. Cells were then fixed 8 h p.i. and CVB1 VP1 was detected by immunofluorescence studies (Fig. 4A). WT-Hrs-GFP overexpression caused a statistically significant ($p<0.0001$ and $p=0.0075$) decrease in CVB1-ATCC and CVB1-CDC11 infections, respectively. CVB1-ATCC infection was decreased approximately for 72% and CVB1-CDC11 by 52%. Whereas, CVB1-CDC7 infection was not affected by a statistically significant manner ($p > 0.018$). In CVB1-ATCC positive cells, the capsid label was found contained in vesicle-like structures (see Fig. 4A for the enhanced image) since no diffuse cytoplasmic label of newly formed capsids was found in the infected cells. This showed a clear blockage in virus replication with no new virus production in the cells overexpressing Hrs. This phenomenon has also seen with CVA9 (19).

In addition to Hrs, we used the dominant negative mutant of VPS4 (DN-VPS4) to investigate the importance of MVBs. VPS4 is AAA-ATPase protein. The function of VPS4 is required in the release of ESCRT-III from endosome-limiting membrane and promotion of the ILV formation. HeLa MZ cells were transfected with VPS4-E235Q-GFP plasmid, as described above, and the effect on CVB1 VP1 production was analyzed (Fig. 5B). As seen with WT-Hrs, DN-VPS4 also had a strong, statistically significant ($p<0.0001$) effect on CVB1-ATCC and CVB1-CDC11 infections, decreasing it by approximately 67% and 78%. CVB1-CDC7 infection was not decreased by statistically significant manner. Furthermore, as with the overexpression of Hrs, CVB1-ATCC capsid was only found in vesicle-like structures 8 h p.i., thus indicating a blockage of entry into the vesicles (Fig. 4A, enhancement). Therefore, these results indicate that CVB1-ATCC and CVB1-CDC11 requires ESCRT-driven MVBs for successful infection. Interestingly, DN-VPS4 did not have statistically significant effect on CVB1-CDC7 suggesting that ESCRT driven MVBs are not needed for efficient CVB1-CDC7 infection.

DISCUSSION

CVB1 is a clinically relevant EV-B virus that mostly causes meningoencephalitis, myocarditis, sepsis, and hepatitis (40, 41) infections in young children and infants (42, 43). It is one of the most frequently

isolated enteroviruses in the USA (43), Korea (44), India (45), Tunisia (46), Western Germany (47) and Finland (10, 48). CVB1 has recently been identified as a risk factor, contributing to the onset of T1D (10, 48). The first findings making a T1D connection appeared around 1970 and 1980 when Jenson et al. (3) and Gamble et al. (2) isolated viral antibodies in the serum samples of patients suffering from islet insulitis. More recently, CVBs have been shown to cause damage to the β-cells of T1D diagnosed patients, in particular (49). Furthermore, the presence of neutralizing antibodies of different CVB serotypes in Finnish and several European populations has shown CVB1 to be a risk factor contributing to the onset of T1D (10, 48).

Due to the importance of CVB1, information has been accumulated on its molecular epidemiology (50), detection techniques using clinical samples have been developed (51, 52), and studies have been undertaken of virus antibody surveys in different populations (10, 48). However, very little information is available about the infectious entry pathway of the virus. In earlier studies, only CVB1 receptor binding has been described in some detail (14, 53), but the relevant details of the entry pathway of the virus have remained unexplored.

We show further that CVB1 infects non-polarized cells in strain specific manner. We studied the entry of CVB1-ATCC and two clinical isolates CVB1-CDC7 and CVB1-CDC11. These strains have already shown remarkable differences in peripheral blood mononuclear cells and islet cell mediated immunogenicity (11, 12). Also here CVB1 revealed strain specific differences in infection kinetics. First, the initiation of replication and production of new viral progeny was studied with the ATCC strain. Efficient replication was seen around 4 h p.i. and the formation of new infectious particles was evident from 5 h p.i. onwards, which is slightly slower than what we observed for CVA9 and E1 (19, 54, 55). As is the case with E1 and CVA9, CVB1 uncoating starts only after virus successfully enters into the cytoplasmic endosomal structures. CVB1-ATCC uncoating was first observed after 45 min to 1 h but it peaked at 2 to 3 h p.i., (19, 54, 55). This suggests that similar to E1 and CVA9, CVB1-ATCC need to enter the endosomes prior to an efficient uncoating event. Interestingly CVB1-CDC11 seemed to be much quicker compared to the other strains, by showing the first signs of efficient uncoating already at 15 min p.i. The early uncoating is observed also with other EVs e.g. poliovirus. Brandenburg et al. (23) showed by live-cell imaging that the poliovirus RNA release occurs at 10 min p.i. close to the

plasma membrane (100 nm to 200 nm away). In addition, Coyne et al. (56) observed that poliovirus uncoating occurs inside the cytoplasmic vesicles. In contrast to CVB1-CDC11 and CVB1-ATCC, CVB1-CDC7 uncoated much later, starting at 4 h p.i.

We wanted to study further the different entry routes of CVB1 strains. The entry route of CVB1-ATCC and CVB1-CDC11, and to some extent CVB1-CDC7, is remarkably similar to other EV-B viruses, E1 and CVA9, and that it bears many similarities to CVB3 as well (25). Generally, the cell entry pathway of CVB1 does not follow the canonical clathrin-dependent pathway according to several criteria: 1) CVB1 entry is not dynamin-dependent; 2) the virus does not enter into early or late endosomes of the clathrin pathway; and 3) the inhibition of acidification has no effect on CVB1 infectivity.

By contrast, CVB1 entry seems to be regulated by several factors, recently, associated with macropinocytosis. Those include PKCs. The chemical inhibitors of PKC decreased the infectivity of CVB1 strains. For E1 it has been shown that PKCs are important factors in E1-receptor complex transport to the cytoplasmic vesicles (18, 26). This suggests that also with CVB1-ATCC, CVB1-CDC7 and CVB1-CDC11, the transport to the cytoplasmic vesicles is needed for the efficient infection. Other important factors in CVB1 entry include Rac1 and Na^+/H^+ exchanger. EIPA is known to have specific inhibitory effects during both the uptake and replication of picornaviruses (18, 19, 28, 57–59) making the interpretation of its effects difficult. However, if administered at the same time during virus entry, the early blocking effect is already effective before the replication phase (19). Even if the inhibition of the Na+/H+ exchanger by EIPA has been a canonical way to inhibit macropinocytosis, its inhibition may also occur indirectly through its inhibitory effect on Rac1 activation, as has been shown previously (30). In our previous studies, Rac1 was clearly needed for the efficient infection of E1 and CVA9 (18, 19) but it is also shown to have an important role in CVB3 movement from the apical surface to the tight junction in polarized CaCo-2 cells (15). Interestingly, the effects of Rac1 and Na^+/H^+ exchanger on E1, CVA9 and CVB1-ATCC entry relate mainly on the endosomal step than on the plasma membrane, suggesting some differences with the entry mechanism of CVB3 (15). Another similarity between the members of enterovirus group B lies in - lack of effect on PI3K inhibition for E1 (18), CVA9 (19) and CVB3 (21).

The lack of colocalization of internalized enterovirus with EEA1 or LAMP1 was shown earlier for E1 (18, 26, 32) and CVA9 (19). Here we showed a similar result in CVB1 entry. In addition, as with other EV-Bs, CVB1 infection was not sensitive to the inhibition of the vacuolar ATPase pump with Bafilomycin A1, demonstrating that CVB1 does not need acidic endosomes for successful infection. This was already seen with other enteroviruses, such as E1, CVA9, CVB3 and poliovirus (19, 20, 28), further suggesting that acidity does not play a role in the EV-B infectious lifecycle. Interestingly, Bafilomycin A1 treatment increased CVB1-CDC7 and CVB1-CDC11 infection drastically, suggesting that low pH might not be beneficial for these viruses.

As already extensively studied using E1 (18) and CVA9 (19), the biogenesis of ESCRT-driven MVBs was required for successful CVB1-ATCC and CVB1-CDC11 infection. The results obtained from DNA transfections, both overexpression of the first component of the machinery (Hrs) and downregulation of the last component (Vps4), decreased CVB1-ATCC and CVB1-CDC11 infection greatly and accumulated CVB1-ATCC in cytoplasmic endosomes, indicating that CVB1 is not able to infect without the formation of MVBs. Previous results using E1 and CVA9 illustrated that these MVBs are non-acidic, thus differing from maturing endosomes in the conventional acidic pathway (32). Our present results suggest that, CVB1-ATCC and CVB1-CDC11 also infects via MVBs that are triggered during virus entry, and which do not rely on acidification. Interestingly, it seems CVB1-CDC7, which already showed much lower efficiency of infection, does not require the ESCRT-machinery for infection. The downregulation of VPS4 did not cause statistically significant decrease in the infectivity. These results further suggest that ESCRT driven MVBs are substantial for sufficient uncoating and infection of EV-Bs.

In conclusion, we have described here the infectious entry pathways of CVB1 strains into non-polarized A549 cells. The pathways of CVB1-ATCC and CVB1-CDC11 closely resembles E1, CVA9 and, in many respects, the CVB3 entry pathways studied earlier despite the fact that these viruses internalize via different cellular receptors (25). As for other EVBs, CVB1s enter the cells using macripinocytic entry, regulated by, PKC, Rac1 and Na+/H+ exchangers, but not by dynamin, Pak1 or PI3K. Furthermore, acidity is not required for their successful infection and they do not enter the early and late endosomes or lysosomes of the clathrin pathway. However, the CVB1-CDC7 strain showed a remarkable difference in the infection kinetics including the uncoating of the capsid. The low

efficiency of uncoating seems to be associated with minor dependency of ESCRT machinery and the biogenesis of multivesicular bodies. The CVB1-CDC11 was more heavily dependent on the ESCRT machinery and as it was shown to cause severe cellular destruction and stronger immune response in comparison to CVB1-CDC7 these results thus indicate MVBs as important for efficient unocating and infection. It will be important to study if the targeting of these isolates to MVBs is also different and less efficient for CVB1-CDC7.

REFERENCES

1. **Tuthill TJ**, **Groppelli E**, **Hogle JM**, **Rowlands DJ**. 2010. Picornaviruses, p. 43–89. *In* Current Topics in Microbiology and Immunology.

2. **Gamble DR**, **Kinsley ML**, **Fitzgerald MG**, **Bolton FRCPR**, **Taylorjj KW**. 1969. Viral Antibodies in Diabetes Mellitus. Br Med J **3**:627–630.

3. **Jenson AB**, **Rosenberg HS**, **Notkins AL**. 1980. Pancreatic islet-cell damage in children with fatal viral infections. Lancet **2**:354–8.

4. **Coppieters KT**, **Wiberg A**, **von Herrath MG**. 2012. Viral infections and molecular mimicry in type 1 diabetes. Apmis **120**:941–949.

5. **Ylipaasto P**, **Klingel K**, **Lindberg AM**, **Otonkoski T**, **Kandolf R**, **Hovi T**, **Roivainen M**. 2004. Enterovirus infection in human pancreatic islet cells, islet tropism in vivo and receptor involvement in cultured islet beta cells. Diabetologia **47**:225–239.

6. **Krogvold, L., Skog, O., Sundström, G., Edwin, B., Buanes, T., Hanssen, K. F., ... & Dahl-Jørgensen K**. 2015. Function of Isolated Pancreatic Islets From Patients at Onset of Type 1 Diabetes: Insulin Secretion Can Be Restored After Some Days in a Nondiabetogenic Environment In Vitro Results From the DiViD Study. Diabetes **64,**:2506–2.

7. **Frisk G**, **Diderholm H**. 2000. Tissue Culture of Isolated Human Pancreatic Islets Infected With Different Strains of Coxsackievirus B4: Assessment of Virus Replication and Effects on Islet Morphology and Insulin Release. Int J Exp Diabetes Res **1**:165–175.

8. **Roivainen M**, **Rasilainen S**, **Ylipaasto P**, **Nissinen R**, **Ustinov J**, **Bouwens L**, **Eizirik DL**, **Hovi T**, **Otonkoski T**. 2000. Mechanisms of Coxsackievirus-Induced Damage to Human Pancreaticβ - Cells 1. J Clin Endocrinol Metab **85**:432–440.

9. **Roivainen M**, **Ylipaasto P**, **Savolainen C**, **Galama J**, **Hovi T**, **Otonkoski T**. 2002. Functional impairment and killing of human beta cells by enteroviruses: The capacity is shared by a wide range of serotypes, but the extent is a characteristic of individual virus strains. Diabetologia **45**:693–702.

10. **Laitinen OH**, **Honkanen H**, **Pakkanen O**, **Oikarinen S**, **Hankaniemi MM**, **Huhtala H**, **Ruokoranta T**, **Lecouturier V**, **Andre P**, **Harju R**, **Virtanen SM**, **Lehtonen J**, **Almond JW**, **Simell T**, **Simell O**, **Ilonen J**, **Veijola R**, **Knip M**, **Hyöty H**. 2014. Coxsackievirus B1 Is Associated With Induction of beta-Cell Autoimmunity That Portends Type 1 Diabetes. Diabetes **63**:446–455.

11. **Hämäläinen S**, **Nurminen N**, **Ahlfors H**, **Oikarinen S**, **Sioofy-Khojine A-B**, **Frisk G**, **Oberste MS**, **Lahesmaa R**, **Pesu M**, **Hyöty H**. 2014. Coxsackievirus B1 reveals strain specific differences in plasmacytoid dendritic cell mediated immunogenicity. J Med Virol **86**:1412–1420.

12. **Anagandula M**, **Richardson SJ**, **Oberste MS**, **Sioofy-Khojine A-B**, **Hyöty H**, **Morgan NG**, **Korsgren O**, **Frisk G**. 2014. Infection of human islets of langerhans with two strains of coxsackie B virus serotype 1: Assessment of virus replication, degree of cell death and induction of genes involved in the innate immunity pathway. J Med Virol **86**:1402–1411.

13. **Cohen CJ**, **Shieh JT**, **Pickles RJ**, **Okegawa T**, **Hsieh JT**, **Bergelson JM**. 2001. The coxsackievirus and adenovirus receptor is a transmembrane component of the tight junction. Proc Natl Acad Sci U S A **98**:15191–15196.

14. **Shafren DR**, **Bates RC**, **Agrez M V**, **Herd RL**, **Burns GF**, **Barry RD**. 1995. Coxsackieviruses B1, B3, and B5 use decay accelerating factor as a receptor for cell attachment. J Virol **69**:3873–7.

15. **Coyne CB**, **Bergelson JM**. 2006. Virus-induced Abl and Fyn kinase signals permit coxsackievirus entry through epithelial tight junctions. Cell **124**:119–131.

16. **Milstone AM**, **Petrella J**, **Sanchez MD**, **Mahmud M**, **Whitbeck JC**, **Bergelson JM**. 2005. Interaction with coxsackievirus and adenovirus receptor, but not with decay-accelerating factor (DAF), induces A-particle formation in a DAF-binding coxsackievirus B3 isolate. J Virol **79**:655–60.

17. **Oikarinen M**, **Tauriainen S**, **Honkanen T**, **Vuori K**, **Karhunen P**, **Vasama-Nolvi C**, **Oikarinen S**, **Verbeke C**, **Blair GE**, **Rantala I**, **Ilonen J**, **Simell O**, **Knip M**, **Hyöty H**. 2008. Analysis of pancreas tissue in a child positive for islet cell antibodies. Diabetologia **51**:1796–1802.

18. **Karjalainen M**, **Kakkonen E**, **Upla P**, **Paloranta H**, **Kankaanpää P**, **Liberali P**, **Renkema GH**, **Hyypiä T**, **Heino J**, **Marjomäki V**. 2008. A Raft-derived, Pak1-regulated Entry Participates in 2 1 Integrin-dependent Sorting to Caveosomes. Mol Biol Cell **19**:2857–2869.

19. **Huttunen M**, **Waris M**, **Kajander R**, **Hyypiä T**, **Marjomäki V**. 2014. Coxsackievirus A9 Infects Cells via Nonacidic Multivesicular Bodies. J Virol **88**:5138–5151.

20. **Patel KP**, **Coyne CB**, **Bergelson JM**. 2009. Dynamin- and lipid raft-dependent entry of decay-accelerating factor (DAF)-binding and non-DAF-binding coxsackieviruses into nonpolarized cells. J Virol **83**:11064–11077.

21. **Delorme-Axford E**, **Sadovsky Y**, **Coyne CB**. 2013. Lipid raft- and SRC family kinase-dependent entry of coxsackievirus B into human placental trophoblasts. J Virol **87**:8569–81.

22. **Myllynen M**, **Kazmertsuk A**, **Marjomäki V**. 2016. A Novel Open and Infectious Form of Echovirus 1. J Virol **90**:6759–6770.

23. **Brandenburg B**, **Lee LY**, **Lakadamyali M**, **Rust MJ**, **Zhuang X**, **Hogle JM**. 2007. Imaging poliovirus entry in live cells. PLoS Biol **5**:1543–1555.

24. **Kankaanpää P**, **Paavolainen L**, **Tiitta S**, **Karjalainen M**, **Päivärinne J**, **Nieminen J**, **Marjomäki V**, **Heino J**, **White DJ**. 2012. BioImageXD: an open, general-purpose and high-throughput image-processing platform. Nat Methods.

25. **Marjomäki V**, **Turkki P**, **Huttunen M**. 2015. Infectious entry pathway of enterovirus B species. Viruses.

26. **Upla P**, **Marjomäki V**, **Kankaanpaa P**, **Ivaska J**, **Hyypiä T**, **F.G. VDG**, **Heino J**. 2004. Clustering Induces a Lateral Redistribution of 2 1 Integrin from Membrane Rafts to Caveolae and Subsequent Protein Kinase C-dependent Internalization. Mol Biol Cell **15**:625–636.

27. **Pietiäinen V**, **Marjomäki V**, **Upla P**, **Pelkmans L**, **Helenius A**, **Hyypiä T**. 2004. Echovirus 1 Endocytosis into Caveosomes Requires Lipid Rafts, Dynamin II, and Signaling Events. Mol Biol Cell **15**:4911–4925.

28. **Krieger SE**, **Kim C**, **Zhang L**, **Marjomäki V**, **Bergelson JM**. 2013. Echovirus 1 entry into polarized Caco-2 cells depends on dynamin, cholesterol, and cellular factors associated with macropinocytosis. J Virol **87**:8884–95.

29. **Bosco EE**, **Mulloy JC**, **Zheng Y**. 2009. Rac1 GTPase: A “Rac” of all trades. Cell Mol Life Sci **66**:370–374.

30. **Koivusalo M**, **Welch C**, **Hayashi H**, **Scott CC**, **Kim M**, **Alexander T**, **Touret N**, **Hahn KM**, **Grinstein S**. 2010. Amiloride inhibits macropinocytosis by lowering submembranous pH and preventing Rac1 and Cdc42 signaling. J Cell Biol **188**:547–563.

31. **Heikkilä O**, **Susi P**, **Stanway G**, **Hyypiä T**. 2009. Integrin αVβ6 is a high-affinity receptor for coxsackievirus A9. J Gen Virol **90**:197–204.

32. **Karjalainen M**, **Rintanen N**, **Lehkonen M**, **Kallio K**, **Mäki A**, **Hellström K**, **Siljamäki V**, **Upla P**, **Marjomäki V**. 2011. Echovirus 1 infection depends on biogenesis of novel multivesicular bodies. Cell Microbiol **13**:1975–1995.

33. **Amyere M**, **Payrastre B**, **Krause U**, **Van Der Smissen P**, **Veithen A**, **Courtoy PJ**. 2000. Constitutive macropinocytosis in oncogene-transformed fibroblasts depends on sequential permanent activation of phosphoinositide 3-kinase and phospholipase C. Mol Biol Cell **11**:3453–67.

34. **Araki N**, **Johnson MT**, **Swanson JA**. 1996. A role for phosphoinositide 3-kinase in the completion of macropinocytosis and phagocytosis by macrophages. J Cell Biol **135**:1249–1260.

35. **Dharmawardhane S**, **Schürmann a**, **Sells M a**, **Chernoff J**, **Schmid SL**, **Bokoch GM**. 2000. Regulation of macropinocytosis by p21-activated kinase-1. Mol Biol Cell **11**:3341–3352.

36. **Claque MJ**, **Urbe S**, **Aniento F**, **Gruenberg J**. 1994. Vacuolar ATPase Activity Is Required for Endosomal Carrier Vesicle Formation. J Biol Chem **269**:21–24.

37. **Rintanen N**, **Karjalainen M**, **Alanko J**, **Paavolainen L**, **Mäki A**, **Nissinen L**, **Lehkonen M**, **Kallio K**, **Cheng RH**, **Upla P**, **Ivaska J**, **Marjomäki V**. 2012. Calpains promote 2 1 integrin turnover in nonrecycling integrin pathway. Mol Biol Cell **23**:448–463.

38. **Raiborg C**, **Malerød L**, **Pedersen NM**, **Stenmark H**. 2008. Differential functions of Hrs and ESCRT proteins in endocytic membrane trafficking. Exp Cell Res **314**:801–813.

39. **Gruenberg J**, **Stenmark H**. 2004. The biogenesis of multivesicular endosomes. Nat Rev Mol Cell Biol **5**:317–323.

40. **Druyts-Voets E**, **Van Renterghem L**, **Gerniers S**. 1993. Coxsackie B virus epidemiology and neonatal infection in Belgium. J Infect **27**:311–316.

41. **Wang SM**, **Liu CC**, **Yang YJ**, **Yang HB**, **Lin CH**, **Wang JR**. 1998. Fatal coxsackievirus B infection in early infancy characterized by fulminant hepatitis. J Infect **37**:270–273.

42. **Wikswo ME**, **Khetsuriani N**, **Fowlkes AL**, **Zheng X**, **Peñaranda S**, **Verma N**, **Shulman ST**, **Sircar K**, **Robinson CC**, **Schmidt T**, **Schnurr D**, **Oberste MS**. 2009. Increased activity of Coxsackievirus B1 strains associated with severe disease among young infants in the United States, 2007-2008. Clin Infect Dis **49**:e44-51.

43. **Khetsuriani N1, Lamonte-Fowlkes A, Oberst S PM**. 2006. Enterovirus surveillance--United States, 1970-2005. MMWR Surveill Summ **Sep 15**:1–20.

44. **Kim H**, **Kang B**, **Hwang S**, **Hong J**, **Chung J**, **Kim S**, **Jeong Y-S**, **Kim K**, **Cheon D-S**. 2013. Molecular characteristics of human coxsackievirus B1 infection in Korea, 2008-2009. J Med Virol **85**:110–115.

45. **Kumar A**, **Shukla D**, **Kumar R**, **Idris MZ**, **Misra UK**, **Dhole TN**. 2012. Molecular epidemiological study of enteroviruses associated with encephalitis in children from India. J Clin Microbiol **50**:3509–3512.

46. **Bahri O**, **Rezig D**, **Ben Nejma-Oueslati B**, **Ben Yahia A**, **Ben Sassi J**, **Hogga N**, **Sadraoui A**, **Triki H**. 2005. Enteroviruses in Tunisia: Virological surveillance over 12 years (1992-2003). J Med Microbiol **54**:63–69.

47. **Roth B**, **Enders M**, **Arents A**, **Pfitzner A**, **Terletskaia-Ladwig E**. 2007. Epidemiologic aspects and laboratory features of enterovirus infections in Western Germany, 2000–2005. J Med Virol **79**:956–962.

48. **Oikarinen S**, **Tauriainen S**, **Hober D**, **Lucas B**, **Vazeou A**, **Sioofy-Khojine A**, **Bozas E**, **Muir P**, **Honkanen H**, **Ilonen J**, **Knip M**, **Keskinen P**, **Saha MT**, **Huhtala H**, **Stanway G**, **Bartsocas C**, **Ludvigsson J**, **Taylor K**, **Hyöty H**. 2014. Virus antibody survey in different european populations indicates risk association between coxsackievirus B1 and type 1 diabetes. Diabetes **63**:655–662.

49. **Richardson SJ**, **Willcox A**, **Bone AJ**, **Foulis AK**, **Morgan NG**. 2009. The prevalence of enteroviral capsid protein vp1 immunostaining in pancreatic islets in human type 1 diabetes. Diabetologia **52**:1143–1151.

50. **Abdelkhalek I**, **Seghier M**, **Yahia A Ben**, **Touzi H**, **Meddeb Z**, **Triki H**, **Rezig D**. 2015. Molecular epidemiology of coxsackievirus type B1. Arch Virol **160**:2815–2821.

51. **Laiho JE**, **Oikarinen M**, **Richardson SJ**, **Frisk G**, **Nyalwidhe J**, **Burch TC**, **Morris MA**, **Oikarinen S**, **Pugliese A**, **Dotta F**, **Campbell-Thompson M**, **Nadler J**, **Morgan NG**, **Hyöty H**. 2016. Relative sensitivity of immunohistochemistry, multiple reaction monitoring mass spectrometry, in situ hybridization and PCR to detect Coxsackievirus B1 in A549 cells. J Clin Virol **77**:21–28.

52. **Laiho JE**, **Oikarinen S**, **Oikarinen M**, **Larsson PG**, **Stone VM**, **Hober D**, **Oberste S**, **Flodström-Tullberg M**, **Isola J**, **Hyöty H**. 2015. Application of bioinformatics in probe design enables detection of enteroviruses on different taxonomic levels by advanced in situ hybridization technology. J Clin Virol **69**:165–171.

53. **Bergelson JM**, **Modlin JF**, **Wielandalter W**, **Cunningham JA**, **Crowell RL**, **Finberg RW**. 1997. Clinical Coxsackievirus B Isolates Differ From Laboratory Strains in Their Interaction With Two Cell Surface Receptors. Journal-of-Infectious-Diseases Mar 1997; 175 697-700 **3**:697–700.

54. **Marjomäki V**, **Pietiäinen V**, **Matilainen H**, **Upla P**, **Ivaska J**, **Nissinen L**, **Reunanen H**, **Huttunen P**, **Hyypiä T**, **Heino J**. 2002. Internalization of Echovirus 1 in Caveolae. J Virol **76**:1856–1865.

55. **Siljamäki E**, **Rintanen N**, **Kirsi M**, **Upla P**, **Wang W**, **Karjalainen M**, **Ikonen E**, **Marjomäki V**. 2013. Cholesterol Dependence of Collagen and Echovirus 1 Trafficking along the Novel α2β1 Integrin Internalization Pathway. PLoS One **8**:e55465.

56. **Coyne CB**, **Kim KS**, **Bergelson JM**. 2007. Poliovirus entry into human brain microvascular cells requires receptor-induced activation of SHP-2. EMBO J **26**:4016–28.

57. **Coyne CB**, **Shen L**, **Turner JR**, **Bergelson JM**. 2007. Coxsackievirus Entry across Epithelial Tight Junctions Requires Occludin and the Small GTPases Rab34 and Rab5. Cell Host Microbe **2**:181–192.

58. **Harrison DN**, **Gazina E V**, **Purcell DF**, **Anderson DA**, **Petrou S**. 2008. Amiloride Derivatives Inhibit Coxsackievirus B3 RNA Replication. J Virol **82**:1465–1473.

59. **Gazina E V**, **Smidansky ED**, **Holien JK**, **Harrison DN**, **Cromer BA**, **Arnold JJ**, **Parker MW**, **Cameron CE**, **Petrou S**. 2011. Amiloride is a competitive inhibitor of coxsackievirus B3 RNA polymerase. J Virol **85**:10364–74.

FIGURE LEGENDS

FIG 1. Kinetics of CVB1 infection in A549 cells. (A) Single-step growth curve of CVB1. At different time points of infection, cell suspension was collected and then serially diluted on new A549 cells. TCID50 values are shown. (B) The sum intensity of dsRNA structures measured from anti-dsRNA antibody (J2)-labeled confocal sections. Approx. 500 cells were quantified from each time point. The results are mean values ± Standard Error (SE). (C) Confocal images demonstrating the dsRNA production at different time points in A549 cells. Anti-dsRNA label (red), anti-CVB (green), nucleus labeled by DAPI (blue). Bars, 25 µm. (D) The uncoating of i) CVB1-ATCC ii) CVB1-CDC7 and iii) CVB1-CDC11 was evaluated by using Neutral Red (NR)-labeled virus. Cells were exposed to light for 10 min at different time points, and infection was continued for 8 h. Fixed cells were labeled with anti-CVB antibody (green) and the percentage of infected cells was quantified. As a control, NR-CVB1 was kept in the dark during the incubation and treated with light before infection. Approx. 600-700 cells were imaged at different time points. Results are mean values from three independent experiments (±SE).

FIG 2. (A) Effects of macropinocytosis inhibitors on CVB1 infection in A549 cells. i) CVB1-ATCC ii) CVB1-CDC7 and iii) CVB1-CDC11. Cells were pre-incubated with the chemical inhibitors described in Table 1, followed by virus binding and CVB1 infection, which was allowed to proceed till 8 h p.i. The newly produced virus capsid was labeled with NCL-ENTERO antibody, and the number of infected cells was quantified with the help of BioImageXD. The infection % was set to 100% in samples treated only with CVB1. Approximately 700-1000 cells were quantified and the results are shown as means (±SE) from three independent experiments. Bisindolylmaleimide (BIM), NSC23766 (NSC), Nocodazole (Noc), Bafilomycin A1 (Baf) and Wortmannin (Wort). Statistical significance between virus-only treated samples and different inhibitors was quantified by an un-paired t-test with Welch's correction (**, $P > 0.001$; ****, $P < 0.0001$). (B) Distribution of CVB1-ATCC (green) was analyzed by immunofluorescence after EIPA and NSC23766 treatments. Non-treated CVB1-ATCC infected cells as a control. Cells were treated with the chemical inhibitors and infected with CVB1 as described above. Brightness was increased similarly with both images. Bars, 25 µm. (C) NSC.

FIG 3. The involvement of early and late endosomes in CVB1 pathway. (A) CVB1-ATCC infection was allowed to proceed to different time points. Fixated cells were labeled with early endosome marker EEA1 antibody (red), CVB1 capsid with CVB antibody (green), and nucleus with DAPI (blue). The representative images are shown as projection stacks. Bars, 25 μm. (B) A549 cells were infected as described in panel A. i) The colocalization of CVB1-CDC7 and CVB1-CDC11 to EEA1 was quantified by BioImageXD. The results are shown as mean values (with SE) independent experiments. ii) CVB1-CDC7 and CVB1-CDC11 infected A549 cells together with transferrin (tf). The infection was let to proceed to different time points. After fixation CVB1 capsid was labeled and the colocalization to transferrin was quatified by BioImageXD. The results are shown as mean values (with SE) independent experiments. C) A549 cells were infected as described in panel A. Late endosomes were labeled with LAMP1 antibody (red) and CVB1-ATCC capsid with CVB antibody (green). Bars, 25 μm. Brightness was increased similarly in all images.

FIG 4. The involvement of ESCRT components in CVB1 infection. HeLa MZ cells were first transfected to overexpress wt-Hrs, DN-Vps4 or control-GFP (green). After 48 h, cells were infected with CVB1 for 8 h, fixed and labeled with CVB antibody (red). (A) The number of infected cells from the transfected cells was quantified. i) CVB1-ATCC ii) CVB1-CDC7 iii) CVB1-CDC11. Approximately 370 transfected cells were quantified per sample. Results are shown as means (±SE) from three independent experiments. Statistical significance between GFP-cntrl and DN-Vps4 or wt-Hrs was quantified by an un-paired t-test with Welch's correction (****, $P < 0.0001$). (B) Representative confocal images of transfected and CVB1-ATCC infected samples. Transfected cells observed as green and infected cells as red. Enhanced images show a typical expression of CVB1-ATCC capsid in each treatment. Bars, 25 μm

TABLE 1. Chemical inhibitors used in this study, and their effects on cells.

FIGURE SET 1.

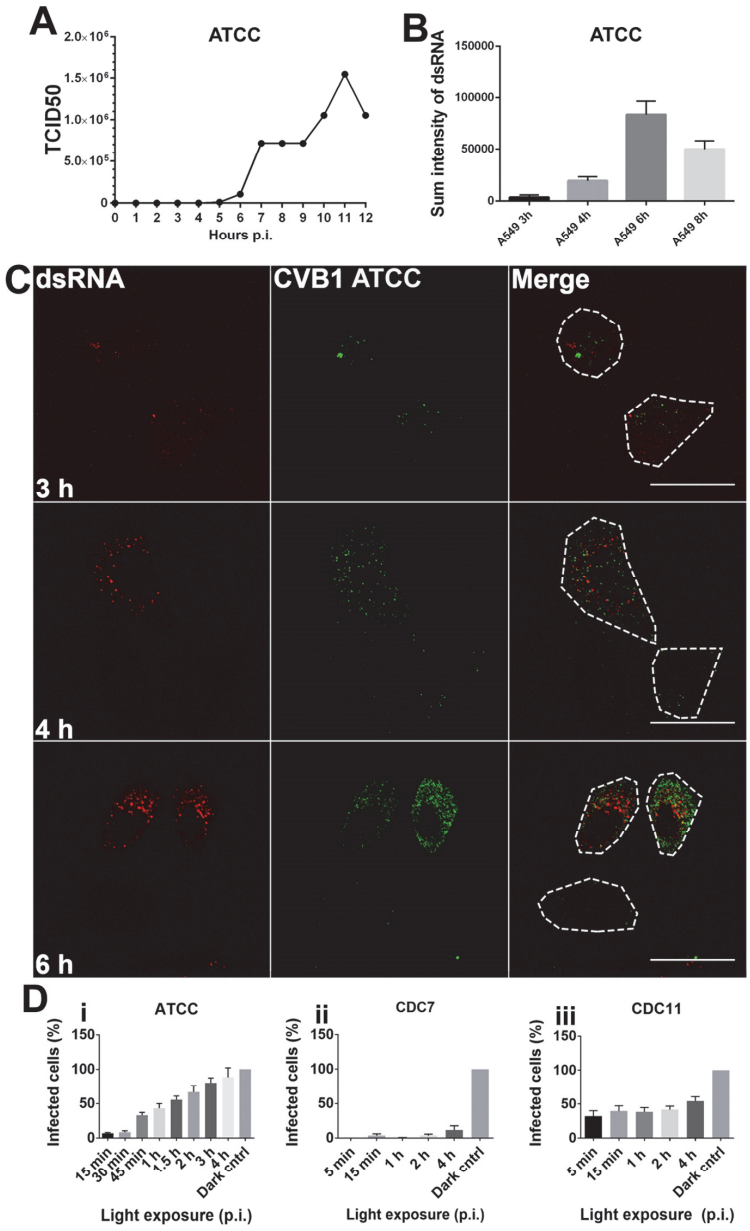
A
ATCC
TCID50
Hours p.i.
B
ATCC
Sum intensity of dsRNA
A549 3h
A549 4h
A549 6h
A549 8h
C
dsRNA
CVB1 ATCC
Merge
3 h
4 h
6 h
D
i
ATCC
ii
CDC7
iii
CDC11
Infected cells (%)
Light exposure (p.i.)
Dark cntrl

FIGURE SET 2.

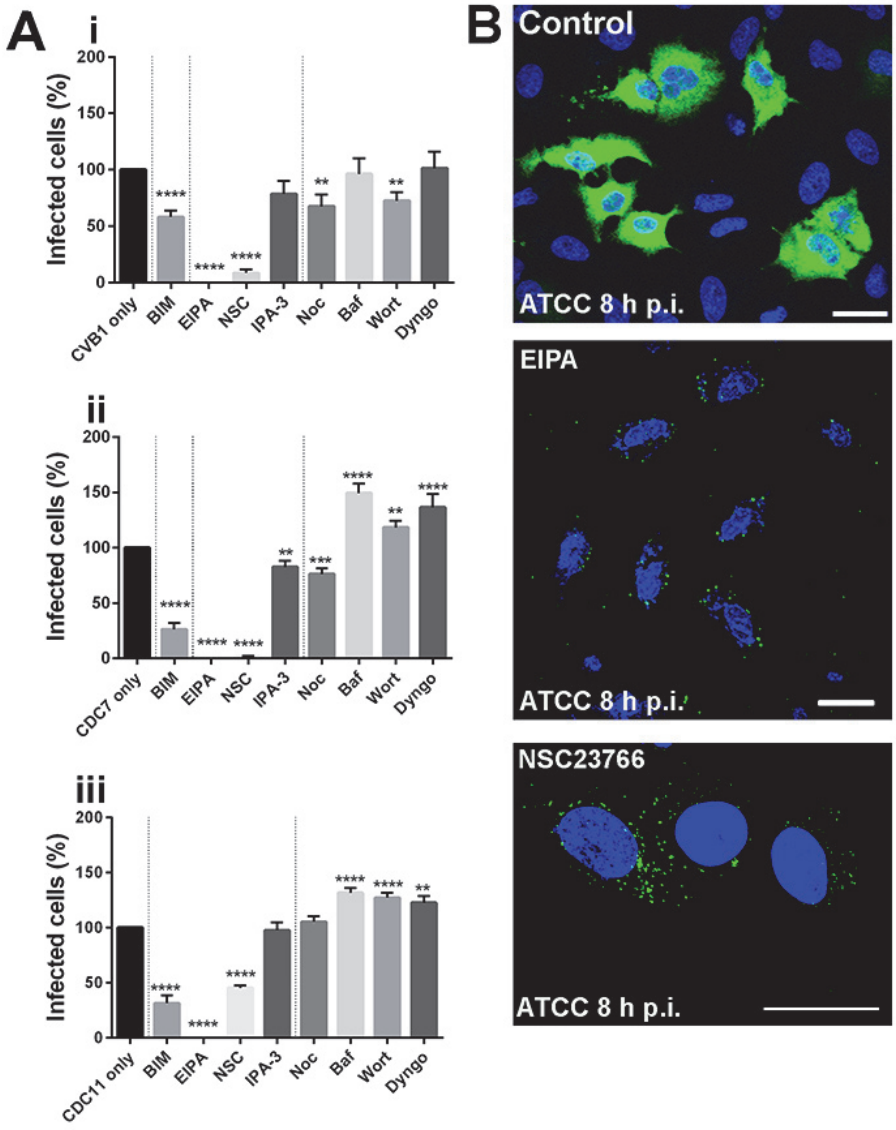
A
i
Infected cells (%)
200
150
100
50
0
****
****
****
**
**
CVB1 only
BIM
EIPA
NSC
IPA-3
Noc
Baf
Wort
Dyngo
ii
Infected cells (%)
CDC7 only
****
****
****
**
***
****
**
****
iii
Infected cells (%)
CDC11 only
****
****
****
****
**
B
Control
ATCC 8 h p.i.
EIPA
ATCC 8 h p.i.
NSC23766
ATCC 8 h p.i.

FIGURE SET 3.

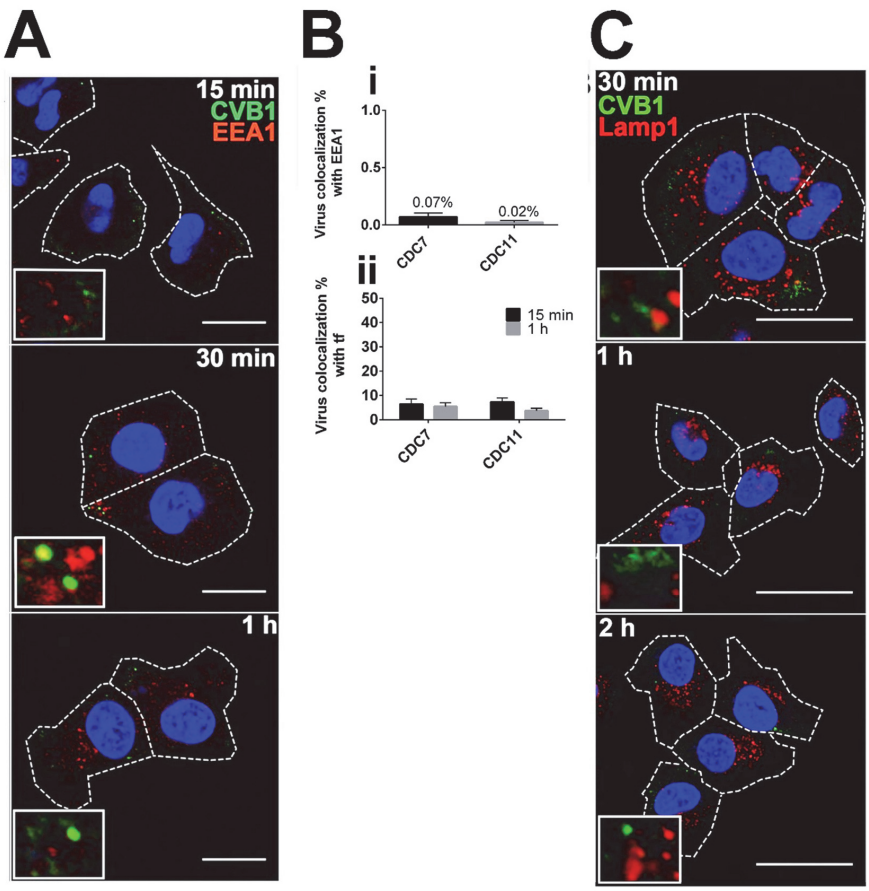
A
15 min
CVB1
EEA1
30 min
1 h
B
i
Virus colocalization % with EEA1
1.0
0.5
0.0
0.07%
0.02%
CDC7
CDC11
ii
Virus colocalization % with tf
50
40
30
20
10
0
15 min
1 h
CDC7
CDC11
C
30 min
CVB1
Lamp1
1 h
2 h

FIGURE SET 4.

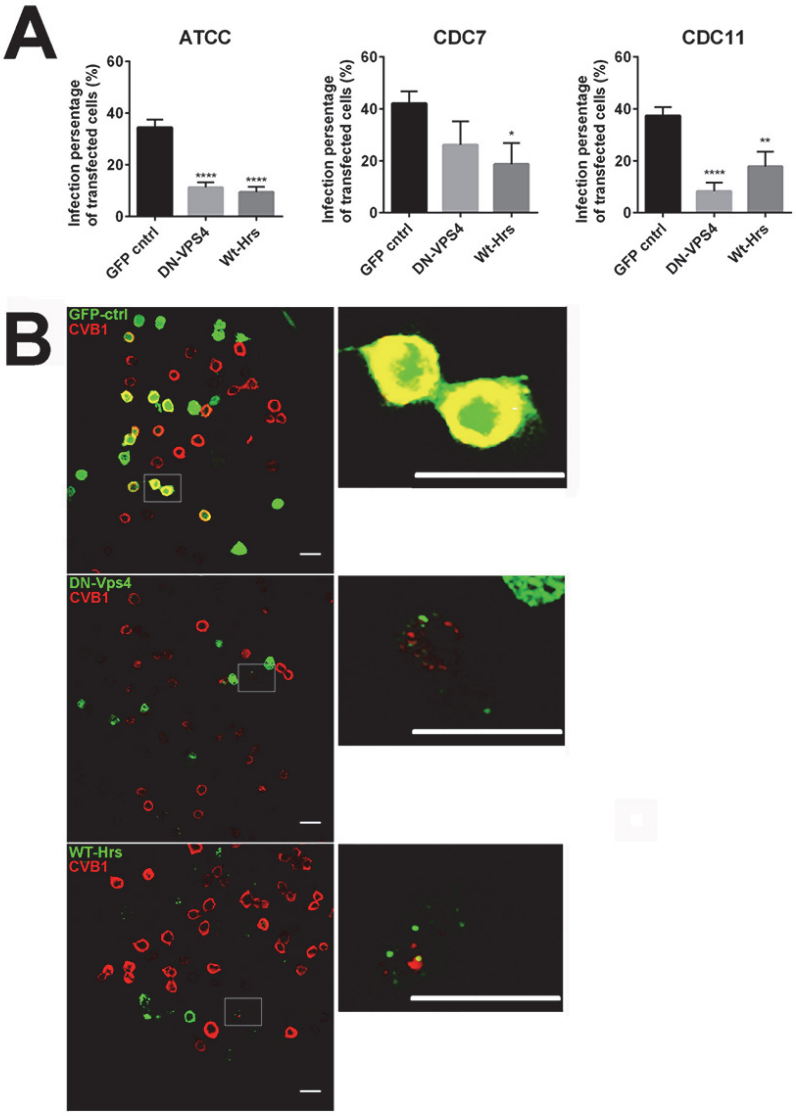
A
ATCC
CDC7
CDC11
Infection persentage of transfected cells (%)
60
40
20
0
****
*
**
GFP cntrl
DN-VPS4
Wt-Hrs
B
GFP-ctrl
CVB1
DN-Vps4
CVB1
WT-Hrs
CVB1

TABLE 1

Target	Drug	Concentration
PKC	Bisindolylmaleimide (BIM)	5 µM
Na^+/H^+ exchanger	EIPA	100 µM
Rac1	NSC23766	100 µM
Pak1	IPA-3	5 µM
Vacuolar ATPase pump	Bafilomycin A1	10 µM
Microtubules	Nocodazole	33 µM
PI3K	Wortmannin	100 nM
Dynamin	Dyngo-4a	12.5 µM